DESIGN OF HUMIDITY SENSOR FOR CONDITION MONITORING OF POWER TRANSFORMER

A Thesis

submitted in partial fulfilment of the requirements for the award of the degree of

Doctor of Philosophy

In Engineering

Submitted by

Shailesh Kumar
Registration No.: 951304002

Under the supervision of

Dr. Kuldeep Kumar Raina
(Ex- Distinguished Professor, SPMS, TIET
Presently Vice-chancellor, DIT University Deharadun)
and
Dr. Tarikul Islam
(Professor, Department of Electrical Engineering,
Jamia Millia Islamia (A Central University), New Delhi

THAPAR INSTITUTE OF ENGINEERING AND TECHNOLOGY
(Deemed to be University)
P. O. BOX 32, BHADSON ROAD, PATIALA, PUNJAB – 147004, INDIA

www.thapar.edu

August 2020

CERTIFICATE

This is to certify that the thesis entitled **"Design of humidity sensor for condition monitoring of power transformer"** being submitted by Mr. Shailesh Kumar to the Department of Electrical & Instrumentation Engineering, Thapar Institute of Engineering & Technology (Deemed to be University), Patiala, Punjab, India for the award of the degree of **Doctor of Philosophy**, is a record of bonafide research work carried out by him under my guidance and supervision and has fulfilled the requirements for the submission of this thesis, which to my knowledge has reached the requisite standard.

The results embodied in the thesis have not been submitted in part or full to any other Institute or University for the award of any degree.

Shailesh Kumar

This is certify that the above statement made by the candidate is correct and true to the best of our knowledge.

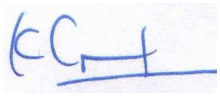

Dr. Kuldeep Kumar Raina
Ex-Distinguished Professor
School of Physics and Material Science,
Thapar Institute of Engineering and
Technology, Patiala, Punjab, India
(Presently Vice-Chancellor DIT University,
Deharadun, Uttrakhand, India

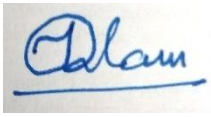

Dr. Tarikul Islam
Professor
Department of Electrical Engineering,
Faculty of Engineering and Technology
Jamia Millia Islamia (A Central
University), New Delhi, India

ACKNOWLEDGEMENTS

I would like to extend thanks and gratitude to the many people, who so generously contributed to the work presented in this thesis. I honestly feel short of words to acknowledge all those who helped me directly and indirectly during this research work.

With due regards and great delight, I convey my heartful gratitude and indebtedness to my supervisor **Dr. Kuldeep Kumr Raina**, Ex- Distinguished Professor, School of Physics and Material Science, Thapar Institute of Engineering & Technology (Deemed to be University), Patiala (presently Vice-Chancellor DIT University Deharadun, Uttrakhand) and **Dr. Tarikul Islam,** Professor, Department of Electrical Engineering, Jamia Millia Islamia (A Central University), New Delhi for skilful guidance, persistent encouragement, proficient evaluation and conscientious supervision throughout this academic endeavour. He was always available to help me with utmost care, kind attention and prudent suggestions during odd hours of the job. His hard working nature and methodical suggestions were a constant source of encouragement to me. It is owing to his guidance, expertise, inquisitive attitude and tireless efforts apart from his working hours that I find my vision even more broadened. I earnestly thank him from the core of my heart for being a consistent source of inspiration right through the beginning till the end.

I am very thankful to **Dr. Mandeep Singh**, Professor, Department of Electrical & Instrumentation Engineering, **Dr. Sanjeev Kumar Agrawal**, Associate Professor, Department of Electrical & Instrumentation Engineering and **Dr. Kulvir Singh**, Professor , School of Physics and Material Science, for being the member of Doctoral Committee and spending their valuable time in reviewing and critically examining the work.

I am also thankful to present Chairman of the Doctoral Committee **Dr. R. S. Kaler**, Senior Professor & Head, Department of Electrical & Instrumentation Engineering for the much needed support throughout the work.

My heartfelt gratitude is due to **Dr. Rafat Siddique**, Senior Professor & Dean, Research and Sponsored Projects and Honourable Director **Dr. Prakash Gopalan** for the support, encouragement and providing the necessary facilities to carry out and complete this work on steady course.

I also wish to express my deep sense of gratitude to all the faculty and staff members, particularly **Dr. Smarjit Ghosh**, Professor of the Department of Electrical & Instrumentation Engineering and all the persons who with their encouraging and caring words, constructive criticism and suggestions have contributed directly or indirectly in a significant way towards completion of this research work. My deepest appreciations are due to the research scholars under the supervision of **Dr. Tarikul Islam**. They have always stood by me in all difficult times and reinforced my confidence. Their never ending support is a constant source of motivation and always keeps me going.

I bow with gratitude for my parents, who are the most precious persons in my life and without their efforts I would have not achieved this milestone. I feel honoured in recognizing the love and affection of my wife **Mrs. Shilpa Singh**.

I express my gratitude to all those, with whom I have worked, interacted and whose thoughts have helped me in furthering my grasps and understanding of the work.

Last but not the least, I bow in reverence to **ALMIGHTY GOD** who has always showered blessings on me at each and every step to complete this thesis.

Shailesh Kumar

Abstract

The life of the transformer highly depends upon the insulation quality of the transformer oil. Moisture is one of the main causes for the degradation of the insulation quality of the oil. It decreases the dielectric strength and accelerates the aging of the insulation system of the transformer. Content of the moisture in insulation is measured in terms of parts per million (ppm). There are two main sources of water contamination of the oil in high voltage transformers such as (i) moisture ingress through cellulose paper used for transformer winding, (ii) moisture ingress by atmospheric humidity through transformer breather. In addition, a fresh oil sample always contains certain amount of moisture. The water contamination rate through the breather greatly depends upon the dehydrating capability of the silica gel present in the breather. The humidity level in the breather varies between 10% RH to 90% RH depending upon the condition of silica ï gel. At present, there is no online method for condition monitoring of the silica gel of the breather. To avoid the need of frequent replacement of silica gel and for condition-based maintenance of the breather, a humidity sensor based auto regenerative dehydrating breather may be an advanced solution. Further, for protecting the high voltage transformer from the dangerous effect of excess moisture, there is a need of a humidity sensor, which directly detects moisture in ppm level (3-100 ppm) in the transformer (T/F) oil. Moisture measurement in ppm level is challenging, and a costly affair. The environment of the transformer is chemically harsh and there is a change in ambient temperature. Metal oxide thin film sensor is stable robust material which may be suitable for moisture measurement in oil and in breather. There are various technologies used for moisture measurement from ppm to ppb level. Popular technologies are Karl fisher titration, chilled mirror hygrometer, cavity ring down spectroscopy (CRDS), electrolytic, and polymer/oxide thin film sensors. Most of the technologies except thin film sensors are costlier and suitable for offline measurement only, require skilled manpower, have long measurement time and are not suitable for field application. A low-cost portable moisture measurement system can be developed using solid state capacitive sensor. Electrolytic sensor has limited life span, and the polymer sensor has low thermal stability. There is a limited work for direct measurement of moisture in ppm level using thin film sensor. Therefore, main objectives of the present thesis are (i) development of a humidity sensor-based system for online condition monitoring and controlling moisture of silica gel of

the breather (ii) online moisture measurement of transformer oil in ppm level using a parallel plate capacitive metal oxide thin film sensor and modelling its long-term drift.

To accomplish the objectives (i) initially, a mathematical model for estimating the moisture content in silica-gel, and the degradation in the performance of the silica-gel inside a breather is developed, (ii) the anodized aluminum oxide parallel plate capacitive sensors and determination of response parameters of the sensors for humidity measurement in the range of 1-97% in breather have been designed and fabricated (iii) a microcontroller based interfacing circuit for auto refreshing of silica gel has been designed and implemented(iv) a thin film capacitive sensor for direct moisture measurement in transformer oil in ppm has been designed and fabricated and finally (v) the modelling the long-term drift due to aging of the ppm moisture sensor has been carried out to estimate the drift due to morphological change.

The developed breather model analyses the saturation condition of the silica-gel. The simulation results of the model closely match the sensor based experimental results. The fabricated anodized aluminium oxide sensors with controlled pore morphology measure the humidity of the breather in the range of 1-97% RH with sensitivities vary from 0.8 pF/%RH to 15 pF/%RH. The automatic control of moisture using heater via moisture sensor in the breather (0.5 kg, used for 150 KVA distribution transformers) increases the refreshing efficiency by 43% and reduces the need of regular replacement of silica-gel. The sol-gel thin film humidity sensor fabricated to measure moisture directly in the oil can measure in the range of 3-100 ppm with the maximum and minimum sensitivity of 1.8 pF/ppm and 0.8 pF/ppm respectively. Effort is also made to measure moisture using anodized alumina capacitive sensor in the range of 180 ppm to 800 ppm. The developed long-term drift model estimates the variation in pore morphology due to the lateral seepage of the moisture in the pore cell of the sensor. Change in pore morphology leads to the variation of the sensitivity of the sensor. It is found that the maximum deviation in the experimental and model response is 2.5%.

CONTENTS

LIST OF FIGURES

LIST OF TABLES

LIST OF ABBREVIATIONS

S1	Fabricated moisture sensor stored in drying agent
S2	Fabricated moisture sensor stored in open environment
$\mathbf{C_{sc}}$	Structural capacitance of the Al_2O_3 film cell (F)
$\mathbf{C_{hd}}$	Humidity dependent capacitance inside the pore (F)
$\mathbf{C_{ap}}$	Capacitance of air pore of Al_2O_3 film (F)
$\mathbf{C_{dw}}$	Capacitance of dry wall of Al_2O_3 film cell (F)
$\mathbf{C_{hw}}$	Capacitance of hydrated wall of Al_2O_3 cell (F)
$\mathbf{C_{scn}}$	Structural capacitance of newly fabricated sensor cell (F)
$\mathbf{C_{sco}}$	Structural capacitance of the aged sensor (S2) cell (F)
$\mathbf{C_{sco1}}$	Structural capacitance of the aged sensor (S2) cell when hydrated layer stretch inside the pore (F)
$\mathbf{C_{sco2}}$	Structural capacitance of the aged sensor (S2) cell when hydrated layer stretch inside the dry wall (F)
$\mathbf{C_{sensor}}$	Capacitance of sensor (F)
$\mathbf{C_{new\ sensor}}$	Capacitance of new fabricated sensor (F)
$\mathbf{R_{dw}}$	Resistance of dry wall of Al_2O_3 film cell (Ý)
$\mathbf{R_{hd}}$	Humidity dependent resistance inside the pore (Ý)
$\mathbf{R_{hw}}$	Resistance of hydrated wall of Al_2O_3 cell (Ý)
$\mathbf{R_{ap}}$	Resistance of air pore of Al_2O_3 film (Ý)
RH	Relative humidity in %
$\mathbf{r_k}$	Pore radius (m)
ũ	Surface tension of water
Ɉ	Density of water
M	Molecular weight of water
P	Partial pressure of water vapour
$\mathbf{P_s}$	Saturation pressure of water
PCB	Printed circuit board
CMOS	Complementary metal - oxide semiconductor
PWM	Pulse width modulation
XOR	Exclusive OR
IC	Integrated circuit
T	Conduction period (S)
$\mathbf{T_{on}}$	On time period (S)
$\mathbf{T_{off}}$	Off time period (S)
$\mathbf{F_{out}}$	Frequency of the train pulses (Hz)

V	Moisture dependent DC voltage (Volt)
V_{out}	Amplified DC voltage (Volt)
V_{cc}	Supply voltage (Volt)
V_{or}	RMS value of output voltage (Volt)
V_{m}	Maximum value of the supply voltage (Volt)
V_{s}	RMS value of the source voltage (Volt)
I_{or}	RMS load current (A)
P_{l}	Power delivered to the load (W)
n	Number of ON cycles
m	Number of OFF cycles
R	Resistance value of the heating load (Ý)
R_1, R_2, R_3, R_4, R_5, R_6, R_7,R_8, R_v	Circuit components (Ý)
C_1, C_2, C_3, C_4, C_r	Circuit components (F
C11	Capacitive response of sensor made on one side of Al sheet (nF)
C22	Capacitive response of sensor made on second side of Al sheet (nF)
C_{RH}	Capacitive response of the oxide sensor (F)
RH_{st}	Moisture concentration at steady-state (% RH)
DC_O	Duty cycle
RH_{in}	Relative humidity at the inlet of the breather (% RH)
RH_{out}	Relative humidity at the outlet of the breather (% RH)
T/F	Transformer
h	Hour
t	Time (S)

Chapter 1

Introduction

1. Overview

Power transformer (T/F) is the important and expensive equipment for the generation and effective utilization of electrical energy. For the un-interrupted continuous operation of power systems, continuous health monitoring of the power transformer is necessary. Investment by the electric utility company to purchase costly transformer is gradually reducing and the maintenance strategies of the devices are changing from time-based maintenance to condition based maintenance. Time based maintenance consists of periodic actions recommended by the manufacturers according to certain standards and sometimes depends on experiences on the working personnel. Condition based maintenance minimizes costs compared to the time-based approach, which may involve unnecessary work. In addition, the maintenance based on experience is sometimes inaccurate leading to early failure of the system. Therefore, there is a need of new diagnostic techniques for the health assessment of the equipment. The life of the (T/F) highly depends upon its cellulose and oil insulation condition. There are various dangerous effects of moisture in the oil as well as in cellulose insulation. It degrades the dielectric strength of the oil and the cellulose insulation, increases the rate of water bubbles release from the cellulose insulation and accelerates the cellulose aging. The moisture concentration of the oil-cellulose insulation is one of the major aspects that should be continuously monitored to determine the transformers condition. There are various sources of water contamination in power transformer. Moisture ingress through the breather is the major sources of water contamination. In cyclic drop of temperature of open breathing transformer, the atmospheric pressure is higher than the pressure inside the tank. Thus, the ambient air moisture of atmosphere ingresses if the breather does not dehydrate the moist air. The water contamination rate greatly depends upon the dehydrating conditions of the breather of specific transformer. The amount of water from the ambient air entering through the breather depends upon the operating mode of the transformer. The grid transformer has the cyclic load and heat recovery system. Due to cyclic temperature drop, it suffers from the high moisture contamination that leads to around 16 kg/annum water contamination through the breather inside the transformer. There is a need of condition monitor of the breather to stop the moisture contamination in the transformer through it. In the recent era of technology, the capacitive relative humidity (RH) sensors are often used to measure moisture relative to

saturation (%), especially under on-site and on-line conditions. There are various advantages of use of the RH/ppm sensor such as easy application in on-site and online measurement. Measurement of low and high humidity range depends upon the fabrication method, type and pore morphology of the sensor. Capacitive type sensor has low hysteresis, very fast response, good repeatability and stability. The sensing film of the sensor gets hydrated as the moisture diffuses inside the pores and it suffers from the long-term drift in response, which leads to measurement error. Therefore, a cyclic calibration of the sensor is required. Silica gel is used in the breather to absorb the moisture of the atmospheric air during the breath in period of the transformer. The moisture absorbing capacity of the gel deteriorates with time. For on line condition monitoring of the silica gel a highly stable humidity sensor monitoring humidity level in the range of 1-97% RH is required. The moisture content in transformer oil is measured in terms of ppm. The maximum allowed moisture depends upon the quality of insulation used in the transformer. For monitoring the moisture content in transformer oil, there is a need of humidity sensors detecting the moisture in ppm are required.

In this thesis work, as per the requirement of the on line monitoring and controlling the moisture to avoid its excess ingresses inside the transformer, initially a moisture model in breather for predicting the saturation level of silica gel has been developed. The model is also validated with the experimental data obtained in the laboratory using commercial humidity sensor by conducting experiments in the artificially designed breather. Two different types of the parallel plate moisture sensors using different methods of fabrication are designed for measuring moisture in different level. One parallel plate capacitive porous alumina (γ-Al_2O_3) humidity sensor for measuring moisture of transformer oil in the range of 3 to 100 ppm has been designed using sol gel technique. The designed sensor is suitable for measuring low level of moisture in the transformer oil. The long-term drift for the duration of one year of the designed sensor has been also investigated in the laboratory. Modelling of the long-term drift with the help of experimental data is achieved. Another parallel plate capacitive anodic porous alumina sensor is designed using electro chemical anodization method for measuring humidity in the range of 1 to 97% RH. This sensor is suitable for monitoring moisture inside the breather of transformer. This type of sensor is also used for measuring the high level of moisture 180-800 ppm in the transformer oil. The moisture inside the breather and transformer oil is monitored using the designed sensors in the laboratory. A simple electronics circuit for converting the capacitor change of the humidity sensor placed inside the breather into the voltage signal is designed and hardware implemented. Finally, the moisture inside the

breather is automatically controlled by heating the silica gel using the heating element via the humidity sensor.

The automatic control of moisture inside the breather with the humidity sensor will reduce the visual inspections of the degree of moisture level inside the drying agent (silica gel), and the regular replacement of the drying agent. This also increases the legibility of the frequent disposal of the drying agent. The operational reliability of the transformer will also increase due to maintenance free breather.

2 Objectives of Thesis

The main objectives of this thesis are:

- Development of moisture model in breather for transformer health assessment
- Design and Fabrication of the sensor for moisture measurement in breather
- Design of a sensor-based instrumentation system for controlling moisture in the breather
- Experimental validation of the designed sensor-based system for monitoring and controlling of moisture inside the breather
- Fabrication of thin film sensor for moisture measurement in ppm in transformer oil
- Long-term drift study of the fabricated humidity sensor and its modelling for the measurement of moisture in ppm level in the oil

3. Contribution of the Thesis

The main contributions of research in this PhD thesis are mentioned below:

(1) A mathematical model for pre-detecting the moisture in the silica gel of the breather considering the natural operation of a high voltage transformer.
(2) A prototype instrumentation system for monitoring and controlling the humidity level inside the breather using a designed thin film capacitive anodized alumina sensor.
(3) Design and fabrication of the humidity sensors using electrochemical anodization method to monitor and control humidity in the breather in the range of 1-97% RH and to fabricate thin film capacitive sensor using sol-gel method to directly measure moisture in the transformer oil from 3-100 ppm.

(4) Development of a mathematical model using the electrical equivalent circuit for the long-term drift analysis of the sol-gel thin film humidity sensor used for the ppm moisture measurement.

4. Outline of the Thesis

Chapter 1 Introduction

In this chapter, a list of thesis objectives is provided. A brief discussion about the scope of research is highlighted and the contributions of research work based on the objectives are explained next. Finally, the way of thesis organization is presented.

Chapter 2 Technical Background and Literature Review

This chapter reports the theoretical background and the literature review of this research. It describes about the power transformer in the liberalized energy market. The components of the power transformer are explained in detail. Different types of solid and liquid insulation used in the high voltage transformer are discussed. Various sources of moisture contamination in transformer and the dangerous effect of moisture on the insulation is also discussed. The details of the different types of sensors used for the measurement of humidity, different types of materials used for designing the humidity sensors are explained. The literatures for monitoring the life of the high voltage transformer using the humidity sensors are reviewed. Different moisture determination methods including the sensor-based condition monitoring of transformer oil are summarized. The literature of the development of the humidity sensor using the electrochemical anodization method is reviewed in details. The possible causes of drift in the response of different types of humidity sensor are explained in details. Types of interfacing circuits used for converting the response of the capacitive sensor into the electrical signal are reviewed, highlighting their merits and demerits.

Chapter 3 Modelling of Breather for Transformer Health Assessment

This chapter reports a mathematical model for estimating the moisture content in silica-gel in the breather of a power transformer. The model equations are derived considering the possible real-time operating conditions of the transformer. These operating conditions are the fast rise or decrease in oil temperature due to a step change in the electrical loads and the cyclic heating and cooling of the oil. An experimental setup has been developed for monitoring the variations in moisture concentration in silica-gel inside an artificially constructed breather. Finally, the validation of the model has been done with the experimentally obtained data and

the standard humidity input signals. The model has been analysed using the equilibrium relations of the moisture concentration between the silica-gel and the environment of the breather. The response of the model indicates the dynamic behaviour of a moisture sensor placed in the breather. The model has been used in predicting the moisture level in the silica-gel, the moisture concentration inside the breather and the degradation in the performance of the silica-gel.

Chapter 4 Fabrication of Anodic Aluminium Oxide Thin Film Humidity Sensor for Breather

This chapter covers the design and fabrication of a capacitive parallel plate relative humidity sensor for monitoring moisture inside the breather and oil of the transformer. The sensing film between the parallel plates of the sensor is of porous hexagonal ordered alumina. It is grown through the electrochemical anodization of pure aluminium (Al) sheet. Experiments have been conducted to determine the response parameters of the sensor with the humidity varying from 10 to 97% RH. The designed sensor is found to be sensitive in the range of 10 to 97% RH. The response parameters are suitable for breather monitoring and T/F oil. The experimental methods and results for measuring moisture in transformer oil are discussed. Further experiments are conducted to measure moisture in ppm level using the sensor in moist nitrogen gas. So, the sensor has wide range for moisture measurement. Efforts are also made to use the anodized capacitance sensor to measure moisture in T/F oil.

Chapter 5 Design and Implementation of an Electronic Circuit for Controlling the Humidity Level of the Breather

The purposes of the sensors, which are fabricated are to measure and control the humidity in the breather. Some of the sensors are also used to measure moisture in T/F oil. This chapter covers the design of an electronic circuit for converting the change in capacitance value of the sensor into the voltage signal. The circuit output is then suitably conditioned to vary the duty cycle of PWM wave. The PWM wave is then used to control the power of the heater placed in the breather, which is used to refresh the silica - gel. Therefore, the moisture inside the breather is automatically controlled using the heating element with the designed humidity sensor. The power across the heating load is controlled using integral cycle controller. The drying efficiency of the breather is estimated for 44 days.

Chapter 6 Thin Film Capacitive Transformer Oil Moisture Sensor and its Long -Term Drfit Modeling

This chapter covers the fabrication and drift study of aluminium oxide thin film capacitive humidity sensor. The sensor has been fabricated by a sol-gel method. This method allows

fabrication of pure formed of porous aluminium oxide for the moisture sensor. Being oxide sensing material, the sensor is thermally and chemically stable for the application in transformer condition monitoring. Experiment has been conducted to study the capacitive response of the sensor with change in moisture in ppm range. The sensor may age due to prolong use in breather or in transformer environment. Due to aging, the capacitance value of the sensor is many times drifted with the passage of time. A mathematical model, the electrical equivalent circuits and long-term drift analysis of the aged capacitive sensors for trace moisture sensing have been developed. The sensors are fabricated for detecting the moisture in the range of 3 to 100 ppm. To study the long-term drift, experiments are performed under different operating conditions over a period of nearly one year. The response behaviours of the sensors are simulated with the help of the model. Comparing the model responses with the experimental results, the proposed model can be used for drift analysis of an aged sensor. It can be used for the determination of hydration level and moisture condensation in the pores of the sensing film. Experimental results showed that when a sensor is kept in drying agent, maximum average drift of only 1.5% is observed but when a similar sensor is kept in open high humidity atmosphere, the maximum long-term drift is found to be ~ 11.2% over a time of 303 days.

Chapter 7 Summary and Conclusions

This chapter summarizes the research work performed in this thesis. Conclusions ofthe research work have been discussed in detail. A brief discussion for future scope ofthe research has also been given in this chapter.

Chapter 2
Technical Background and Literature Review

2.1 Introduction

This chapter deals with the specific requirement of high voltage transformer for the generation and utilization of electricity. The details of various components of the transformer and the effect of moisture on the life of the insulators are explained. There is a need of various types of the sensors for the health monitoring of transformer. It is explained in section 2.7. The various sources of water contamination in oil filled high voltage transformers are explained. Section 2.6 and section 2.8 discuss the different methods and types of humidity sensors used for the moisture measurement in transformer. Different techniques used for the development of humidity sensors are discussed in section 2.9 and section 2.10. Drift in the response of the humidity sensor is an important phenomenon. The possible causes of the drift in different types of humidity sensors are discussed in section 2.11.Section 2.12 provide the literature to model the response of the humidity sensor. Literatures on electronics circuit used for signal processing of the capacitive sensors are discussed in section 2.13.

2.2 Power Transformers

Power transformer is one of the most expensive devices of power sector. Reliability of the power system directly depends upon its reliable operation. Due to combined electrical and mechanical stress during the transformerôs operation, its cellulose-oil insulation system can fail. The moisture concentration of oil-cellulose insulation is the one of the major aspects that should be continuously monitored to determine the transformerôs condition. For the un-interrupted continuous operation of the power system, the continuous health monitoring of power transformer is necessary. There are three major factors that cause stresses to the transformers are: (1) the varying demand of electrical energy (2) improvement in the average age of the transformer and (3) improvement in maintenance strategies due to its high cost.

Investment by the electric utility company is reduced in the new devices and maintenance strategies of devices change from time based to condition based. Time based maintenance consists of periodic actions advised by the manufacturerôs recommendations, industrial standards and the experiences of the working personnel. Condition based maintenance minimizes the cost compared to the time-based approach, which may involve needless work. Therefore, there is a need of new diagnostic techniques for the health assessment of the equipment [1-2]. Reliability centred maintenance considers the probability of a failure in a forward-thinking approach. In order to get more benefits, power utilities are forced to utilized

the maximum capacity and lifetime of the equipments, decrease the cost of service and specialized stuff and suggest revised maintenance strategies. Utility company wantsquality, reliability, and maintenance free solutions that provide timely information on the transformerôs health.

2.3 Components of Transformer

Transformer consists of various components such as laminated core, winding, insulation (liquid or solid), tap changer, buchholz relay, explosion vent, cooling tubes, dehydrating breather and the conservator tank. The schematic diagram of a high voltage transformer showing the various components is shown in Fig. 2.1.

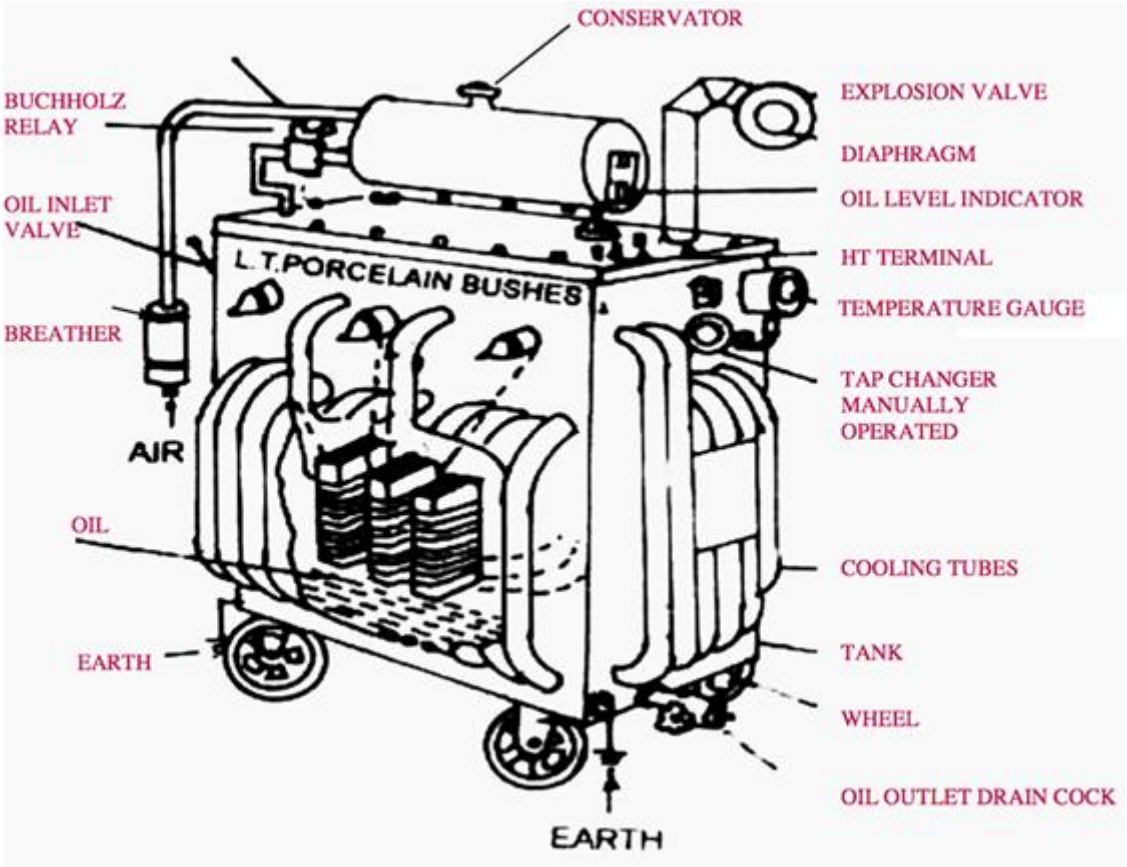

Fig. 2.1 Schematic diagram of the transformer showing the various components.

The Transformer Core

The transformer core provides the low reluctance path to the magnetic flux linking to both the primary and the secondary winding. The arrangements of both the windings are in such a way that the core reduces the flux leakage in the transformer. The core has two types of losses namely, the hysteresis and the eddy current loss. It is also called the iron loss, which produces

heat. The material used in the core has low loss and producing low noise. The loss is only 2-4% of the total loss in the T/F. Major loss occurs in T/F winding. Annealed copper coil is used in the transformer winding. Nowadays, aluminium coil is also used, its used depends upon the rating and the cost of the transformer. Various types of insulations are used in T/F such as liquid mineral oils, vegetable oils in conductor insulations and the insulation for barriers and spaces made of pressboard [3].

The Winding of Transformer

Two sets of winding insulated from each other are placed over the core of the transformer. There are several turns of copper or aluminium conductor in each set of winding. Conductors are bundled together and connected in series. Windings are classified in two different ways: (i) based on the input and output supply and (ii) based on the voltage range.

Based on the input excitation and the output supply, there are two types of winding namely the primary winding and the secondary winding. Based on the voltage range the windings are classified as the high voltage winding, this is made of copper or aluminium conductor. The number of turns of the conductor is the multiple of the number of turns in the low voltage winding. The conductor used will be thinner than that of the low voltage winding. The low voltage winding has the smaller number of conductors. Current in the low voltage winding is higher than that of the high voltage winding [3].

The Conservator

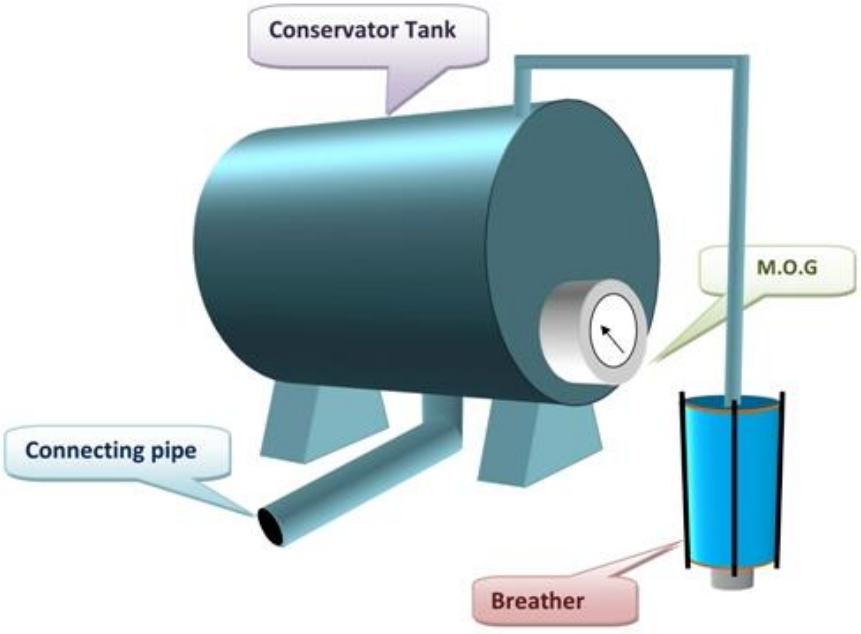

Fig. 2.2 Conservator without air cell.

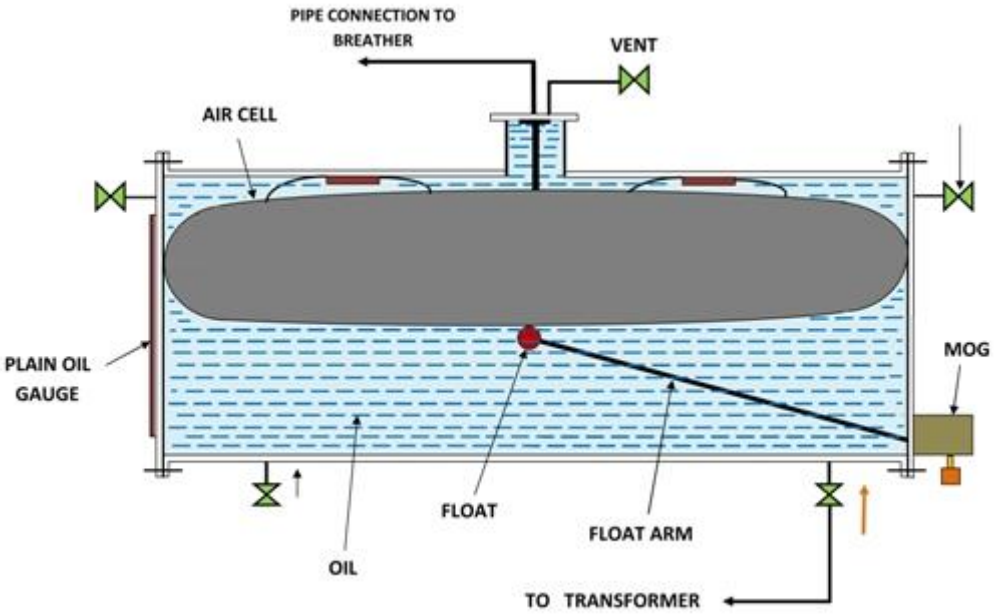

Fig. 2.3 Conservator with air cell.

Conservator stores the transformer oil. It is airtight cylindrical drum and made of metal. It is fitted above the transformer. The conservator tank is vented to the atmosphere at the top, and the normal oil level is approximately in the middle to allow the oil to expand and contract as the temperature of oil varies. The conservator is connected to the main tank inside the transformer, which is completely filled with transformer oil through a pipe line. An air cell inside the conservator of high voltage transformer (above 5 MVA) is provided for avoiding direct contact of air with the oil [3]. The schematic diagram of conservators with air cell and without air cell is shown in Fig. 2.2 and Fig. 2.3 respectively.

The Breather

Breather is a cylindrical container and filled with silica gel. It is used to controls the moisture level in the transformer. Due to cyclic loading of the transformer, there is a variation in the temperature of the insulating oil and causes expansion and contraction of the oil. Change in oil level causes the pressure to change inside the conservator. Pressure changes are balanced by a flow of atmospheric air in and out of the conservator. In this way, the air moisture can enter into the transformer. If the moisture is dissolved in the oil, it deteriorates the quality of the paper insulation or may even lead to internal faults. Therefore, it is necessary that the air entering the tank is moisture-free. When the atmospheric air passes through the silica gel of the breather, the silica crystals absorb the air moisture [4-5]. The moisture absorption capacity of the silica - gel depends upon its type.

Table 2.1

Data used for the selection of breather in transformer [5]

Breather Capacity (kg)	Maximum oil contents (Litres) of Transformer	Transformer Rating (MVA)	Maximum Air Space Volume (Litres) of Transformer	Approximate Daily Breathing Rate(Litres) of Transformer	Maximum Air Volume before Recharge (Litres)	Cycle Time (Days) of Breather
0.60	1500	<1.25	230	15	6000	400
1.20	3000	3	500	30	12000	400
1.90	4750	6	1100	55	20000	400
5.00	11350	9	2400	140	45450	320
10.00	22700	30	4800	280	90900	320
14.50	34050	60	7250	420	136500	320
17.50	45450	100	9685	570	181800	320
27.30	68150	180	14500	840	272700	320
17.5X2	90900	240	19370	1140	363600	320
27.30X2	136360	500	29000	1680	545400	320
17.5X3	136360	500	29055	1700	545400	320
27.30X3	204550	750	38750	2280	818100	360

Some silica - gels are sensitive above 50 %RH and some are sensitive below 50 %RH [6].The type of silica - gel used in the breather depends upon the local climate of the working transformer. The breather acts like an air filter for the transformer.

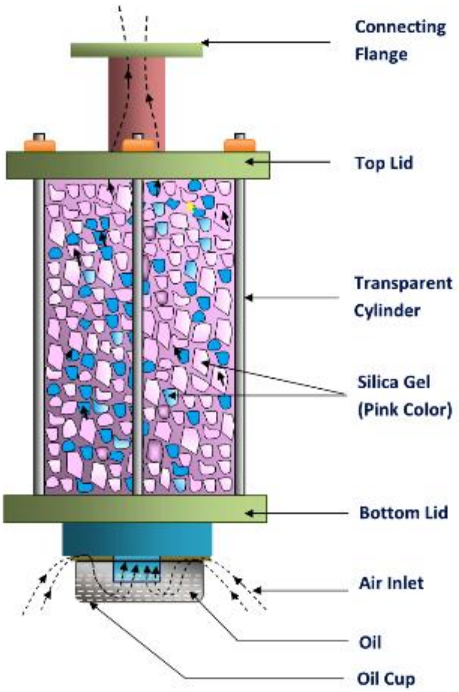

Fig. 2.4 Dehydrating breather of transformer.

It is connected to the end of a breather pipe. Maintenance free breather in the industry is also available but working principle is not clear in any literature [7]. The conventional dehydrating breather used in high voltage transformer is shown in Fig. 2.4. The size of the breather depends upon the rating of the transformer, the maximum oil contents, approximate daily breathing rate, etc. The details of the requirement of the size of the breather used in high voltage transformer are shown in Table 2.1.

Tap Changer

The output terminal voltage of the transformer depends upon the input supply voltage, turns ratio and the connected load. The terminal output voltage decreases during loaded conditions and increases during the off load conditions. Tap changer is used to balance the voltage variations. It can be either on-load or off-load. In an on-load tap changer, the tapping can be changed without isolating the transformer from the supply. In an off-load tap changer, it is done after disconnecting the transformer from supply. Automatic tap changers are also available in some of the T/F [3].

Cooling Tubes

Cooling tubes are used to cool the transformer oil. These tubes increase the surface area. The transformer oil is circulated through the cooling tubes. The circulation of the oil may either be natural or forced. In natural circulation, when the temperature of the oil raises the hot oil naturally rises to the top and the cold oil sinks downward. Thus, the oil naturally circulates

through the tubes. In forced circulation, an external pump is used to circulate the oil. The hot oil passing through the tubes gets cool down [3].

Buchholz Relay

Buchholz relayis a protective device, which is housed in the connecting pipe from the main tank to the conservator tank. It senses the faults occurring inside the transformer. Buchholz Relay operates by the gases emitted from the decomposition of the transformer oil due to the internal faults. It protects the transformer from internal faults [3].

Explosion Vent

The explosion vent is used to expel very hot oil in the transformer during heavy internal faults in order to avoid its explosion. During heavy faults, the oil rushes out of the vent. The level of the explosion vent is normally maintained above the level of the conservatory tank [3].

2.3.1. Insulating Materials

The insulation used in transformer is of dielectric insulating materials. It is used to provide the insulation between the windings turns, between the windings and to separate the winding from the tank and core. The insulation used in the oil cooled transformer is either liquid or cellulose type. The internal insulation consists of mineral oils, paper and cellulose in the form of pressboard. Dry type insulation is used in the distribution transformer upto a few MVA. However, the oil filled is suitable for the high rating transformer [3].

2.3.2. Electrical Properties of the Insulating Materials

The electrical current under the influence of an electric field does not flow through the electric insulator. The current through the semiconductor and conductor flows easily. The resistivity of the insulator is much higher than that of the semiconductor and conductors. An ideal insulator does not exist practically and it carries small numbers of movable charges due to which it carries current. When sufficiently large voltage is applied across the insulator, the high electric field breaks away electrons many from the atoms and this is called break down voltage of an insulator. There are various materials which has high resistivity and used as the electrical insulator such as paper, glass, and teflon. In electrical apparatus, insulator provide support and insulate the electrical conductors. The used insulator has good electrical properties to survive the impulse voltage of peak values, which is several time the operating voltage. The important electrical properties of the insulators are their electrical stress, permittivity, resistivity, and dielectric loss, etc. A perfect insulator consists of high dielectric strength, high resistivity, superior thermal conductivity, high tensile and shear force of solid insulation and high level of thermal stability. The other important properties apart from the above, it must have excellent mechanical properties such as ability to resist moisture (being

non-hygroscopic), withstand vibrations, bending and abrasion. Good thermal stability during the life of the transformer [8-10].

2.3.3. Transformer Oil

The core of the transformer is winded with the set of coils. The coils are insulated with paper insulation and separated from each other by radial spacers. The tube of oil- impregnated paper or pressboard is used to insulate the low and high voltage coils. The coils and core are housed in oil filled steel walled tank. The oil is thermally stable and does not react with any other element of the transformer. It has very good electrical properties and remain electrically insulating at normal operating voltage and impulse voltages arising from the lightning strokes or switching surges. Transformer oil is the combination of various types of hydrocarbons molecules that is formed from the crude oil. It is composed of three types of molecules: (1) linear chains and branched chains paraffins (2) cyclical paraffins (naphthenes) and (3) cyclical structures having carbon-carbon double bonds (aromatics). The transformer oil is either paraffinic or naphthenic type as in as shown in Fig. 2.5 [11]. The compositions of the used transformer oils are given in Table 2.2. The source of crude oil decides the relative percentage of paraffinic and naphthenic constituents. The physical properties of both the oils are same and independent from its relative compositions. The physical properties of oils are shown in Table 2.3 [12]. Important physical properties of the oil are refractive index, viscosity, cloud point, pour point, sulphur content and wax content.

Table 2.2: Percentage compositions of different types of transformer oils

Transformer Oil	Paraffinic (% Composition)	Naphthenic (% Composition)
Paraffins	60	20
Naphthenes	25	65
Aromatics	15	15

Table 2.3: Physical Properties of Transformer Oil

Physical Properties	Standard Values
Index of Refraction, K	2.1 ï 2.7
Density, 15^0C (g/cc)	0.876
Viscosity, 40^0C (cSt)	9.48
Cloud Point (^{0}C)	− 54
Pour Point (^{0}C)	− 54
Sulfur (wt. %)	0.05
Wax Content (− 40^0C)	0

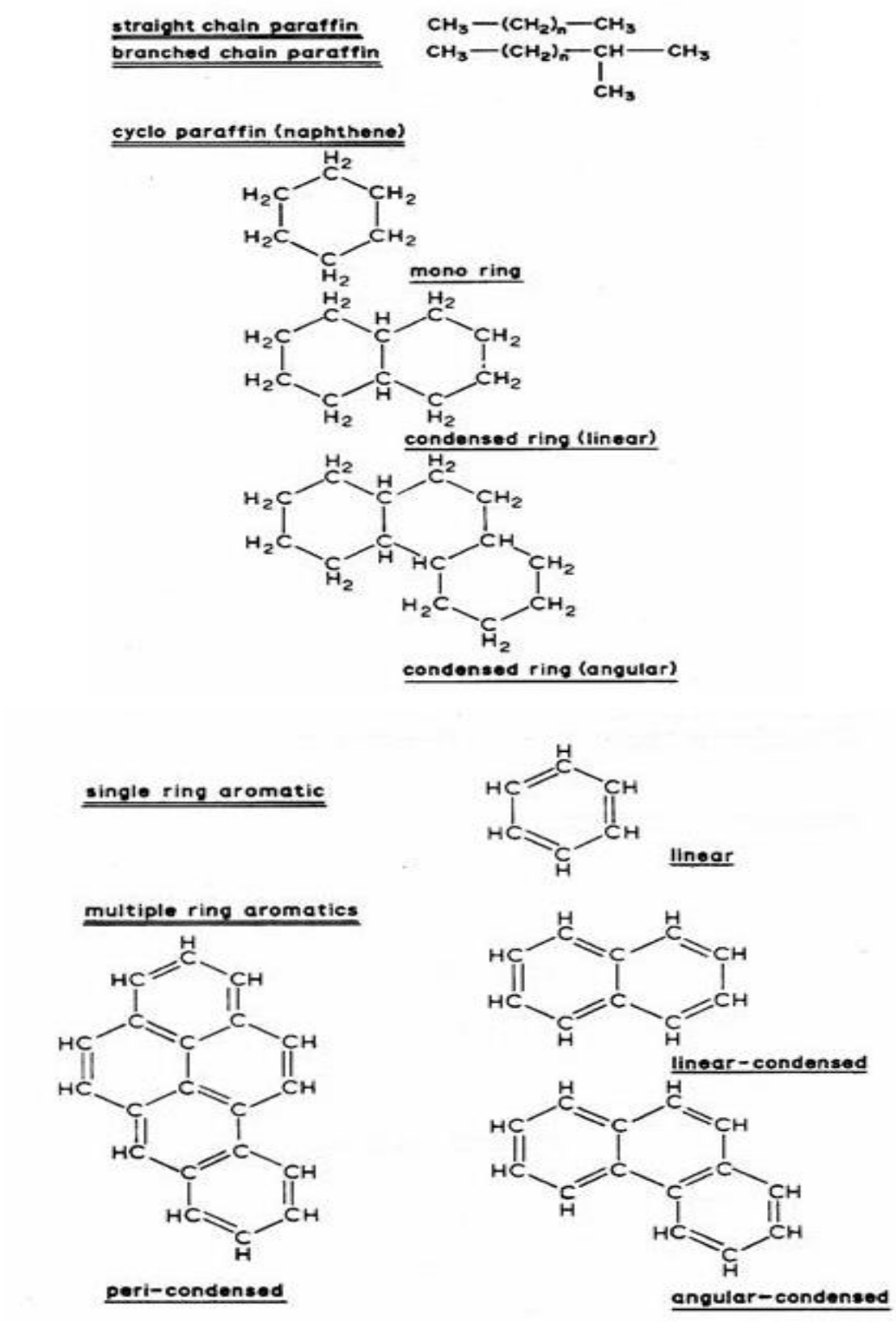

Fig. 2.5 Paraffinic, Naphthenic and aromatic hydro carbons.

The physical parameters such as viscosity, pour point, cloud point and wax content should be low so that the oil can freely flow through the tubes for cooling purposes. The electrical properties of the oil are listed in Table 2.4 [13-16].

Table 2.4: Electrical Properties of transformer oil

Electrical Properties	Standard Values
Resistivity, 80^0C, (Ω-cm)	$10^{\square\square}$
Tan δ	0.002
Corona Inception level (KV)	22.4
AC Break down voltage (KV/ inch)	400
Impulse Break down voltage, Positive needle (KV/ 0.25 inch)	30
Impulse Break down voltage, Negative needle (KV/ 0.25 inch)	50

Presence of moisture in the oil is another important concern for the reliable operation of the T/F.As the moisture content increases the breakdown voltage of the oil reduces. So, the insulating property decreases. The reduction of break down voltage with water content is shown in Fig. 2.6 [14].

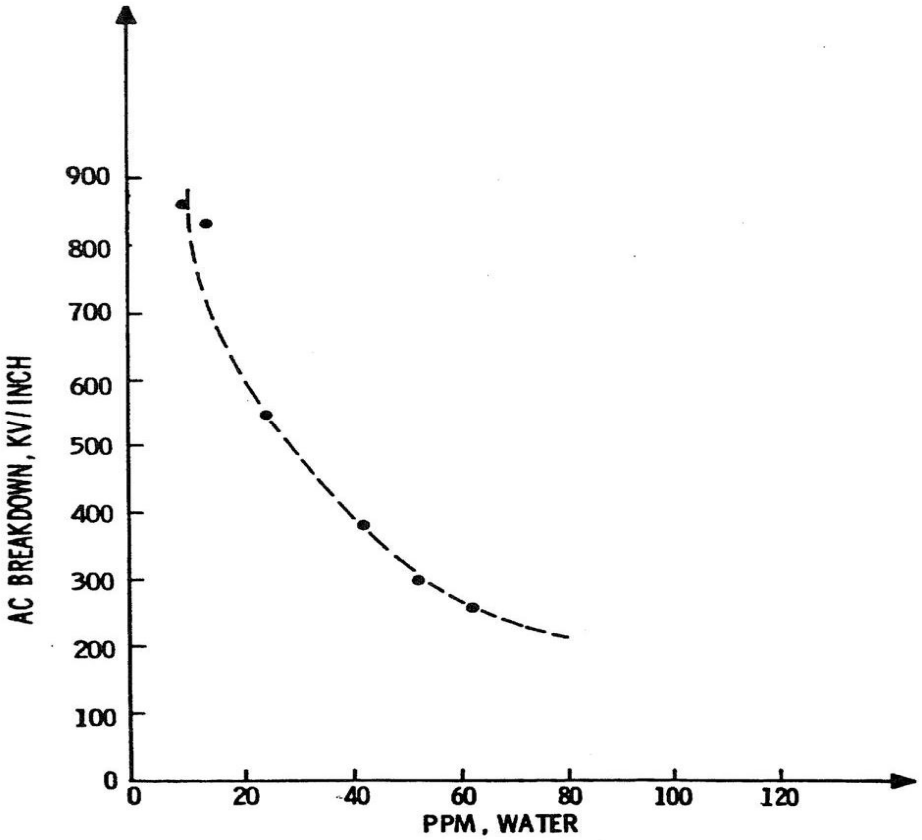

Fig. 2.6. AC breakdown voltage as a function of water content.

It shows that there is a sharp decrease in the break down strength as the moisture level increases. The graph also shows that as the concentration of water increases from the 20 to 60 ppm, the breakdown strength of the oil reduced to one-third of its initial value. This result

highlights the need to reduce the moisture level in the oil and avoiding the contact of the oil to moisture. Oxidation is another degradation process that happens in the practical transformer. Oxygen reacts with the oil at high temperature and liberates water, peroxides and weak organic acid. It deteriorates the insulation strength and the metal surface of the tank. So, the contact of oxygen with the oil is avoided. The oil is degassed, dehydrated and nitrogen filled in the transformer instead of air. Oxidation rate can be slow down through the employment of a sealed container or by filling the gas space in the bigger transformers with nitrogen gas.

Sludge is the product of the organic molecular reaction, which also presents a problem in the oil. It is generated from molecules, which are ionized by the partial electric discharges. It precipitates at the coils and walls and at the bottom of the tank. It causes hindrance to the flow of the oil.

2.3.4 Paper Insulation

Paper insulation in the transformer is necessary for the survival of high electrical and mechanical stresses generated at its windings and core. The pressboard for the insulation of the winding is prepared by compressing the layer of papers jointly and drying them thoroughly to remove moisture from it. Cellulose insulation is used as the solid insulation in the power transformer and it is available in the form of natural renewable source. The insulating paper is prepared through the kraft process followed by the delignification of wood pulp. Cellulose is the major component of the paper insulation. It is about 90% of the total insulation and 6 to 7% is lignin and the rest is hemicelluloses. The percentage of water in paper is 4 to 5% by weight. The insulator is dried after the winding to reduce the percentage of water to 0.5% [17-18]. Transformer oil is acting as the coolant for the winding and the dielectric constant of the dried paper increases when it is soaked with insulating oil. The major problem with the cellulose paper insulation is that it is hygroscopic material. It adsorbs moisture, so the dielectric strength of the paper insulation also reduces. When the paper is impregnated with oil, the moisture molecules are not allowed to get adsorbed in the pores of the paper. However, even though it is properly dried and impregnated, some moisture molecules remain trapped in the pores, which become troublesome issue at the latter stage.

2.4. Humidity

Humidity is available everywhere in the atmosphere of the earth. Amount of water vapour present in air is called humidity. Amount of water in air is expressed as relative humidity represented by %RH. Humidity is different from the moisture. Amount of water present in any solid or liquid material is called the moisture. Trace moisture indicates very small amount of water vapour in the range of parts per million to parts per billion. The dynamic range of

humidity is very large. Its range is from ppb (parts per billion) to %RH. Measurement of humidity is performed in different environmental conditions such as in corrosive or non-corrosive gases, at different temperature in the range of -80℃ to 1000℃ and at different types of contaminants [19-20].

2.4.1 Fundamental of Humidity

There are different ways to express the humidity such asabsolute humidity, relative humidity, Parts Per Million (PPM), mixing ratio, Dew/Frost point (D/F PT), and specific humidity.

- **Absolute Humidity**

It is defined as the ratio of the mass of water vapour to volume of dry air and expressed in terms of g/m^3.

- **Relative Humidity**

Relative humidity is measured in percentage and expresses as %RH. It is defined as the ratio of amount of water vapour present in air to the maximum amount of water vapour the air can hold or the ratio of partial pressure of water vapor to the saturation vapor pressure of the water. Relative humidity is expressed as relative measurement because it is temperature dependent quantity [19]. As the temperature increases, the relative humidity decreases. The saturation vapour pressure is also the function of temperature. As the temperature increases, the saturation vapour pressure increases. The partial pressure of water vapour is expressed as the individual pressure of the water vapour in the total pressure. At 100 %RH, the partial pressure is equal to the saturation pressure and the water vapour is in equilibrium with the liquid water.

- **Parts Per Million by Volume (ppmv)**

Moisture measurement in ppmv is known as theabsolute humidity measurement. Low level of moisture in industry is measured in terms of ppmv. It is defined as the ratio of volume of water vapour in total volume of moist gas or water vapour pressure to total moist gas pressure

- **Parts Per Million by Weight (ppmw)**

Concentration in ppmw is defined as the ratio of the mass of the water vapor occupies to the total mass of the solid liquid [20].

- **Specific Humidity**

Specific humidity is the ratio of the weight of water vapor to the total weight of air containing it [20].

- **Mixing Ratio**

It also called humidity ratio and it is defined as the ratio of the mass of water vapor to a unit mass of dry air containing it.

- **Dew-Point and Frost-Point Temperature**

Temperature at which the water vapour present in air or gas condenses into liquid form is called the dew point. Frost point is defined as the temperature (below 0ºC) at which the water vapor present in air/gas condenses to ice. Dew point and frost point do not depend upon the temperature, it depends upon the pressure. Therefore, it is defined as absolute humidity [19-20]. At dew point temperature, relative humidity is 100%. The relation among the dew/frost point, parts per million by volume and relative humidity is shown in Fig. 2.7. Parts per million by volume covers the lower measurement range of humidity, relative humidity covers the higher range of measurement and dew pint and frost point covers the all measurement range of humidity.

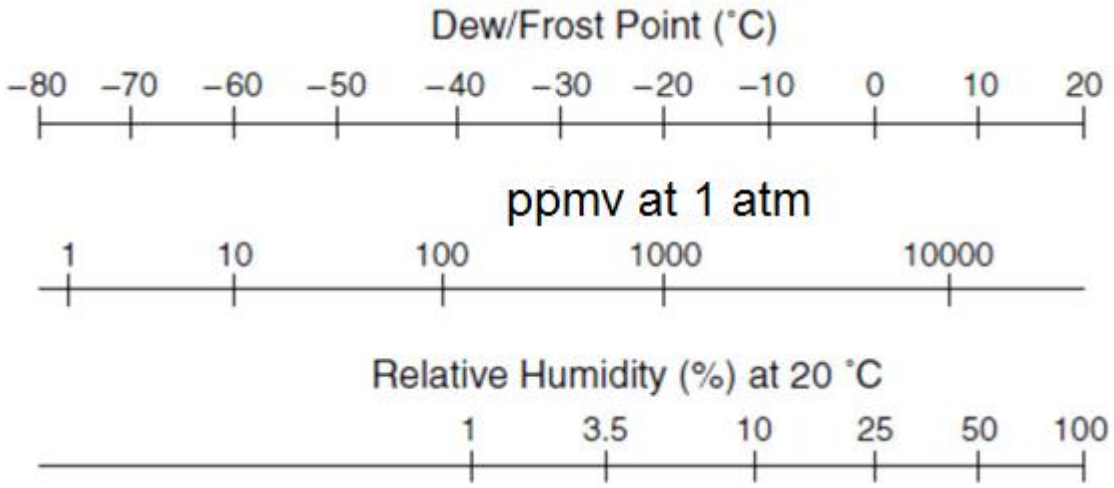

Fig. 2.7 Correlation among humidity units: relative humidity, dew/frost point, and ppmv.

2.5 Dangerous Effects of Moisture in Transformer Insulation Systems

There are three dangerous effects of moisture in the oil- cellulose insulation system.

1) degrades the dielectric strength of oil and cellulose insulation. 2) increases the rate of water bubbles release from the cellulose insulation and 3) accelerates the cellulose aging.

- **Degradations of the dielectric strength of oil and cellulose insulation**

Moisture deteriorates the dielectric strength of oil and insulator, which is the most important part of the transformer operation. The bubbles are generated due to the injection of current at the negative electrode and originate from the area of low density. The breakdown process of

dielectric strength of oil-insulation system is influenced by the relative availability of water molecules due to moisture content relative to the saturation. Water does not dissolve above saturation level but generate small droplets. The moisture relative to saturation depends upon the temperature influence. The effect of moisture on breakdown process is explained more appropriate by moisture content relative to the saturation (%) than the moisture relative to the weight (ppm). According to the IEC 60422 standard, moisture limit of transformer is given in terms of relative to weight (ppm) without considering the effect of temperature and aging phenomena.

- **Evolution of Water Vapour Bubbles**

At high temperature, the gases bubbles are emitted from the wet insulator in oil-filled transformer. This phenomenon causes two harmful effects. It decreases in the dielectric strength of the oil and cellulose insulation due to the formation of the bubble on its surface. It causes the displacement in insulation oil and de-impregnation of the conductor turns insulation. Insulating liquid has higher dielectric strength than that of the gases. The breakdown process starts with a microscopic area of large distances between corpuscles, where ions or electrons can initiate avalanches. Microscopic bubbles are originated from the current impulse on the electrode. Charge carrier is injected into the bubbles from the next current impulse that causes current amplification and the break down occurs [21-22]. Bubbles generate from the oil paper insulation, when it is heated that leads to significant decrease in dielectric strength. The thermal stability of the new kraft paper is minimum. Due to the microstructure of the thermally upgraded paper, the bubble inception within it starts at high temperature. It is made resistant to thermal aging by filler material that leads to decrease in pores volume and capillaries. Bubbles are generated at high temperature as the capillary forces increase. During the thermal aging, -OH groups are the active part of the cellulose chain and become attracted to each other that leads to decrease in volume, diameter and number of the pores, which increase the capillary forces [23]. Aging of oil besides the paper aging is also equally important for the inception temperature. The surface tension and inception temperature of bubble decreases due to the aging by-products.

- **Accelerated Aging of the Cellulose**

The mechanical strength of the cellulose in power transformer decreases due to its hydrolysis, oxidation and pyrolysis effects. Hydrolysis is considered as the major factor for the aging process. The chemical reaction of hydrolysis takes place even at the service temperatures. The

longer chain of the cellulose breaks into the smaller pieces during the hydrolysis process. Water is added in this reaction, and acid serves as a catalyst [24].

2.5.1. Sources of Water Contamination in Transformer

There are three major sources of water contamination in power transformer: (1) moisture ingress from the ambient air of atmosphere, (2) aging of oil-cellulose insulation system and (3) residual moisture after manufacturing.

The cellulose insulation of new transformer has 0.4-1% moisture by weight. Per year water contamination in service transformer is approximately 0.1% that leads to a typical value of 3% for 30 years old transformer. There is a need of long drying time to remove the residual moisture from the cellulose insulation in the manufacturing process. In the duration of change in temperature due to the cyclic loading of the transformer, the moisture is transferred from the oil to thin structure of the insulation. Moisture available in the atmospheric air is the major source of water [25] and contributes through the three mechanisms: firstly, the adsorption of moisture from atmosphere during the maintenance and repair. Secondly, the moisture ingresses into the tank due to the pressure gradient between the gas space or oil inside the transformer and water vapour in the atmosphere. The third is the cyclic drop of temperature of open breathing transformer. In this duration, the atmospheric pressure is higher than the pressure inside the tank of the transformer.

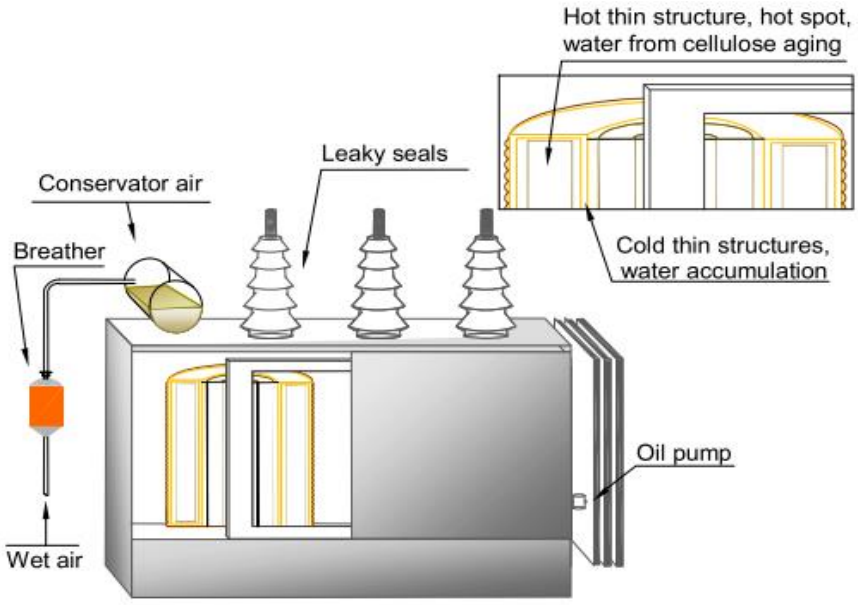

Fig. 2.8 Transformer showing various sources of water contamination.

Thus, the ambient air moisture of atmosphere ingresses if the breather does not dehydrate it. The water contamination rate greatly depends upon the dehydrating conditions of the breather of aspecific transformer.

Table 2.5

Rate of water contamination in a large grid (150 MVA) transformer [25-29].

Conditions	**Rate of water contamination**
Ingress of moisture due to oil-impregnated insulation with the direct exposure to the air	0.5 mm depth of water sorption in 1000 square meter of surface area
At temperature-20°C, Relative humidity (RH) = 75%	13.5 kg in 16 hours
At temperature-20°C, Relative humidity (RH) = 40%	8 kg in 16 hours
Water vapor molecular flow	
Via capillaries in seals	1-5 gm per year
Via loose gaskets	30 -40 gm per year
Viscous flow of air: core and coil covered with oil	
Adequate sealing	0.6 kg per year
Insufficient sealing	15 gm in a day
Operation with open breathing conservator, having no any heat recovery system	1.5 kg per year
Operation with open breathing conservator, when transformer assemble with heat recovery system and suffer from rapid temperature change	16 kg per year
Insufficient sealing with rain water present	200 gm in an hour as free (liquid) water

The amount of water from the ambient air goes through breather depends upon the operating mode of the transformer. The grid transformer has the cyclic load and heat recovery system. Due to cyclic temperature drop, it suffers from the high moisture contamination that leads to around 16 kg/annum water contamination through the breather inside the transformer [25]. Additional sources of water contaminations are the leaks such as the top seal of draw-lead bushings, leakage between the main tank and the coolers in case of forced oil circulation systems and the seals in explosion vents. Furanic compound and water is the by-product of

aging of the cellulose material due to the molecular chain scissions. Each chain scission produces approximately 0.2 % water by weight. Water contamination is also due to the chemical reaction such as pyrolysis, hydrolysis in the cellulose and oxidation of oil during the aging of the oil-insulation systems. Fig. 2.8 indicates the sources of moisture contamination in the transformers in service. Water is also generated due to the aging of the hot winding [26-29]. Water migrates from the hot insulation area to the colder insulation structure between the windings through the oil and during this process, it accumulates the moisture.

2.6. Moisture Determination Methods in Transformers

2.6.1. Karl Fischer Titration Method

Karl Fischer Titration (KFT) technique is used for the measurement of trace level of moisture in the oil.In this method a reagent which consists of sulphur dioxide, iodine, a base and a solvent such as alcohol is used. The measurement accuracy of the moisture depends upon the reaction of the reagent with the water. Volumetric or coulometric titration systems is used in this method and the more details are available in [30-31]. Small level of moisture content such as 1-2 ppm is measured using the automatic coulometric Karl Fischer titration technique. This titration method was developed by the German chemist (Karl Fischer) in 1935. In titration method, a reagent of predetermined concentration (called titre) is added to an unidentified substance until the concentrations are balanced. In volumetric titration, the added volume is measured and demanded value (water content) is calculated by stoichiometric equation. This method is applicable for dry insulation oil and its sensitivity is approximately 10εgof water. In coulometric titration iodine reagent is liberated from the generator electrode which eliminates the requirement of standardization. The stoichiometric equation representing thereactions of the titration vessel is given by (2.1). The detection edge of coulometric titration comes down toa few εg of water.

$$2H_2O + SO_2 + I_2 \rightarrow H_2SO_4 + 2HI \qquad (2.1)$$

The moisture relative to weight C_w is calculated by (2.2), which is the ratio of the measured water mass to the mass of dry and oil free paper m_p multiplied with 100%. Moisture access into the system is defined by the drift D (εg/min) and the moisture inside the emptysample vessel (blind value $m_{H2O,B}$ in εg) must be subtracted from the total moisture m_{H2O}.

$$C_w = \frac{m_{H2O} - t*D - m_{H2O,B}}{m_p} * 100\% \qquad (2.2)$$

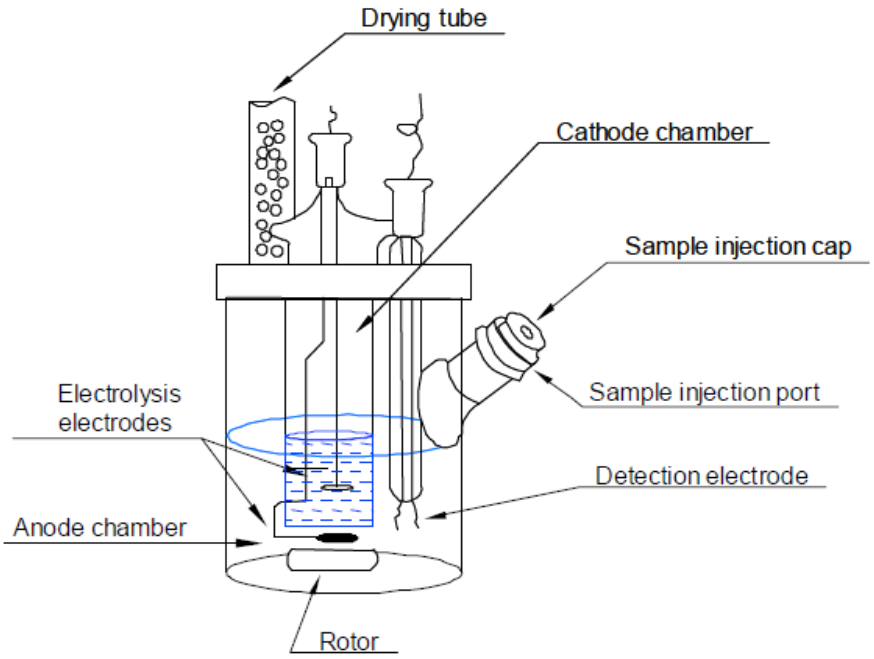

Fig. 2.9 Electrolysis cell for coulometric Karl Fischer titration.

There are three different methods to bring the material moisture into the reaction vessel as shown in Fig. 2.9 [30]. In the first method, an option for the injection of the material directly into the reaction vessel is available. This technique pollutes the reagent. The side reactions of ageing products or inhibitors with the reagent are possible. Secondly, the water can be dissolved in another medium, e.g. methanol. This is applicable for the samples of cellulose. The water will be extracted out of the cellulose when the sample will be immersed into methanol. The methanol and water is injected inside the reaction vessel. In the third method, the sample is heated in an external oven and gas stream with water vapour is taken into the reaction vessel. The advantage of this process is that reaction vessel is left clean. A drawback of this system is the blank value of the heating vessel and the gas stream, which reduces the sensitivity, compared to the direct injection method.

2.6.1.1 Merits and Demerits with the Karl Fischer Titration Method

The important features of the Karl Fischer titration technique are

- high accuracy and precision
- the response is selective for water only
- the need of quality of sample is very less
- the preparation of sample is very simple
- the period of analysis is short
- the measuring range is wide(1ppm to 100%)
- appropriateness for analysing the moisture content in solid, liquid and gases

- free from of existence of other volatile materials
- accurate for automation.
- Linearity - single-point calibration, no calibration curves is required

However, the demerits of this method are

- moisture ingress from atmosphere air during the transportation and sample preparation
- water binds with the cellulose through chemical bonds of different strength. It is uncertain, if the thermal energy releases all the water or not
- The results of moisture in the oil are different in direct injection and heating techniques. This is due to the aging of oil
- the instrument is not portable and is costly
- the instrument is not suitable for online measurement. It can be used for the offline measurement only

2.6.2 Moisture Determination by Equilibrium

This is another technique used to determine the moisture content in the sample of oil.

The temperature transient disturbs the steady state of moisture during the operation of the transformer that leads to the transfer of moisture. Transformer oil is hydrophobic and the insulating paper is hydrophilic in nature. The value of moisture in pressboard is 0.5-5%. The moisture content in oil at room temperature in saturation level is around 50 ppm. Therefore, the moisture content in pressboard is very high. As the electric load of the transformer increases, the heat dissipated by the winding of the transformer also increases. Consequently, the water is discharged by the insulation paper and moves into the transformer oil. The solubility of the water in aged oil increases with increase in temperature and it is around 800% in the range of 20^0C to 80^0C. As the transformer-winding cool down due to the cyclic variation of the power demand, the moisture available in the oil migrates slowly into the insulation paper. However, some amount of moisture remains in oil. It causes super saturation of the oil and formation of free water in the oil. The direction of the water mass flowed between the oil and paper depends upon its equilibrium moisture content. This equilibrium moisture depends upon the temperature as shown in Fig. 2.10 [38]. The steady state is reached when themoisture inside the pressboard diffuses to the surface to set up a uniform moisture distribution [32-37]. The time taken to reach the moisture equilibrium between the paper and theoil depends upon the rate of diffusion of moisture through the oil and paper. The diffusion constant of water in oil and paper is shown in Table 2.6 [38].

Table 2.6

Diffusion coefficients of water in transformer oil and paper.

Diffusion Coefficient	Symbol	Value at 15^{0}C	Value at 70^{0}C
In oil	D_o	$1.3 * 10^{-11}$ m^2/s	$1.1 * 10^{-10}$ m^2/s
In pressboard	D_p	$6.7 * 10^{-14}$ m^2/s	$6.0 * 10^{-12}$ m^2/s

Practically, the moisture equilibrium between the oil and the paper never occurs but a small change in temperature significantly changes the moisture content in the oil and the paper. To predict these changes, isotherms showing the relationship between the water content present in the oil and paper might be used. These isotherms are obtained after the combination of sorption curves for oil and paper. This method is used for the determination of the moisture equilibrium curves between the oil and paper. Moisture content of aged insulation paper can be obtained from the measurement of moisture from the oil when the transformer is in equilibrium operation. A significance of temperature on moisture measurement is reported [39-40].

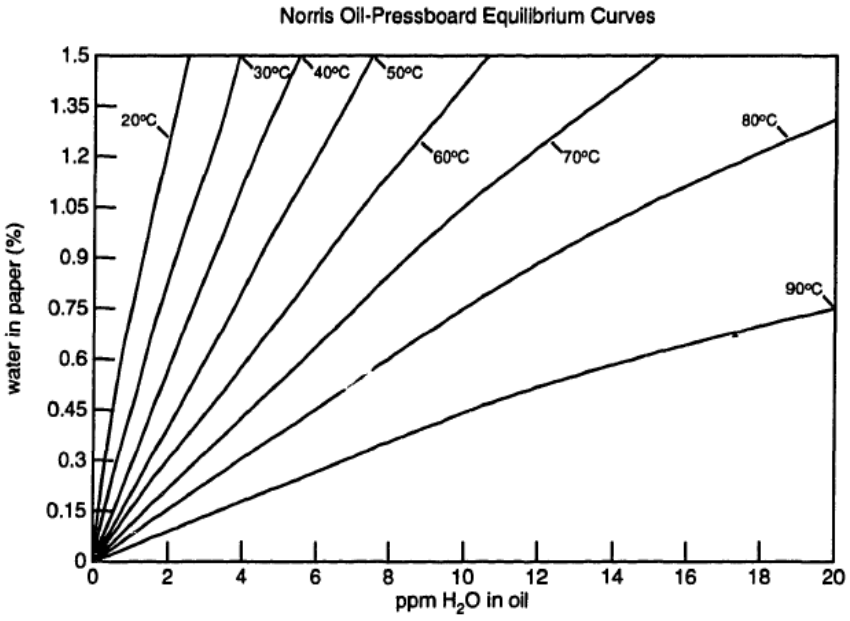

Fig. 2.10 Equilibrium relationship between the moisture content of transformer oil and pressboard for temperatures ranging from 20^{0}C to 90^{0}C.

2.7 Sensor based Condition Monitoring of Transformer

The blackout of the transformer has major impact on connected electrical system. Therefore, it is very necessary to assure precise assessment of the transformer condition.

For the maximum reliability and accessibility non-invasive tests is utilized to diagnose the integrity of the transformer. There is a need to know the internal condition for its growing average age of use. The on and off line technique is utilized for its monitoring. The on-line monitoring is used continuously for recording the relevant stresses at various points, which effect the life time of the transformer. Faults occurs in the transformer will be detected early if the information of these data collected automatically. Different types of measurable variables are collected from the on-line monitoring. The entire spectrum of the data is not useful. Therefore, sensors are utilized for the transformer depending on its conditions.

For the sensor-based condition monitoring, the types of sensors used in a 400 kV power transformer are:

(1) PT100 used for the measurement of top oil temperature and ambient temperature

(2) C.T. used for the measurement of load current (single phase)

(3) measurement of voltage next to measurement tap of bushing (three phase)

(4) measurement of pressure of the oil of bushing

(5) sensor designed for measurement of oil humidity

(6) sensor designed for measurement of gas-in-oil content

(7) tap changer position

(8) power consumed by motor drive

(9) digital inputs meant for switching status of fans and pumps

The standardized web browser technology can easily be used to utilizing the advantages of modern IT-technology, the sharing of information about the condition of the equipment. Optical sensor is used for the condition monitoring of the power transformer. It detects the various parameter of the oil like moisture and partial discharge occurs due to the breakdown of the oil. Different types of chemical sensors are used for the detection of different types gases generated through the degradation of the insulation system in power transformer. Major challenges related to the sensing of the gases in dissolved gas analysis (DGA) have been discussed. Some of the important sensors which can be used for the DGA technique are acetylene sensor, methane sensor, ethane sensor, ethylene sensor, 2FAL detection, etc [41-44].

2.8. Humidity Sensor used for the Detection of Moisture in Transformer

Optical fiber sensor is used for the measurement of moisture in the transformer oil. An instrumentation system using optical fiber sensor, temperature sensor and microcontroller was designed for monitoring the moisture in transformer oil. ANN trained algorithm is also used for the detection of moisture [45].

Measurement of humidity is done by the optical methods. The moisture concentration depends upon the amplitude, frequency and polarization of the optical signal. Due to the presence of humidity, the dielectric constant of the medium, where the signal propagates changes and its impact is observed on the signal parameters. It is fabricated by using a hydrophilic gel (agarose) on the thinner zone of a biconically tapered single mode optical fiber [46]. The refractive index of the gel changes with humidity. In the range of 30- 80% RH, a change of 6.5 dB in the transmitted optical power has been found. The material of the sensor shows excellent reproducibility and low hysteresis. Similar types of sensor structures, where change in refractive index with humidity has been found in the literature [47-48]. Ceramic sensor prepared through the oregano metallic precursor by sol gel process is used for the measurement of moisture in transformer oil. The designed sensor measures the ppm level of moisture in the oil. The response of the sensor was found to be almost linear in the trace level of measurement of moisture in oil [49]. A scheme for on line measurement of moisture in the transformer oil using ceramic humidity sensor was developed. The sensor is parallel plate capacitive sensor having thin film of ɔ- Al_2O_3 for moisture. The electrical characteristic of the sensor with the change in temperature and moisture content in oil are also studied [50]. An instrumentation system using polymer optical fiber as a moisture sensor for the measurement of moisture in transformer oil is designed. The developed system has been used for the online condition monitoring of the transformer [51-52]. Harley CT-8804 is a thin film based moisture sensor. It is used for online measurement of relative humidity of transformer oil. It measure humidity in the range of 0 to 100% RH. Thin film platinum RTD is used for the measurement of temperature in the designed instrumentation system. The moisture solubility of the oil is determined with the help of linear relation of relative humidity of the oil and moisture content in the oil. Various types of chemical and electrical methods are explained for the diagnosis of transformer [53]. The thin film of micro dielectrometry is used for the moisture measurement in transformer oil. The dielectric constant of the layer of Plasma with coated bromobenzene on interdgitated electrode changed after the absortion of moisture of transformer oil. The phase and gain of the chip changes with the variation of the moisture in oil [54]. The dielectric constant of the material placed between the electrode changes due to variation of moisture in the oil. The response of the sensor is indicated by frequency signal [55].Optical fiber sensor is used for the detection of moisture inside the transformer insulation. The response of the sensor is found to be independent of electric field generated in the winding of the transformer. The sensor is placed in the area of the winding [56].

Polymethyl methacrylate (PMMA) based optical fiber bragg grating is used for the measurement of moisture in transformer oil. The refractive wavelength of the gratting depends upon the refractive index. The output of the sensor is observed interms of change of its refractive wavelength with the variation of the moisture in oil [57]. A mathematical model for measuring the moisture in the transformer oil has been developed and validated experimentally. Mathematical model is developed considering the phenomena of moisture release from the insulator to the oil when the transformer is loaded. Temperature and moisture in the oil are considered as the variable of the model. Experimental results were found to be consistent with the result of the model [58]. Three-wavelength interdigitated sensor has been used for the measurement of moisture in pressboard of transformer. The depth of penetration of electric field depends upon the wavelength. Sensor can be used for the measurement of dielectric loss of pressboard. The diffusion coefficient of moisture in pressboard is estimated with the help of experimental data [60]. A comparison table of various techniques of moisture measurement in oil is given in table 2.7.

2.8.1 Comparison of Different Techniques used for the Moisture Determination in Oil

Table 2.7

Comparison of different techniques used for the moisture determination in oil

Prior art	Moisture measurement technique	Merits	Demerits
30-31	Karl Fischer Titration Method	• better precision and accuracy • moisture sensitive response only • less amount of sample is needed • simple process of the sample preparation • the need of short period for analysis	• the instrument is costly and not portable • it is offline method of testing • moistureingress from atmosphere air during the transportation and sample preparation

32-37	Moisture Determination by Equilibrium	• moisture is measured in solid insulator • moisture in oil is measured using Karl Fischer method • moisture in insulator is measured via equilibrium diagrams	• equilibrium conditions are rarely achieved (due to temperature variations) • equilibrium depends on moisture solubility in oil and moisture adsorption capacity of cellulose • One obtains different results using different diagrams from the literature
45-46, 57	Optical Fiber Sensor	• Poly methyl methacrylate based optical ýber bragg grating is used for the measurement of small amount of moisture in oil • An instrumentation system using polymer optical fiber sensor was developed for measuring moisture from 15 ppm to 65 ppm • refractive index of oil changes as the moisture content changes • The wavelength of the optical ýber bragg grating is very sensitive towards the changes in moisture in the oil	• Response time of the polymer optical sensor is very high. It is approximately 200 min. • Effect of the temperature on the sensor performance was not tested • Response of the sensor due to polymer decomposition degrades. Drift in the response of the sensor with time due to aging of the polymer was not tested

49	Capacitive Type Humidity Sensor	• Parallel and cylindrical type capacitive sensor is used for the moisture detection • Sensor was found to be sensitive from 400 ppm to 800 ppm	• Designed sensor is sensitive in highly contaminated oil • Response time of the sensor was not discussed • Effect of temperature on sensor response was not discussed
58	Analytical Method Based on Mathematical Model	• A mathematical model for detecting moisture in solid insulator was developed • Effect of temperature in model was considered as one input • Model was validated with the experimental data	• Aging effect of insulator in the model was not considered

2.9 Capacitive Humidity Sensors

There are various types of materials, which are used as the moisture sensing film such as porous silicon, ceramic and polymers [61-62]. Polymer thin film based capacitive humidity sensorwas presented in many papers [63-65]. Polymide film based sensor for monitoring humidity level of anodically bonded hermetic micropackages has been developed [62]. The capacitive humidity sensor based on polymide film columns and integrated with polysilicon heater has been developed in literature [64]. The polymide based humidity sensor has linear response, high sensitivity, and low power dissipation. It is compatible with CMOS fabrication, which allows the monolithic integration of the sensors with the readout circuitry [65]. Humidity sensor was made using surface acoustic wave (SAW) resonator. Resonator is covered with photolithographically patterned poly vinyl alcohol (PVA) film [66]. An optical fiber Fabry-Perot (FP) is used for the measurement of relative humidity (RH).The fabryperot is developed through the splicing the short length of hollow silica tube in a single mode fiber. A coating of polyvinylidene fluoride (PVDF) on fiber has been done to work as a mirror [67].

Polymer film based sensor has some disadvantages such as hysteresis, low working temperature, large response and recovery time, durability problem in harsh environment and long-term drift [68-70]. It cannot be used for the measurement of high humidity. The characteristics of these materials have been improved in the recent research and polymer based humidity sensors are commercially available [71]. It is useful for measuring RH level of humidity and continuous effort is continued to improve its undesirable characteristics [72]. Another humidity sensitive material is porous silicon. It is formed by galvanic etching of silicon in acid medium [73]. Porous silicon based capacitive humidity sensor with integrated refresh resistor was designed [74]. Humidity response of the porous silicon sensor depends upon its electrochemical formation parameter. Sensor was found to be highly stable at elevated temperature. The response of the sensor was found to be non-linear and it is the major disadvantage of the porous silicon based sensor. Film is also highly unstable. Oxidized porous silicon is also used for the humidity measurement [75]. In some literature, it is reported that the porous silicon is capable for detecting the trace moisture level. The etching of the silicon substrate forms porous silicon. T. Islam has done the measurement of humidity in ppmv level using porous silicon based humidity sensor [76-78]. Different types of ceramic materials also used for the humidity detection such as WO_3, $MnWO_4$, Fe_2O_3, TiO_2, Al_2O_3 and SnO_2 [79]. Trace level of moisture detection using solid state devices is only done through the porous silicon, Al_2O_3 and P_2O_5. The response of the Al_2O_3 based humidity sensor is mostly temperature independent in all range of humidity. It is found to be suitable for the humidity measurement application in the industry. The process of fabrication of nanostructure to enhance the surface activity is very simple and well established [80]. Different methods are used for the fabrication of the humidity sensor using Al_2O_3 ceramic material [81-84]. For the humidity measurement, transparent Al_2O_3 is generally used due to ease of its fabrication process and low-cost. The amorphous ɔ-$A1_2O_3$ is used as moisture sensing film because of its very high surface area [85-86].Pore morphology has important role in improving the sensitivity of the sensor for detection of wide range of humidity [87].

2.10 Humidity Sensor based on Anodic Alumina

First time in 1950, it was found that amorphous anodic aluminum oxide (AAO) has humidity sensitive property. In 1978, the researchers have investigated it and form its regular micro structure.The layer of Al_2O_3 through the anodization of pure Al metal surface for the measurement of humidity was formed in 1953 [88]. M.G. Kovac et al. fabricated the porous alumina based moisture sensor through the anodization by H_2SO_4 solution in 1978. Sensor

was found to be suitable for measuring the low level humidity and can be used to detect the absolute humidity [89]. Feiyue Li et. alreported the hexagonal structure of domain in anodic alumina films prepared by the repeated anodization and stripping of the porous oxide. The size of the domain is the function of anodization time and temperature of the electrolyte. The density of the pores decreases as the anodization time increases. The nucleation of the pore before the anodization is an important parameter and has been achieved by electropolishing. The pore starts growing as the electric field at the pore bottoms increases and oxides dissolve in the acid locally [90]. Azadeh Nazemi et. al established the condition for anodization such as its voltage, concentration of electrolyte and the time of the first electrolysis for the development of porous anodic alumina oxide tempelate [91]. Lujun Yao et. aldeigned the porous anodized alumina based highly sensitive humidity sensor. Anodization was done using high-field for shorter time. The sensitivity of the sensor was adjusted through the uniform distribution of anion impurities on the pore wall [92]. Alaa M. Abd-Elnaiem et. aldeveloped the porous alumina film via anodization of aluminium (Al) deposited on SiO_2/Si substrate. Anodization of Al was explored using different electrolytes such as H_2SO_4 (1M), Oxalic acid (0.3M), Phosphoric acid (0.75M). The effect of anodization parameters on the morphology of the pores has been discussed [93]. Jihun Oh et. alreported the role of electric field in the pore formation during the aluminium (Al) anodization. The electric-field enhanced the dissolution rate at the base of the pores. Based on the experimental evidence a cellular- like model for steady-state growth of anodic oxide has been proposed [94]. Highly sensitive parallel plate capacitive humidity sensor was fabricated using the anodic alumina. Thin film of aluminium oxide was grown through the anodization of aluminium sheet in 0.3 M oxalic acid at different excitation voltage. The designed sensor was found to be sensitive in the range of 20 to 80% RH. Electrical equivalent circuit of the sensor was proposed and modelling of its capacitive response was studied [95]. Parallel plate capacitive humidity sensor using anodic aluminium oxide as the thin film sensing layer was designed. Parallel plate of the sensor was made by tantalum. The effect of pore morphology on the sensitivity of the designed sensor was analysed. The sensor was found to be sensitive in the range of 20 to 80% RH [96]. Humidity sensor using anodic aluminium oxide grown on silicon substrate was designed . The designed sensor was having interdigitated electrode on the oxide thin film made by vacuum evaporation deposition method. The capacitive response of the sensor is linear in the range of 25 to 95% RH [97]. Anodic aluminium oxide based humidity sensor with temperature measuring capacity was designed. Sensor was prepared using electrochemical oxidation and semiconductor processing steps. The designed p-n junction below the capacitive structure is

used to heat the sensor. The designed sensor has drift free response [98]. Anodic aluminium oxide grown on flexible paper substrate based thin film for measurement of humidity was designed. Highly ordered nano porous structure of oxide was developed on the substrate. Phasphoric acid was used for the anodization. The electrical characteristics of the sensor was analysed using the 4192A LF network analyser. The capacitive response of the sensor was analysed with respect to the moisture concentration and frequency [99]. A humidity sensor compatible with the wireless sensor network was designed. The sensing film of the sensor was grown through the anodization of aluminium sheet under anodic bias. Two different types of the sensor structure were made on the silicon substrate using semiconductor processing and oxidation process. Paladinum and gold mesh are used as the electrode in the designed sensor [100]. The capacitive response of the anodic aluminium oxide based humidity sensor was improved using the magnetic effect produced by NbFeB magnet. The response was found linear from low to high range of humidity (10 to 90% RH) due to orderly arrangement of water molecule in the pore of aluminates in the presence of magnetic field. Due to the presence of magnetic field in the operation of humidity sensor, the linearity and sensitivity of the sensor was improved [101]. The effect of rectangular spiral type and interdigitated electrode on anodic aluminium oxide based humidity sensor was studied. The sensitivity of the designed sensor is better in rectangular spiral type electrode if the hysteresis and linearity is improved by heating. The sensitivity of the sensor is better in the porous electrode than nonporous electrode [102]. The properties of the anodic aluminium oxide for sensing and MEMS devices have been explained. The morphology of the pore of the grown oxide through the electrochemical oxidation was controlled with the selection of the types and molar concentration of electrolytes [103]. The change in the impedance due to the moisture absortion in the porous anodic aluminium oxide was studied. The electrical property of the porous alumina changes in the atmospheric environment. The electrical properties were explained with the help of equivalent circuit of physical structure of the porous alumina. The resistive components of the alumina found to be decreases exponentially with the humidity [104]. The surface conductivity of the Al_2O_3 sensor varied with the humidity level. In presence of moisture, the charge transport in anodic alumina takes place through two mechanisms. At low humidity, photon induced electron tunnelling between donor water sites occurs and at high humidity, photonic conduction dominates. The physical model of surface conduction has been developed using energy band concepts [105]. The effect of current density in the preparation of anodic Al_2O_3 for moisture sensing was explained. Thin film of anodic aluminium oxide grown through the anodization process carried out at lower current

density shows the negligible response at low humidity and the steep rise in response at high humidity. The response at low humidity improved if film developed through the high current density [106]. The process of fast anodization of Al sheet in two steps was explained. The anodization was carried out at 150 V in 0.3 M oxalic acid for 10 minutes in the first step and then 3 minutes for the second step. The effects of temperature and anodization time in pore distribution of grown anodic aluminium oxide were studied. Characterization of the anodized sample was carried out using XRD and FESEM [107]. High density anodic porous alumina based MIM capacitor has been developed using the electrochemical anodization of Al sheet on Si. The designed capacitor was found highly thermally stable. It can be used as a passive component in the analog circuits [108-110]. Capacitive humidity sensor using thin film of aluminates was designed. The developed sensor was found to be highly sensitive in the range of 10 to 97% RH. The developed sensor was used for condition monitoring of high voltage transformer [109-110]. Moisture in the transformer oil is measured in terms of parts per million (ppm). Its range varies between 5 ppm to 500 ppm. It depends upon the quality of the insulation used in the transformer. The designed sensor through the sol-gel method is suitable for the low level of moisture in the range of 5 ppm to 200 ppm. Breather is another source of water contamination in the transformer. The level of humidity in the breather depends upon the saturation level of silica gel, where the humidity level varies between 5- to 90% RH. The designed sensor using electrochemical method is suitable for the condition monitoring of breather.

2.11 Drift in Humidity Sensor

The long ï term drift of the polymer based humidity sensor was investigated in hot temperature and humid atmosphere. The atmospheric temperature and humidity was 40ŮC and 90% RH respectively. The reason of the drift in the sensor is the increase in water sorption ability of the sensing polymer with aging due to the presence of oxygen containing group at its surface. Morphological change in the sensing film is also responsible for drift in the humidity sensor output [111].The drift of the polymer humidity sensor was analysed in the range of 5 to 95% RH. The average drift in the sensor was found to be 5% RH [112].

The impact of the thickness of the polymer humidity sensor on its drift phenomena was also investigated. Due to the high water sorption capability of the polymer, the sensing film swells. The sensitivity of the sensor increases due to the aging as the water sorption capability increases with passes of time [113]. Drift of the resistive humidity sensor was analyzed in [114]. The designed sensor was used to monitor the moisture in clay loam soil. The sensor

was made using the plaster of paris material. The improved model of the sensor with drift compensation was proposed. Without compensation, the drift was found proportional to the sensitivity. The estimated drift with time was found lower in bare sensor than that of apvccasting based sensor [114]. Micro-centiliver based humidity sensor was reported. Polyamide was used as moisture sensing film on the silicon suspended on the glass substrate, which act as a movable plate of the capacitor. A thin film of platinum resistor is used for the compensation of the drift, which occurs at high humidity. The response of the sensor was highly sensitive due to low stiffness and large surface area of the cantilever [115]. A polyamide based humidity sensor was reported using inkjet-printing process. The sensor had silver interdigitated electrode made on the film of the polyamide. The sensing area of the sensor was optimized using the simulation study. Drift in the thermal coefficient of the sensor was minor with respect to operating frequency of the sensor. The sensor showed minor thermal drift. So, it had high thermal stability [116]. The qualities of the hygrometers depend upon the quality of the humidity sensor used inside to fabricate the meter. Long-term drift is an important issue for most of the humidity sensors, which work on moisture adsorption and desertion principle. This phenomenon is mostly observed for the sensor which uses porious material as moisture adsorption film for high sensitivity [117]. Long-term stability test of aluminium oxide humidity sensor was performed for thirty days in the environment of 75% RH. The operating range of the sensor was 10- 90% RH. Drift in the sensor response was found minor below 45% RH but it was approximately large around15% above 90% RH [117]. Study of drift in the response of the porous silicon based humidity sensor was explained. Sensor is highly stable in the range of 20 to 98% RH. To understand the aging phenomena in sensor, it was stored in open atmosphere at 75% RH for 10 days. Approximately 49% of drift was found in response at 98% RH. An artificial neural network based model was developed and hardware implemented to compensate the drift [118-119]. The porous silicon is an excellent material for sensing but it suffers from the stability problem that leads to change its morphologies and causing degradation in the response [120]. The stability of the porous silicon was improved by its carbonization [121]. Drift analysis of polymer based humidity sensor was studied in open environment for 200 days. The sensor output was highly stable in the range of 40 to 98% RH. Approximately 4% and 5% drift was found at60% and 90% RH respectively [122].The electrical equivalent circuit of an aged aluminium oxide sensor prepared through the electrochemical anodization was reported. Simulation of the response of the aged sensor based on the electrical equivalent circuit was performed. The possible reason of the aging of the sensor was explained. However, the model was not verified experimentally

[123]. Due to gradual change in porosity, the surface area of the film decreases [124]. Long ï term drift is the major problem of aluminium oxide sensor. The sensitivity of the sensor decreases with time. Due to drift, the sensitivity of the sensor decreases due to the pore widening, lateral diffusion of the moisture inside the wall of the pore. The base value of the sensor decreases due to the formation of the hydrated alumina inside the wall of the pore [125-127]. To solve the drift problem different types of deposition techniques such as anodic spark deposition and reactively evaporation have been used [128-130]. The drift is improved by dipping the alumina film in some ion solution or treating it in boiling water. However, the drift cannot be completely removed from the sensor output. Even today, the commercial alumina moisture sensors are to be recalibrate in every six months. The drift due to morphology degradation in high humidity can be controlled by storing the moisture sensor in drying agent [131]. All the methods for film deposition such as electron beam, sputtering, evaporation, spray pyrolysis and reactive evaporation suffers from the problem of degradation. Heat treatment of alumina at400°C was done for improving the stability of anodized Al_2O_3 sensors. Porous α-Al_2O_3 phase was obtained by reactive evaporation method. This phase is found to be very sensitive and stable for the moisture detection. In this method, Al is evaporated at temperature (800ï 1300^oC) and particle becomes oxidized before depositing on the substrate [132]. Drift in the response of aluminium oxide capacitive sensor used for the measurement of trace level of moisture was found. The operating range of the sensor was 1 to 15 ppm moisture. For the estimation of the drift in the metal oxide sensor, it was stored in the environment of 15 ppm moisture for 274 hours. The estimated drift at 2 ppm moisture was found 12% [133]. Drift analysis of polyamide based capacitive humidity sensor has been studied at 85% RH for thirteen days. Total number of samples used for the experimental verification was thirteen. The operating range of sensor was 10 to 90% RH. The significant drift in the operating range of sensor was found to be 1-20% [134].

2.12. Modelling of Humidity Sensor

Modelling for the prediction of the response of the capacitive humidity sensor has been developed. The approach of modelling is based on the electrostatic and diffusion process. The developed model was validated with the experimental results of the sensor and finite element simulation. The model also predicts the uncertainty of the fabrication process [135]. A model for simulating the response of polymide based humidity senor was developed. It was developed considering the effect of vapour diffusivity, film porosity, Fickôs law and Looyenga's empirical equation. The response of the model was validated with the

experimental results of the sensor. The variation in the response time found to be minor due to the environmental effect [136]. A model for the transient response of the sensor for measuring humidity in the air was developed. It was verified experimentally by the step humidity variation. The model was analysed through the diffusion process in the polymer film [137]. Modelling of the drift in polymer sensor considering the effect of temperature was indicated with the help of Arrhenius equation. Experimental validation of the model was not reported [138]. For predicting the reliability of the sensor, a model combining the effect of soft failure with self recovery was developed. Conditional probability was utilized to understand the effect of self recovery on degradation of the sensor. The model of reliability test was verified with the experimental data of humidity sensor [139]. Modelling of ZnO based capacitive humidity sensor was studied in [140]. The sensing mechanism was explained with the help of an equivalent circuit model. COMSOL multi physics software was used for the simulation study. There was a close agreement between the simulated and experimental results [140]. The modelling of the sorption humidity sensor made by ink-jet printing technology was also presented. Modelling is based on the principle of RC transmission line distributed parameters. The developed theoretical model was validated with the comparison of the measured empirical parameters of the sensor in different frequency range. The number of RC distributed parameters should not be limited for validating the experimental results of the sensors [141]. A dynamic model based on the principle of diffusion for measuring the concentration of water on the surface of sensor by measuring the water content in the polymer of the sensor was developed. The state space model of the sensor variable has been developed. The state space model was converted into the transfer function. The time response of the model was used for the estimation of moisture. The %RH on the surface of the sensor was estimated through the calibration process [142]. A model to improve the non-linearity and cross sensitivity of the capacitive humidity sensor was developed with the help of ANN in matlab environment. In the model, variation in the humidity is shown by the variation of capacity, which is the passive magnitude and realized by switch capacitor circuit (SCC). Three different types of model represent the smart sensor: capacity/voltage converter, ANN model and model inverse INV ï ANN [143]. A model for the response of impedance of humidity senor was developed. The developed model consists of two resistors and two constant phase element. Effect of humidity on the selection of model parameters was studied [144]. A model for the correction of temperature effect and improvement in the non - linearity in the response was developed. The design of the smart humidity sensor incorporating the artificial intelligence model was realised. The response of the model was simulated [145]. Modelling of four-electrodes

humidity sensor through the finite element analysis (FEA) for monitoring the humidity in natural gas transportation line was studied [146]. An analytical model changing the capacitive response of the sensor due to the change in dielectric constant of the film after absorption of the moisture was developed. The response of the model was validated with the response obtained through the FEM software [147]. With the help of theoretical model of Looyenga and Shibata, the effect of moisture and temperature on change in dielectric constant of the polymer film was studied. The proposed model was used to predict the capacitive response of the humidity sensor. The effect of sensor designed parameters on its response was studied. The design of the sensor was optimized with the help of simulation results [148]. The response of the fiber bragg grating (FBG) humidity sensor was simulated through the COMSOL multiphysics simulation tools. Light propagation and reflecting wavelength were simulated using Snell's and Fresnel's laws [149]. Electrical equivalent circuit of ceramic humidity sensor was presented. Impedance of equivalent circuit was determined. The equivalent circuit consist of two RC parallel components in series with two constant phase elements. The simulation of cole-cole and bode plots of titania thick film humidity sensor was presented in [150]. An electrical equivalent circuit of the sensor was developed. The impedance value of the sensor consists of three different impedances which depends on its the chemical and physical properties. Three different impedances are (i) temperature dependent ohmic resistance due to the electronic conductance (ii) constant phase element in parallel with ohmic resistance due to the ionic pathway depending upon the concentration of humidity on the sensor surface and (iii) the capacitance of the double layer formed by combination of electrode and sensing film and represented as the second constant phase element in series with the first constant phase element [151]. The electrical equivalent circuit of ceramic capacitive humidity sensor has been developed. The electrical circuit was simulated experimentally [152]. Drift modelling of the metal oxide gas sensor was done experimentally. However, the electrical equivalent circuit of the drift model was reported. A significant drift in the response with time was found [153]. Reliability modelling of humidity sensor was proposed. Model was developed with the help of conditional probability [154].

It has been observed through literature survey that mainly two types of the capacitive structures such as interdigitated electrode (IDT) and the parallel plate electrode are used for humidity over wide dynamic range. The interdigitated electrodes are widely used for percentage relative humidity measurement. There is a very limited work reported for low moisture measurement below 1000 ppm. For RH humidity measured, the hydrophilic sensing

film is either deposited on the IDT electrode or the IDT electrode is deposited on the sensing film. The parallel plate capacitive structure where the sensing film is sandwiched between the metal pales are reported to measure humidity over wide dynamic range from %RH to low ppm. As written above, mainly three types of sensing materials are used for humidity sensing such as polymer, porous silicon and the metal oxide thin film. Polymer and porous silicon are reported for %RH level humidity sensing. Both the materials are not suitable for chemical harsh environment like transformer. Polymer and porous silicon sensors rarely reported for humidity measurement in transformer. Metal oxides are suitable for humidity sensing over wide dynamic range and these materials are relatively chemical inert and have high temperature stability. Among different oxides, nanostructure alumina film is very much suitable for humidity sensing. Nanostructure of alumina having different pore morphology can be made by different methods like electrochemical anodization, sol-gel method or spray pyrolysis technique. Desirable pore morphology of the nanostructure of the sensing film can be achieved easily by the anodization and sol-gel method. Preparation of nanostructure of the alumina by the sol-gel method requires high temperature sintering of the film above 400ºC. In this work, the parallel plate capacitive sensors are fabricated using alumina sensing film by anodization and sol-gel method.

2.13 Interface Electronics for Capacitive Sensor

To develop an electronic test system to measure moisture using the designed sensor, it should be interfaced with an electronics circuit. For the capacitive humidity sensor, the sensor should be interfaced with the properly designed electronics circuit. The output of the interfacing circuit should be an electrical signal in the form of change in voltage amplitude, frequency or the time of the output signal. It is desirable that output should be in the form which can be directly interfaced with digital devices like microcontroller for further processing like mathematical manipulation to compensate non-linearity , temperature error etc. Ultimately, the signal in the calibrated form will be displayed, stored and transmitted if necessary. The output signal frequency by the sensor is too noisy and too weak, which also contains unwanted components. The output of the sensor is not compatible for data acquisition because it contains an incorrect format. For processing the signal, there is a need of matching device. The generated signal from the sensor is conditioned previously to feed into the processing device (a load) [155-156]. Voltage or current signal is used as the input for the load. The signal conditional circuit is used to format the signal generated through the sensor. Fig. 2.12 shows the stimulus acting on a sensor that is coupled to a load through an interface circuit.

For the sake of an effective interface between the sensor and the load, the interface circuit must be a dependable slave of two masters that is the sensor and the load device. Its input characteristics must be matched with the output characteristics of the sensor and its output must be such that it can be interfaced with the load. For the measurement of capacitance value, a signal conditioning circuit is required to convert the capacitance change into the frequency [157], voltage [158-160], current [161] or pulse-width [162-163], etc. Depending on the output signals, different topologies of readout circuits can be employed [164-166]. Different types of conversion techniques used to enhance various design factors in capacitive sensing systems, such as resolution, dynamic range, power and linearity, etc.

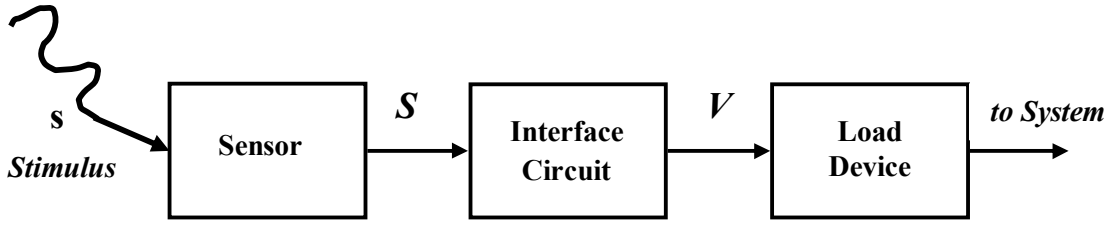

Fig. 2.11 Interface circuit matches the signal formats of a sensor and a load device.

Some common interfacing circuits are

- Opamp based interfacing circuit for a capacitive sensor

  An inverting opmap based interface circuit was utilized to interface the porous silicon/porous alumina/polymer humidity sensor. The amplitude or the phase angle of the output voltage signal of the inverting conýguration varies according to the variables [187-188].

- Oscillator based transformer ratio arm bridge for interfacing the capacitive sensor

  For the measurement of small change in capacitance, the transformer bridge based AC bridge method is used. But it suffers from the limited range of capacitance measurement. For the measurement of wide range of capacitance of the sensor, oscillator-based interfacing circuit is used. With the combination of both transformer bridge-based AC bridge method and oscillator-based method, more accurate wide range of capacitance of the sensor was measured [167].

- A Microcontroller compatible oscillator based active bridge circuit for interfacing capacitive sensors. It is the combination of the properties of the capacitance to frequency convertor and the capacitive ratio arm bridge technique with an output signal. The output signal is compatible to the microcontroller [163, 184ï 186]. The circuit offers all the features of the TRA bridge, including the CMOS compatibility.

- The circuit requires few hardware components and is easy to integrate for an application septic integrated circuit in a standard CMOS technology with high sensitivity.
- An Impedance measurement technique for wide-range lossy capacitive sensors

  An auto balancing approach was utilized for improving the modiýed active De Sauty bridge performance for the measurement of sensor parameters. A voltage controlled variable capacitor is used in auto balancing bridge. It nullifies the quadrature component of the output phase shifted signal. The output voltage of the circuit is proportional to the resistance component. The phase and the amplitude of the output signal change due to the variation of the resistance and the capacitance of the sensor arm [189].
- Current mode oscillator circuit for the grounded capacitive sensors

  The current mode oscillator offers large dynamic range, wide bandwidth, high linearity, possibility of designing with low power consumption and simple analog circuit design. An oscillator-based interface circuit for the grounded capacitive sensors with wide dynamic range using CCII has been discussed in [190]. Its main operation is basically adopted from the voltage mode of current integration and the conýguration is designed in such a speciýc way that minimizes the effect of the parasitic components of CCIIs.

2.14 Research Gap

Based on the literature review, pointed research gaps are listed below:

- Need of auto regenerative dehydrating breather for controlling the moisture ingresses in high voltage transformer
- Need of model based monitoring of moisture inside the breather for predicting the saturation level of silica gel
- Sensor based monitoring of moisture of transformer oil and breather
- Need of optimization of anodization parameters of electrolyte to achieve the different level of sensitivity of anodic aluminium oxide (AAO) based humidity sensor
- Need of development of mathematical model to analyze the drift in aged humidity sensor

2.15 Scope of the Thesis

- The life of the paper insulation deteriorates due the presence of moisture. Water dissolve in oil is measured in terms of parts per million (ppm). The level of dissolved water in the oil allowed in industry depends upon the rating of the transformer and types of oil used for the insulation.

- Chemical method (Karl Fischer Titration) is used for the measurement of water in oil in the industry, which has certain limitation. Capacitive humidity sensor measures the relative moisture content and this method applies to all measurement techniques based on moisture equilibrium.
- During the temperature variation of the oil due to cyclic variation of the load of the transformer, there is constant moisture exchange between oil and solid insulation. As temperature increases, water is released from cellulose and air above the oil inside the conservator comes out through the silica gel breather. Again, as the temperature of the oil decreases, the volume of the oil is decreased and water dissolved in the oil is transferred to the solid insulation.
- During the period, when the temperature of the oil decreases, the atmospheric air enters into the conservator through the breather. The silica-gel crystal inside the breather absorbs moisture of the airflow inside the breather, when the temperature of the oil of the transformer varies due to the cyclic variation of the load. The silica-gel crystal has finite capacity to absorb the moisture. It is saturated, when its threshold value is reached. It has need of frequent replacement, when it is saturated. The colour of gel is dark blue, when it is fresh and becomes pink when it is saturated. Silica-gel inside the breather is monitored through the visual inspection and suffers from the regular replacement in high humid area.
- Atmospheric air moisture is major source of moisture contamination in transformer due to the poor condition of the dehydrated breather. For the protection of the life of the transformer insulation, there is need of continuous real time monitoring of the breather. The real time monitor of the humidity level inside the breather through the humidity sensor will indicates whether the drying capacity of the silica-gel is decreased. It will indicate whether there is risk of moist airflow through the breather into the conservator. It will give better indication of moisture in solid crystal of silica-gel inside the breather. Silica-gel dryer can also be used to remove moisture after achieving preset value of humidity level inside the breather.
- Capacitive humidity sensor can be used to indicate the relative humidity level. It consists of two electrodes with a hydroscopic dielectric material sandwiched between the electrodes. The hygroscopic material may be polymer or ceramic types. The electrode used in the sensor may be interdigitated type or parallel plate type.

- Water molecules penetrate into the hygroscopic dielectric material depending on the relative saturation of the ambient material. Water penetration changes the capacitance because of the high relative permittivity. Most of the humidity sensor used in the industry is capacitive type. Capacitive sensor has fast response, high thermal stability, repeatability, and minimum hysteresis.
- The capacitive sensor designed for the measurement of relative humidity suffers from long term drift due to lateral seepage of moisture inside the pore and change in the pore diameter of the sensing material. Therefore, there is need of a periodic calibration of capacitive sensor. The signal conditioning electronics circuit is used to measures the change of capacitance by a change of voltage or frequency. This variance is calibrated to relative saturation.

Chapter 3

Modelling of Breather for Transformer Health Assessment

3.1 Introduction

A silica-gel breather is an important accessory of a power transformer. The breather as shown in Fig. 3.1, is connected with a conservator of the transformer through a breathing pipe. Silica-gel in the breather is used for filtering the air from moisture, which may enter the transformer due to change in the volume of oil. Oil in the transformer is used as an insulating medium, and for cooling of the transformer winding. The volume of the oil is changed due to the temperature gradient, which is caused by the variation of the electrical loads of the transformer. Silica-gel desiccant without moisture is dark blue in its colour and after saturation with moisture, it becomes pink. Whenever there is a step change in load either in summer or in winter season, the temperature of the oil increases or decreases and consequently, the volume of the oil either increases or decreases. The transformer breathes in or breathes out the air as the air pressure inside the tank change. The temperature of the air inside the tank is equal to the temperature of the oil. When the volume of the oil increases, the air above the oil level inside the transformer comes out in the breather through the conservator tank. The temperature of the breather air and air inside the tank is different due to the difference in pressure and volume between them. Similarly, when the volume decreases, the atmospheric high moisture content air enters into the conservator tank through the breather and the temperature of the breather air is almost equal to the temperature of the atmospheric air.

Fig. 3.1 Silica-gel breather used in power transformer.

In both the situations, the moisture in the air is adsorbed properly by the silica-gel crystals. Over the period of time, the silica gel loses the moisture adsorbing capability and therefore, it requires frequent replacement.

The maintenance of the breather depends on human inspection and hence, the measurement is prone to human error. Due to the poor condition of the silica-gel, the moisture available in the air is mixed up with the oil.Moisture ingress inside the transformer through the saturated silica-gel is one of the significant causes of oil contaminations and transformer failure. Therefore, there is an urgent need to develop a model to estimate the condition of the silica-gel in the breather.

In this chapter, a mathematical model is proposed, which monitors the moisture and predicts the failure of the silica-gel in breather at different working conditions of a power transformer. For modelling, two conditions are considered for the improved dynamic analysis of the moisture migration between the breather atmosphere and the silica-gel. These conditions are the equilibrium condition of moisture in a breather and the transient phenomena of moisture ingress. It is to be noted that the equilibrium conditions of the moisture in a breather hardly occurs due to the variable loads of the transformer. Thus, the role of the second condition, the transient phenomena of moisture ingress becomes very critical for the dynamics of the moisture inside the breather. Validation of the model is done using the standard input signals of humidity namely (i) the unit rectangular pulse, and (ii) the hyperbolic. Finally, some of the simulated results are validated by the experimental work. Thus, with the help of the model, we can (i) estimate the moisture level in the oil, (ii) estimate the condition of the silica gel for its usefulness for practical application,

3.2. Theoretical foundation

3.2.1 Steady-state sub model of the breather

During the transient phenomena of water adsorption and desorption between the breather air and silica-gel, the moisture content in the gel is estimated by the steady-state sub model. Moisture and temperature of the breather air are taken as inputs to the sub model. The equilibrium moisture concentration (EMC) of silica-gel at different %RH level is obtained from the literature [6]. The EMC of the gel in percentage is the ratio of the weight of water adsorbed by the gel to the weight of the gel at the dry condition. Fig. 3.2 shows the EMC at different %RH for three different types of silica-gel usually employed in the breather. Typically, Art-Sorbôs gel shows better performance at higher RH above 50% but the Regular Density gel shows the better performance in lower RH below 40%. Depending on the conditions of the atmospheric air, the different types of silica-gel can be used in the breather for controlling the moisture ingress.

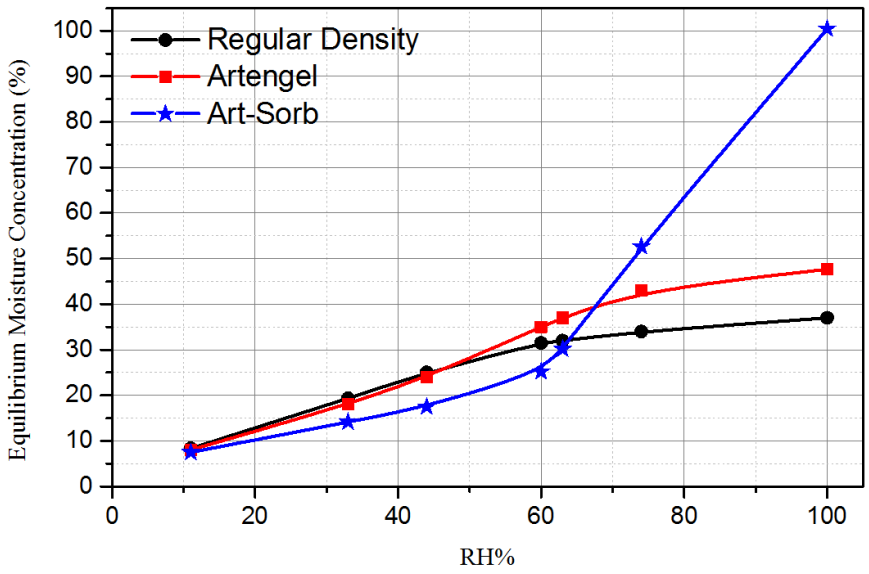

Fig. 3.2 Equilibrium moisture capacity at different relative humidity in the range of 11-100% of three different silica-gels.

3.2.2 Transient sub model

Due to slow process of water migration between the air of breather and the silica-gel, moisture takes several hours to reach the steady state condition. The transient process is the combination of three different processes including (1) the water transfer from the breather air to silica-gel, (2) the water transfer in the entire volume of silica-gel and (3) the transient response of the moisture sensor. Moisture dynamics in the breather depend on the operating modes of the transformer, such as a sharp rise in loads or sharp fall in loads or the natural cyclic of the loads. Therefore, the model equations are different according to the loading conditions of the transformer. The model equations are derived to estimate the moisture content inside the silica-gel at different RH.

3.3 Transient state sub model for fast rise or decrease in oil temperature

3.3.1 Transient of water adsorption/desorption from breather air to silica-gel

The temperature of the air above the oil inside the transformer tank is almost equal to the temperature of the oil. However, there may be different temperature of the air in oil and the air in breather. The relation between the temperature of the breather air and the air of the transformer can be approximately given by (3.1).

$$T_1 = \frac{P_1 \text{ x } V_1 \text{ x } T_2}{P_2 \text{ x } V_2} \tag{3.1}$$

Where, T_1 is the temperature of the breather air in Kelvin, T_2 is the temperature of the oil in Kelvin, V_1 is the volume of the breather in m^3, V_2 is the volume of the main tank of the m^3, P_1 is the pressure inside the breather in mm Hg and P_2 is the pressure inside the main tank of the transformer in mm Hg. Further, the capacitance value (C) of the sensor in the breather with moist air permittivity (Ų) can be given by [85].

$$C = \frac{\varepsilon_O * \varepsilon_{r*A}}{d} \tag{3.2}$$

Where, A is the area of the parallel plate and d is the gap between the plates. For the moist breather air, the relative permittivity is determined by the following equation [85].

$$\varepsilon_r = 1 + \frac{211}{T}(P + \frac{48P_S}{T} RH) * 10^{-6} \tag{3.3}$$

Where, T is the temperature of the breather air in Kelvin, P is the pressure of moist air, P_s is the saturated vapor pressure at T and RH is the relative humidity in the breather air. Therefore, if there is a temperature difference between the air of the oil tank and the breather, the moisture adsorption depends on only the temperature and pressure of the breather air. However, the temperature and the pressure of breather air will depend on the temperature and the pressure of the oil air in the transformer tank as given in (3.1). The moisture in the breather will be adsorbed by the silica-gel. Silica-gel is a non-homogeneous moisture adsorbent. It consists of large varieties of pores with different sizes. The distribution of the pores includes micro, meso and macro pores. The density of the micro pores plays an important role for the adsorption of the water in the silica-gel. A typical process of moisture transfer from the air to the entire volume of the silica-gel in the breather is shown in Fig. 3.3. The figure shows the distribution of moisture in the silica-gel. In the beginning, the moisture molecules are present in the breather air, then gradually adsorbed by the gel. Therefore, the pores are gradually filled up. After certain time elapsed, the moisture concentration reaches an equilibrium condition. At equilibrium, moisture level indicated by the sensor is almost equal to the moisture level present in the gel. The moisture present in the breather air at any particular temperature is properly adsorbed by the silica gel. Dubinin-Astakhov (D-A) had proposed a model for the adsorption of moisture in the silica-gel crystals [174-176]. D-A equation can be used to evaluate the EMC in cm^3/g and is expressed as

$$q = q_0 \exp[-(\frac{A}{E_0})^{n_1}] + q_1 \exp[-(\frac{A}{E_1})^{n_2}] \tag{3.4}$$

where, A is the adsorption potential at temperature T, n_1 and n_2 are the structural heterogeneity parameters of the micro pores, E_0 and E_1 are the characteristics energies of the adsorption of the gel in cal/mole, q_0 and q_1 are the limiting uptakes of adsorption space of the gel in cm^3/g. The parameter A can be given by

$$A = RT \ln(\frac{1}{RH}) \tag{3.5}$$

Where, R is universal gas constant in $JMol^{-1}K^{-1}$, T is equilibrium temperature in Kelvin and RH is the relative humidity and the EMC in percentage is expressed as the

$$EMC\% = q \times 100 \tag{3.6}$$

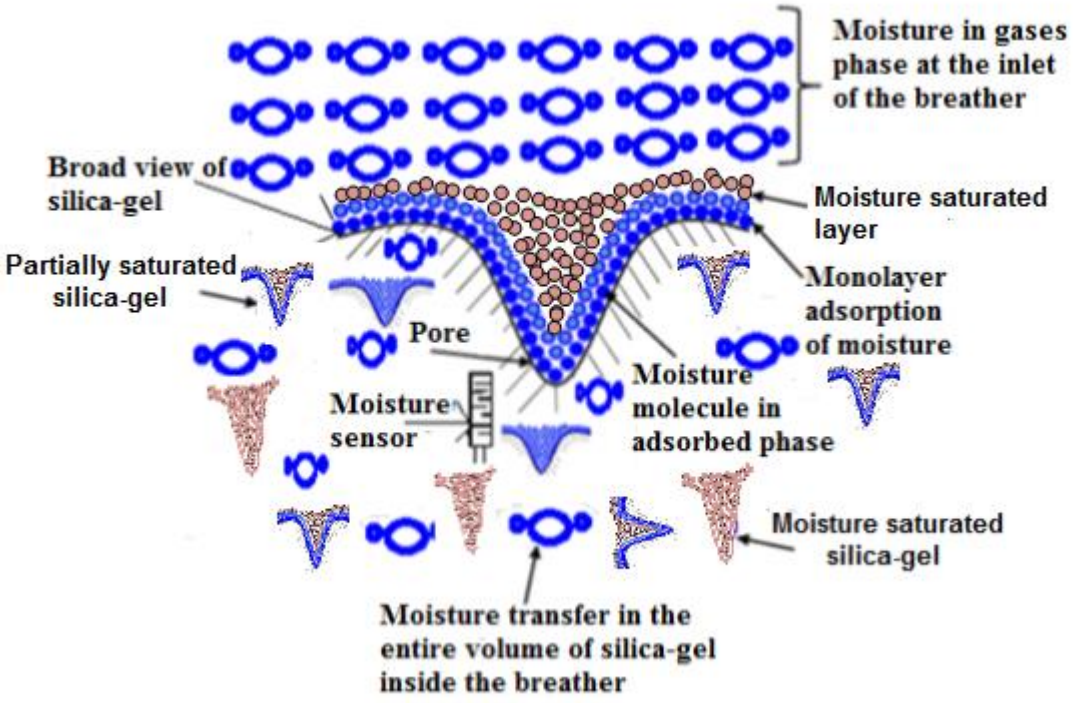

Fig.3.3 Adsorption process of moisture from gaseous phase to the adsorbed phase in silica-gel inside the breather.

Thus, an analogy exists between the heat transfer and the mass transfer of water at particular condition [177]. So, it is possible to relate the process of heat and mass transfer with the equation given in (3.7).

$$\Gamma_{air} \frac{dM_{sgel}}{dt} + M_{sgel} = M_{sgel-ss} \tag{3.7}$$

Where, M_{sgel} and $M_{sgel-ss}$ are the masses of water in silica-gel at any time and at the steady state condition respectively. Γ_{air} is the time required by the breather air to reach a steady state equilibrium with the silica-gel. The value of $M_{sgel-ss}$ varies with the variation of the ambient temperature. To determine the value of temperature dependent $M_{sgel-ss}$ over a certain period of time, the (3.7) is modified as

$$\Gamma_{air}\frac{dM_{sgel}}{dt}+M_{sgel}=M_{sgel-ss}+\overline{\Delta t}\frac{dM_{sgel-ss}}{dt} \tag{3.8}$$

where, $\overline{\Delta t}$ is the incremental integration step.

3.3.2 Transient of water transfers in the entire volume of silica-gel

For monitoring the moisture inside the gel, the moisture sensor can be placed in the silica-gel at the suitable location. The sensor is placed deep inside the gel. This arrangement is done to monitor the moisture concentration inside the breather. When the temperature of the oil decreases quickly, the transformer sucks atmospheric air through the breather. There exists a homogenous distribution of water in the gel inside the whole breather volume. The mass of water at the position of the sensor is assumed to be equal to be the water mass in the silica-gel as

$$M_{sens}(t)=M_{sgel}(t) \tag{3.9}$$

Where, $M_{sens}(t)$ is the moisture mass in the silica-gel at the sensor position at any timeátô in days.

3.3.3 Transient response of the moisture sensor

The response of the sensor depends on the moisture concentration inside the silica-gel of the breather. The response can be in the form of capacitance/ impedance/ resistance depending upon the working principle of the humidity sensor. The capacitive technique is one of the most widely used methods of humidity sensing. Often, the response of the capacitive type moisture sensor is of first order equation [83]. The sensor time constant is defined as the time taken to attain the moisture equilibrium with the moisture of silica-gel. The sensor response is modelled as a first order equation with a time constant Γ_{sens} and is given by

$$\Gamma_{sens}\frac{dM_b}{dt}+M_b=M_{sens} \tag{3.10}$$

Where M_b and M_{sens} are the measured moisture in the breather and silica-gel in the zone where the sensor is installed respectively. Using (3.8), (3.9) and (3.10), the equation of the model can be expressed as

$$\Gamma_{air}\Gamma_{sens}\frac{d^2M_b}{dt^2} + (\Gamma_{air}+\Gamma_{sens})\frac{dM_b}{dt} + M_b = M_{sgel-ss} + \overline{\Delta t}\frac{dM_{sgel-ss}}{dt} \tag{3.11}$$

Equation (3.11) is a second - order equation of the model, which indicates the dynamic response of the moisture sensor at steady state.

3.4 Transient state sub-model for the natural operation of the transformer

3.4.1 Transient of water desorption/adsorption from breather air to silica-gel

In this case, the operation of the power transformer depends upon the ambient temperature cycles of the oil due to the variable electrical loads. The air flows through the breather as the volume of the oil changes due to a temperature gradient. Equation (3.8) can be used to model the water migration between the breather air to silica-gel (vice-versa).

3.4.2 Transient of water transfer in entire volume of silica-gel

The process of water transfer in the whole volume of silica-gel inside the breather is slower than when there is a sudden step change in temperature as described previously. The transfer process can be modelled in a simplified way by a first-order equation with a time constant Γ_{sgel}.

$$\Gamma_{sgel}\frac{dM_{sens}}{dt} + M_{sens} = M_{sgel} \tag{3.12}$$

Where Γ_{sgel} is the time required by silica-gel to maintain the moisture equilibrium with sensor.

3.4.3 Transient of the moisture adsorption to the sensor

The transient behavior of the humidity sensor can be represented by the equation given in (3.13), which is obtained using (3.10) and (3.12)

$$\Gamma_{sgel}\Gamma_{sens}\frac{d^2M_b}{dt^2} + (\Gamma_{sgel}+\Gamma_{sens})\frac{dM_b}{dt} + M_b = M_{sgel} + \overline{\Delta t}\frac{dM_{sgel-ss}}{dt} \tag{3.13}$$

and finally substituting (3.13) into (3.8), the model equation under the natural operation of the transformer can be represented as

$$\begin{aligned}&\Gamma_{air}\Gamma_{sens}\Gamma_{sgel}\frac{d^3M_b}{dt^3}+(\Gamma_{air}\Gamma_{sens}+\Gamma_{sens}\Gamma_{sgel}+\Gamma_{sgel}\Gamma_{sens})\frac{d^2M_b}{dt^2}\\&+(\Gamma_{air}+\Gamma_{sens}+\Gamma_{sgel})\frac{dM_b}{dt}+M_b\\&=M_{sgel-ss}+\overline{\Delta t}\frac{dM_{sgel-ss}}{dt}\end{aligned} \tag{3.14}$$

Equation (3.14) indicates the dynamics response of the moisture sensor.

3.5 Computational validation of the model

The validity of the model is verified by the frequency domain analysis. Two different inputs are considered to study the performance of the models. These inputs are selected on the basis of the moisture ingress phenomena in real - time situation. Two inputs are shown in Fig. 3.4. In Fig. 3.4(a), the amplitude of the moisture increases in a hyperbolic manner for the first 15 days and then for the next 15 days, the amplitude remains constant. Number of days in Fig. 3.4 (a) has been selected arbitrarily. This number of days can be changed. In the present case, we have assumed that initially for the first 15 days, the moisture has sharp rise may be due to heavy rain, then it becomes constant for rest of the time. For example, in rainy season, there is very high humidity in the atmosphere for some times, and then it becomes constant. This type of situation can be represented by the Fig. 3.4 (a). But, the nature of moisture variation varies according to the geography of the transformer location. The performance of the silica gel depends upon the equilibrium moisture concentration in the breather. There are different types of silica gels, which are used for breather. Some gels like regular density arten gels are sensitive at lower relative humidity and get saturated at higher humidity level within short period of time as shown in (Fig. 3.2). It loses moisture adsorbing capability after almost 98% RH level. X2 (t) = 0.98 for t > 15, indicates the saturation condition of the silica gel. Beyond this humidity, the silica gels are further not useful for the adsorption of moisture. The second input is shown in Fig. 3.4 (b), where the amplitude of the moisture is the rectangular pulse. In the beginning, the moisture amplitude is maintained at certain fixed value and then, there is a step change in the moisture amplitude. These inputs show different forms of the moisture variation in the silica-gel. Rectangular shape input has been considered to indicate that there is a sudden sharp rise in moisture and then, it becomes constant. It basically represents the transient phenomena of the moisture level.

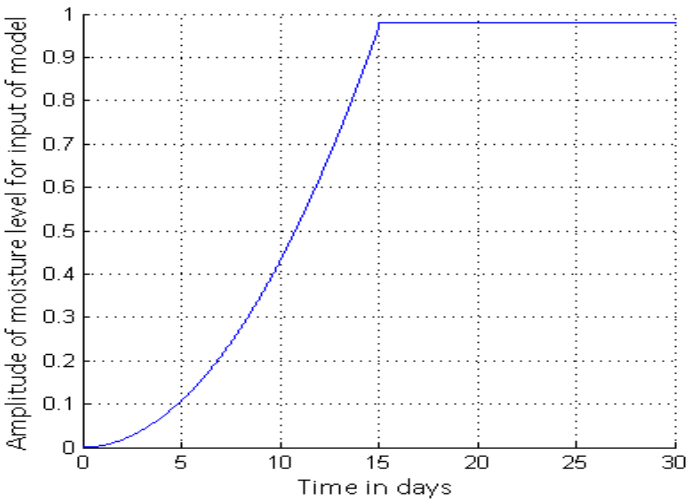

Fig. 3.4a Signal of hyperbolic variation for first 15 days then remains constant till 30 days.

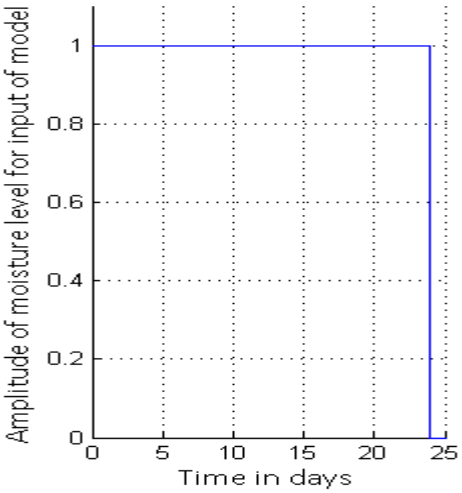

Fig. 3.4 b Rectangular signal

3.5.1 Validation of the response of the model for fast rise or decrease in oil temperature

When the temperature of the oil of the power transformer decreases or increases quickly, the moisture content in silica-gel, at a particular relative humidity inside the breather is given by (3.11). Considering $M_{sgel-ss}$ as the input and M_b as the output parameter, the output of the model in frequency domain is given

$$Y(S) = \left[\frac{\overline{\Delta t} s + 1}{p_1' S^2 + p_2' S + 1} \right] X(S) \qquad (3.15)$$

Where $p_1' = \Gamma_{air}\Gamma_{sens}$, $p_2' = \Gamma_{air} + \Gamma_{sens}$, $X(S)$ and Y(s) are the Laplace transforms of the input signal and the output response respectively.

Case I: Response of the model for the input signal shown in Fig. 3.4 (a)

The input signal has two distinct moisture amplitudes at the different time periods (t). For the first 15 days (0 < t <15), the input signal is hyperbolic, which is represented by

$$X_1(t) = 0.0043\, t^2 \qquad (3.16)$$

and for the next 15 days (30 > t Ó15), the amplitude of the input is constant, which is given by,

$$X_2(t) = 0.98 \qquad \text{for t Ó15} \qquad (3.17)$$

The response of the model in frequency domain for the period (0 < t <15) is given by

$$Y_1(s) = \frac{(0.0087 + 0.130s)}{(900s^4 + 60s^3 + s^2)s} \tag{3.18}$$

and the transfer function of the model for the period t Ó15 is given by

$$\frac{Y_2(s)}{X_2(s)} = \frac{1+15s}{900s^2 + 60s + 1} \tag{3.19}$$

Where, $Y_2(S)$ is the output for the input $X_2(S)$.The equation can be expressed in differential form as

$$900\ddot{y}_2 + 60\dot{y}_2 + y_2 = 15\dot{x}_2 + x_2 \tag{3.20}$$

Taking the Laplace transform of (3.20), the output response in frequency domain is

$$Y_2(s) = \frac{(15s+1)0.98}{s(900s^2 + 60s + 1)} + \frac{900s^2 y_1(15) + 900s\dot{y}_1(15) + 60s\dot{y}_1(15) - 15sx_2(0)}{s(900s^2 + 60s + 1)} \tag{3.21}$$

where, the initial conditions are $y_2(0) = y_1(15)$ and $\dot{y}_2(0) = \dot{y}_1(15)$.

The total response of the model, for the entire period is obtained by adding the individual response of $Y_1(s)$ and $Y_2(s)$ respectively.

The computation of the model for the desired input is performed using the MATLAB software [19]. The simulation result of the model is shown in Fig. 3.5 (a). It shows the dynamic response of the sensor immersed in the gel inside the breather. The output response, the moisture concentration at the position of the sensor follows the nature of the input signal. However, the amplitude of the response is smaller. The closed-loop poles of the model equation are located at s = - 0.03398 and s = - 0.03267. All poles are in the left-half of the s plane, and hence, the model shows stable behavior. The response curve gives satisfactory results. The p at s = -0.03267 acts as a dominant closed-loop pole. The response has better rise time due to the presence of derivatives terms in the numerator of the model equation. The steady-state response of the model corresponds to the saturated response of the silica-gel. At this stage, it indicates the maximum moisture adsorption by the silica-gel. It shows the silica-gel reaches its maximum capacity and the gel is not useful for further moisture adsorption. This necessitates the replacement of the gel from breather. For better visualization, the input is also shown in the same graph.

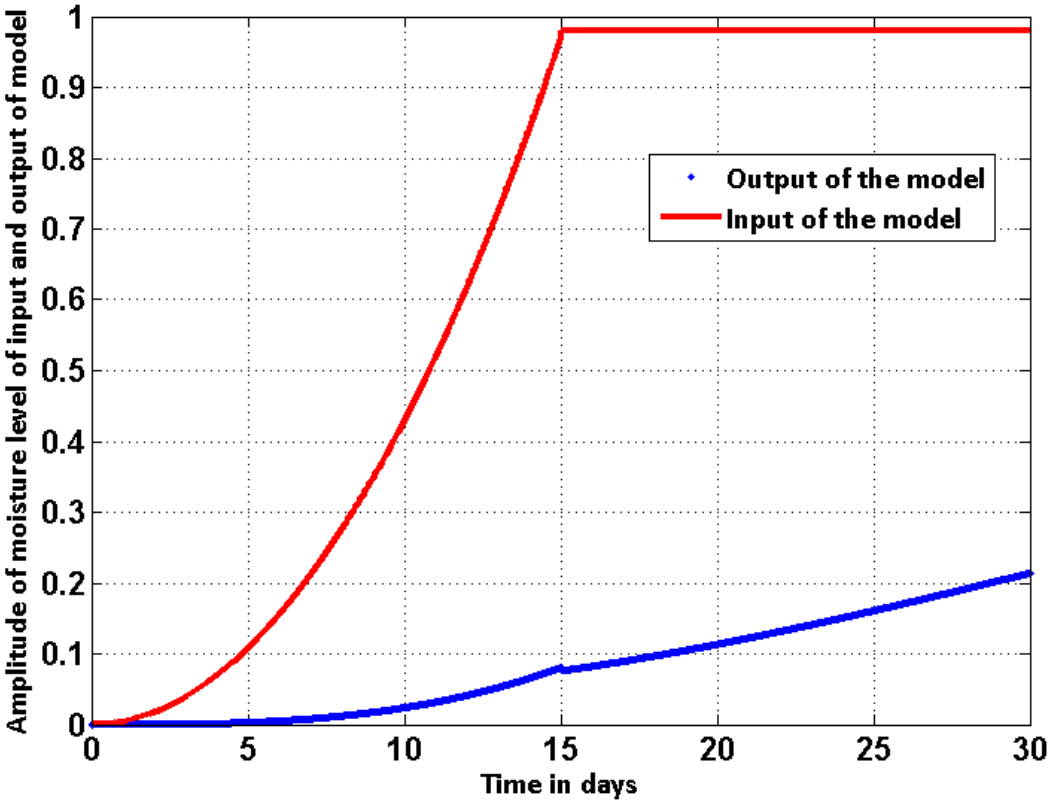

Fig. 3.5a Simulation result of the model equation (3.21) along with input signal.

Case II: ***Response of the model for the input signal shown in Fig. 3.4(b)***

The input signal, which is shown in Fig. 3.4 (b) is rectangular in shape. The time domain representation of the input signal is

$$X(t) = U(t) - U(t-24) \tag{3.22}$$

The Laplace transform of the input given by (3.22) will be

$$X(s) = \frac{1}{s} - \frac{e^{-24s}}{s} \tag{3.23}$$

Expanding the expression and neglecting the higher order terms, X(S) can be written as

$$X(s) = \frac{1}{s}\left(1 - \frac{2-24s}{2+24s}\right) = \frac{48}{2+24s} \tag{3.24}$$

The Laplace transform equation of the model for $\Gamma_{air} = \Gamma_{sens} = \Gamma = t = 24 days$ the input signal as shown in Fig. 3.4 b, is

$$Y(s) = \frac{(48s + 576s^2)}{(13824s^3 + 2304s^2 + 120s + 2)s} \tag{3.25}$$

The simulation result of the model for the desired input is shown in Fig-3.5 (b). The results show that the moisture level indicated by the sensor follows the moisture input signal of the gel. The simulation results are also observed for the longer periods of the input signal and are shown in Fig. 3.5b (i) and 3.5b (ii) respectively. It is clear that a large time (Γ) is desirable for faithful reproduction of the input due to the presence of decay and undershoot of the response at $\Gamma = t$ [31].

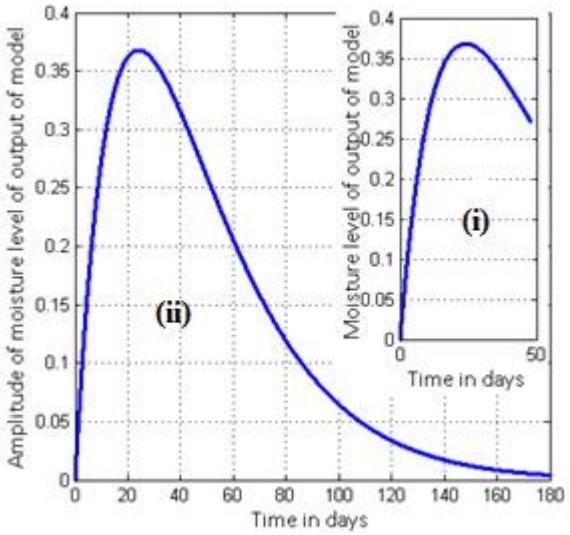

Fig-3.5b Simulation result of the model equation (3.25).

3.6 Computational validation of the model for the natural operation of transformer

During the natural operation, the power transformer has acyclic rating. Its operation depends on the need to meet the day to day demand of the customer. It is overloaded at peak times, while is lightly loaded during the lean periods of the time. During this natural operation, the temperature of the oil inside the transformer goes up and comes down. Due to the change in the level of the oil, the air flows through the breather and the moisture of the air is adsorbed by the gel. The mathematical equation for the moisture content in the silica-gel at different

RH, at steady state condition, is given by (3.14). Again, considering $M_{sgel-ss}$ as the input and M_b as the output parameter, the frequency domain output response of the model is given by

$$Y(s) = \left[\frac{\overline{\Delta t}s + 1}{p_1 s^3 + p_2 s^2 + p_3 s + 1} \right] X(s) \tag{3.26}$$

where, $p_1 = \Gamma_{air}\Gamma_{sgel}\Gamma_{sens}$, $p_2 = \Gamma_{air}\Gamma_{sgel} + \Gamma_{air}\Gamma_{sens} + \Gamma_{sgel}\Gamma_{sens}$, $p_3 = \Gamma_{air} + \Gamma_{sgel} + \Gamma_{sens}$ respectively.

Case I: Response of the model for the input signal shown in Fig. 3.4 (a)

For the time period, 0 <t <15, the output response of the model is

$$Y_1(s) = \frac{(0.0087 + 0.130s)}{(27000s^5 + 2700s^4 + 90s^3 + s^2)s} \tag{3.27}$$

For the time period, t Ó15, the transfer function of the model is

$$\frac{Y_2(s)}{X_2(s)} = \frac{1+15s}{27000s^3 + 2700s^2 + 90s + 1} \tag{3.28}$$

The transfer function in differential form can be written as

$$27000\dddot{y}_2 + 2700\ddot{y}_2 + 90\dot{y}_2 + y_2 = 15\dot{x}_2 + x_2 \tag{3.29}$$

With the initial conditions $\ddot{y}_2(0) = \ddot{y}_1(15)$, $\dot{y}_2(0) = \dot{y}_1(15)$ and $y_2(0) = y_1(15)$, the output in the frequency domain can be given by the expression

$$\begin{aligned} Y_2(s) &= \frac{(15s+1)0.98}{s(27000s^3 + 2700s^2 + 90s + 1)} \\ &+ \frac{27000s^3 y_1(15) + s^2[2700y_1(15) + 27000\dot{y}_1(15)] + s[90y_1(15) + 2700\dot{y}_1(15) + 27000\ddot{y}_1(15) - 14.7)]}{s(27000s^3 + 2700s^2 + 90s + 1)} \end{aligned} \tag{3.30}$$

The simulation result of the model is shown in Fig. 3.6a. The model output is similar to the input as shown in Fig. 3.4a. The closed-loop poles of the model are located at s = - 0.03092, (- 0.03453 ï 0.00208j), and (- 0.03453 + 0.00208j) respectively. The response of the model is dominated by the pole at s = - 0.03092. The complex-conjugate poles also lie close to the

dominant pole, which make the transient response very slow. Because of these complex conjugate poles, the steady state response is too long.

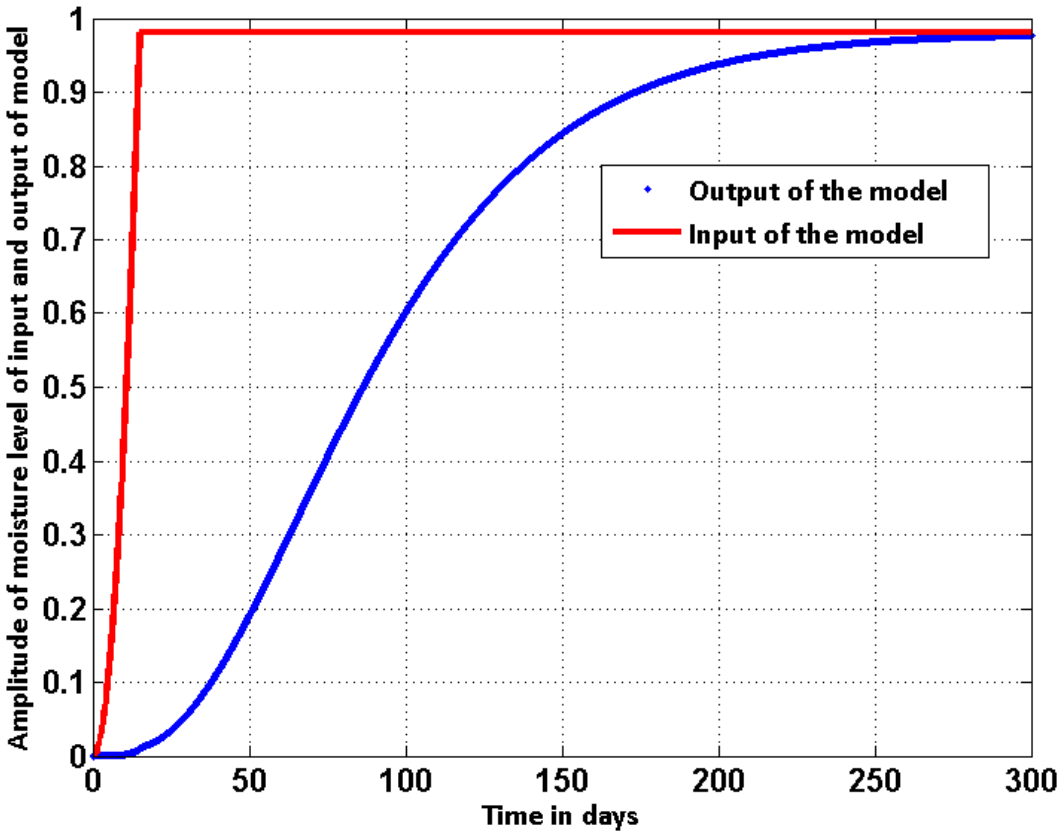

Fig-3.6a Simulation results of the model (3.30) along with the input signal.

Case II: Response of the model for the input signal shown in Fig. 3.4 (b)

For the input signal, the model equation with time constant $\Gamma_{air} = \Gamma_{sens} = \Gamma_{sgel} = 24\,days$ is obtained by substituting (3.22) in (3.26) as

$$Y(s) = \frac{48s + 576s^2}{S(331776s^4 + 69120s^3 + 5184s^2 + 168s + 2)} \qquad (3.31)$$

The simulation result of the output response of the model is shown in Fig. 3.6b at different time constants. The results show that the amplitude of the output initially increases up to the maximum value and then decreases. At higher time constant, the output amplitude decreases to zero value. The output amplitude of the model varies according to the change in amplitude of the input signal. The model consists of two real distinct and a pair of complex-conjugate poles. The closed-loop poles of the model are located at s = -0.09086, - 0.02954, (- 0.04395 ï 0.01767j) and (- 0.04395 + 0.01767j). All the poles lie in the left half of the s plane. The

response of the model is dominated by the pole at s = -0.02954, as it is close to the imaginary axis (jw). Due to the presence of derivatives terms in the numerator of the model equation (3.31) and a pair of complex-conjugate poles in the left side of the s plane, the model response is under shooted and takes more time to reach the steady-state condition.

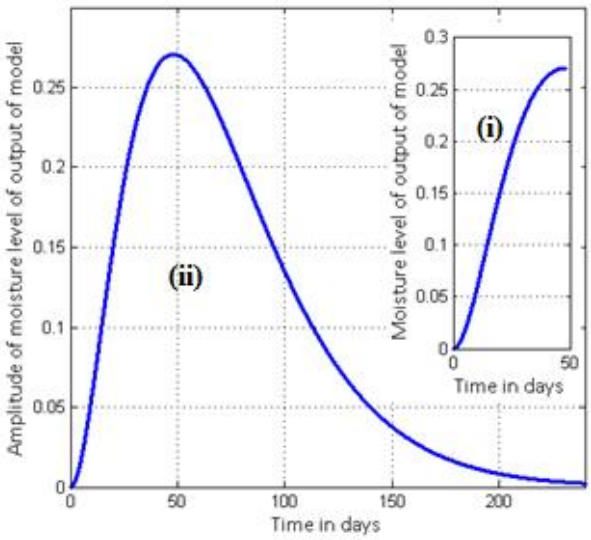

Fig. 3.6b Simulation result of model equation (3.31).

3.7 *Model* for monitoring the moisture concentration of the breather for short period

Depending upon the working conditions of the transformer, moisture concentration in the breather changes at a particular time and then remains at that state for some time. Discrete model is used to estimate the moisture variation for a short period of time. Discrete model more easily determines the variation of moisture in a breather for a short period.

3.7.1 Model when there is a step change (rise or fall) in the oil temperature

Equation (3.11) is a second-order equation of the model. For converting the second-order equation into the discrete form, a variable Z is introduced.

$$Z = \frac{dM_b}{dt} \tag{3.32}$$

The variable Z indicates an incremental change in measured moisture for the incremental change in time.

By substitution Z, (3.11) can be expressed as

$$\Gamma_{air}\Gamma_{sens}\frac{dz}{dt} + (\Gamma_{air}+\Gamma_{sens})z + M_b = M_{sgel-ss} + \overline{\Delta t}\frac{dM_{sgel-ss}}{dt} \quad (3.33)$$

The Euler approximation of the (3.32) is

$$Z(t) = \frac{M_b(t) - M_b(t-1)}{\Delta t} \quad (3.34)$$

where, $M_b(t)$ and $M_b(t-1)$ are the masses of the moisture in the breather at any time t and (t-1) respectively.

Similarly, the Euler approximation of (3.33) is

$$\Gamma_{air}\Gamma_{sens}\frac{Z(t)-Z(t-1)}{\Delta t} + (\Gamma_{air}+\Gamma_{sens})Z(t) + M_b(t) = M_{sgel-ss}(t) + \overline{\Delta t}\frac{M_{sgel-ss}(t) - M_{sgel-ss}(t-1)}{\Delta t} \quad (3.35)$$

Substituting (3.34) into (3.35), the expression of the M_b in discredit form can be given by

$$M_b(t)\left(\frac{\Gamma_{air}\Gamma_{sens}}{\Delta t^2} + \frac{\Gamma_{air}+\Gamma_{sens}}{\Delta t} + 1\right) + M_b(t-1)\left(\frac{-2\Gamma_{air}\Gamma_{sens}}{\Delta t^2} - \frac{\Gamma_{air}+\Gamma_{sens}}{\Delta t}\right) + M_b(t-2)\frac{\Gamma_{air}\Gamma_{sens}}{\Delta t^2} = M_{sgel-ss}(t) + \overline{\Delta t}\frac{dM_{sgel-ss}}{dt} \quad (3.36)$$

Or

$$M_b(t) = K_{1td}M_b(t-1) + K_{2td}M_b(t-2) + K_{3td}M_{sgel-ss}(t) + K_{4td}M_{sgel-ss}(t-1) \quad (3.37)$$

where, K_{1td}, K_{2td}, K_{3td} and K_{4td} are the model parameters.

3.7.2 Moisture estimating model for shorter time under the natural operation of the transformer

Similarly, the model for estimating the moisture concentration for the short duration in discrete form under natural operation is given by

$$M_b(t) = K_{1no}M_b(t-1) + K_{2no}M_b(t-2) + K_{3no}M_b(t-3) + K_{4no}M_{sgel-ss}(t) + K_{5no}M_{sgel-ss}(t-1) \quad (3.38)$$

3.8 Experimental validation of the model

For enhancing the effectiveness of the design, the model is also validated using the real-time humidity data obtained from the experimental setup developed in the laboratory. The schematic of the setup is shown in Fig. 3.7 (a). For recording the real-time data, the developed experimental setup consists of a breather like close chamber having the capacity to store 0.5 kg silica gel. A commercial Honeywell humidity sensor was placed inside the silica-gel. The voltage output of the capacitive Honeywell sensor was measured by an Arduino microcontroller kit integrated with a digital display system. The accuracy of the utilized sensor is of 3.5% RH at 25°C and the zero offset at dry condition is 0.82421 V. The voltage output of the sensor, displayed on the Arduino board was calibrated in terms of the humidity (%RH). The simulated breather chamber has inlet and the outlet holes at the bottom and the top of the chamber. The atmospheric humidity is allowed to enter the chamber andtherefore, the sensor output increases with increase in humidity. The experiments have been conducted to measure the RH level in the chamber for the periods of 93 days. Fig. 3.7 (b) shows the variation of RH level in the chamber at the natural atmospheric condition in the laboratory.

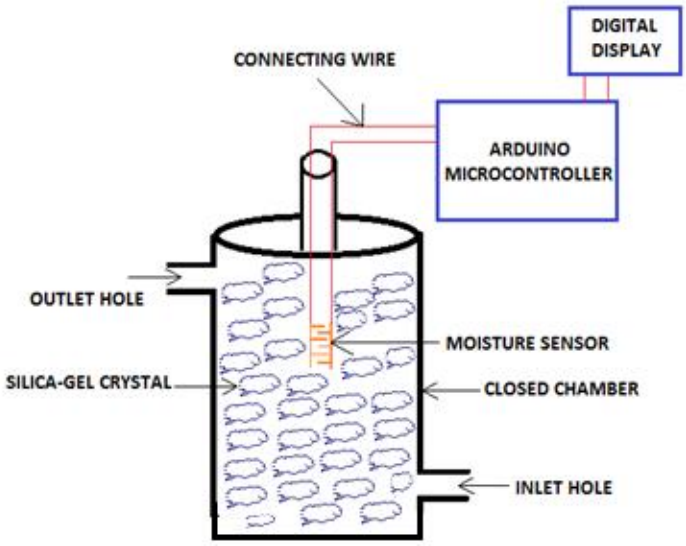

Fig.3.7a Schematic diagram of the experimental setup.

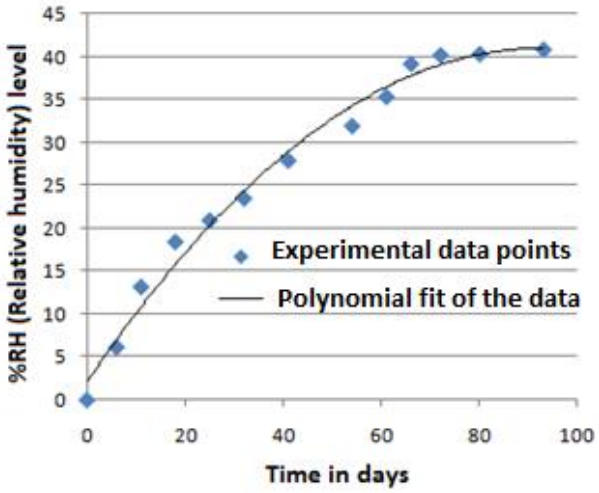

Fig. 3.7b Experimental value of moisture ingress in silica-gel.

It is observed that the humidity indicated by the sensor monotonically increases as the time progresses and then reaches the saturation after nearly 80 days. The experimental data has been curved fitted using the least square method and it shows a second order polynomial function. The RH level is shown in Fig. 3.7 (b) is used as the input to validate the model equations proposed for the breather condition analysis.

Case I: Validation of the model with experimental data for fast rise or decrease in oil temperature

Thetime domain equation of the experimental data obtained by the least square method of trend analysis is

$$X(t) = -0.004t^2 + 0.837t + 2.135 \tag{3.39}$$

The Laplace transform of the input (3.39) is given by

$$X(s) = \frac{-0.008 + 0.837s + 2.135s^2}{s^3} \tag{3.40}$$

Putting (3.40) into (3.15), the output response of the model in frequency domain is given by

$$Y(s) = \frac{99.27s^3 + 41.055s^2 + 0.465s - 0.008}{s(8649s^4 + 186s^3 + s^2)} \tag{3.41}$$

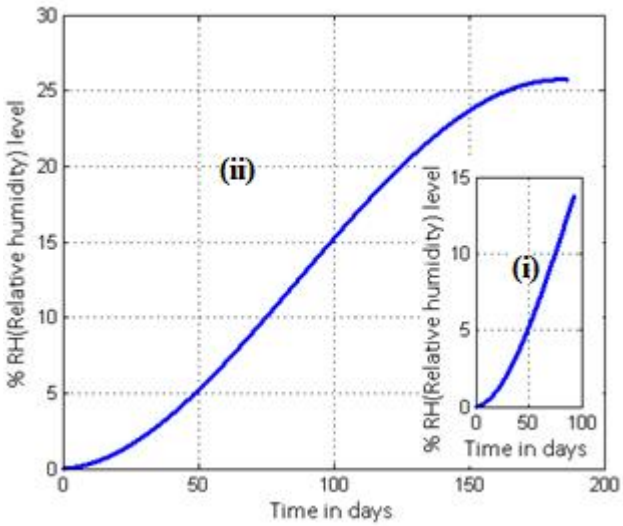

Fig-3.7c Response of the model for the input fig 3.7b (model eq. 3.41).

The simulation result of the model for the input for a time period of 93 days is shown in Fig. 3.7c.The output response again follows the moisture variation in silica-gel as indicated by the input Fig. 3.7b. The response for the longer time periods is also shown in the same graph (Fig. 3.7c (ii) for 180 days). The model consists of three distinct zeros and two multiple poles. The zeros are at and s = -0.40139, -0.02150, and 0.0093 and poles are at s = 0, and -0.0107. Due to the presence of one zero in the right side of s-plane and multiple poles at origin, the response of the model is under shooted. The response of the model first increases then saturates at higher time constants.

Case II: Validation of the model with the experimental data for the natural operation of transformer

Similarly for the input shown in Fig. 8b, the model equation for $\Gamma_{air} = \Gamma_{sens} = \Gamma_{sgel} = 93 days$ can be expressed as

$$Y(s) = \frac{-0.008 + 0.465s + 41.055s^2 + 99.27s^3}{S(s^2 + 279s^3 + 25947s^4 + 804357s^5)} \qquad (3.42)$$

The simulation result of the model for the input is shown in Fig. 3.7d. The results show that the amplitude of the output of the model increases with time up to certain maximum values then becomes constant at a higher time constant

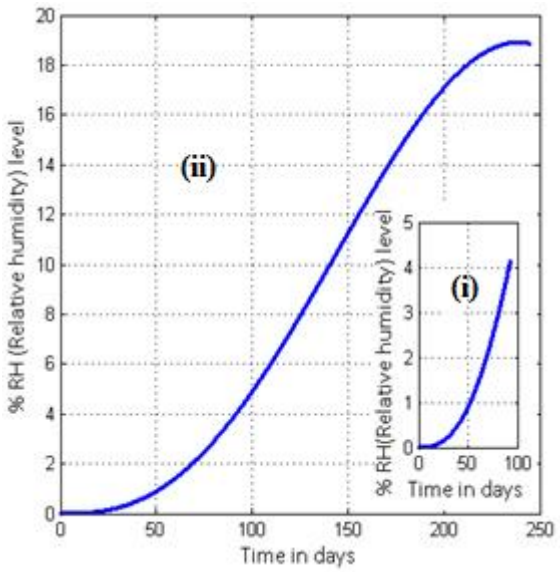

Fig. 3.7d Simulation result of model equation (3.42).

Fig. 3.7d shows the response of the model for different time constants. The saturation of the response curve occurs at higher time constant. Therefore, the faithful reproduction of the input requires higher time constant due to presence of undershoot and decay in a second or third order model.

3.9 Conclusions

In this chapter, the mathematical models are developed for estimating the moisture content inside the breather of a power transformer. Two different models namely the steady-state model and the transient sub model are developed for the same purpose. The transient sub model involves three different processes: (i) transfer of water from the air to silica-gel, (ii) transfer of water in the entire volume of silica-gel and (iii) the moisture sensor response. When there is a step change in electrical loads, the model equations are of second order type but for the natural cyclic load, the model equations are of third order type. The analysis of the model is performed by assuming (1) an equilibrium condition of moisture transfer between the silica-gel and air inside the breather, and (2) the transient phenomena, till a steady state condition is reached. The model is capable of predicting the failure of the silica-gel, thus suggesting abnormal water flow inside the transformer through the breather. The moisture content in the silica-gel is calculated using the Dubinin-Astakhov equations. Simulations of the model under different loading conditions are performed with two different types of inputs. The output amplitude of the model varies according to the change in amplitude of the input signal. It is established that the large time constant of the output is desirable for the faithful

reproduction of the input signals. For validating some of the simulation results, an experimental setup is developed in the laboratory. The moisture content in the silica-gel in the simulated breather environment is measured using a calibrated Honeywell humidity sensor. The saturation analysis of the silica-gel using the experimental set up closely matches the simulation results. The model is effective to predict the conditions of the gel. This exercise allows the end-users of the transformer to develop a more accurate monitoring system to aware from possible saturation of the silica-gel.

Chapter 4

Fabrication of Anodic Aluminium Oxide Thin Film Humidity Sensor for Breather Condition Monitoring of Transformer

4.1 Introduction

In chapter 3, we have introduced about the breather and its importance in T/F operation. It is an accessory of the high voltage transformer filled with silica ï gel. It is used to provide the protection from the ingress of excess moisture of ambient air during the breathing. The level of the humidity inside the breather of the transformer varies between 10% RH to 90% RH. In fresh condition of the silica ï gel, the humidity level inside the breather is around 10% RH. Silica ï gel has limitation to absorb the moisture. It is saturated, when its threshold is achieved. Saturation level depends upon its types. It varies from 50% RH to 90% RH. In fresh condition, the colour of the silica ï gel is dark blue and becomes pink when it is saturated. For on line condition monitor or self-dehydrating breather, there is a need of a stable humidity sensor, which detects humidity level from 10 % RH to 90% RH [4-7]. Therefore, in this chapter, development of a capacitive humidity sensor using porous alumina prepared through the anodization of 99.9% pure aluminium (Al) sheet has been reported. The designed capacitive humidity sensor works on the principle where the dielectric constant of anodic Al_2O_3 film changes after the absorption of the moisture. The response characteristics of the sensor were studied with varying %RH. The sensitivity of the sensor was optimized by controlling the pore morphology of the nano structured thin film of Al_2O_3. The pore morphology of the anodic aluminium oxide (Al_2O_3) was controlled by selecting the proper anozation parameters such as molar types of electrolyte, molar concentration of electrolyte, anodization voltage, duration of anodization conductivity of aluminium (Al) sheet and current density of the anodizaton. During anodization of the Al sheet dipped in electrolytic solution, the oxide layer is formed on each side of the sheet. But between these two oxide layers, there is the bulk pure Al layer which can be used as one electrode of the capacitive sensor. The silver metal plate was deposited on the oxide layer of each side. The capacitive sensor was formed in each side of the Al sheet. Both the sensors were connected in parallel for enhancing the sensitivity. Three sensors were fabricated with different anodic parameters. The response of the three sensors developed through the different anodization conditions was compared.

Output of the sensors was used to measure the moisture in parts per million (ppm). The sensor was found to be sensitive for detection of moisture in the range of 200 ppm to 1000 ppm. It was used for the detection of moisture generated in highly contaminated transformer oil.

4.2 Fabrication of the Porous Alumina Capacitive Sensor using Anodization of Aluminium Sheet

4.2.1 Pre-treatment of the substrate of the Al sheet

An Al sheet (99.9% pure) was initially annealed at 450°C for 3 h for reducing the mechanical stress then degreased in 0.75 M NaOH at 70°C for 30 s, the sheet was then rinsed in acetone and deionised water ultrasonically for several minutes. Then the sample was electropolished at a constant voltage of 20 V in a solution mixture of perchloric acid and ethanol ($HClO_4$:C_2H_5OH=1:4 v/v) at current density > 300 mA/cm^2 for 1 min at temperature below7°C. After electro polishing, the sample was rinsed again in acetone then deionised water ultrasonically for several minutes. Scan electron microscopic image of Al surface after the electropolishing for 60 s is shown in Fig. 4.1.

.

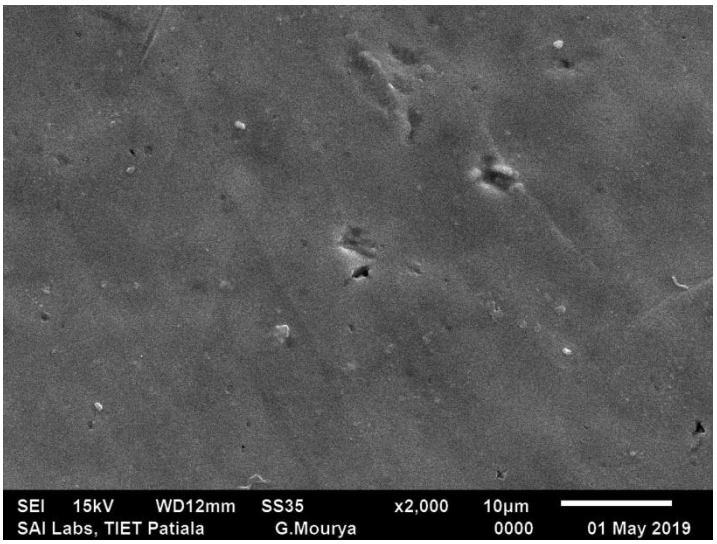

Fig. 4.1 Scan electron microscopic image of electropolished Al sheet for 60 s.

Electropolishing was done for reducing the surface roughness and for the generation of controlled nano pores. The density and the depth of the nano pores in the Al sheet depend upon the current density and duration of the electropolishing [137-140]. The variation of thecurrent density with time during the electropolishing for three different samples for 60 s are shown in Fig. 4.2. In electro polishing, the Al atoms are removed uniformly. Consequently, in a very short period of time, the current density achieves minimum value and

then becomes constant. The nature of the variation of the current during the electropolishing of the three samples was found to be almost similar.

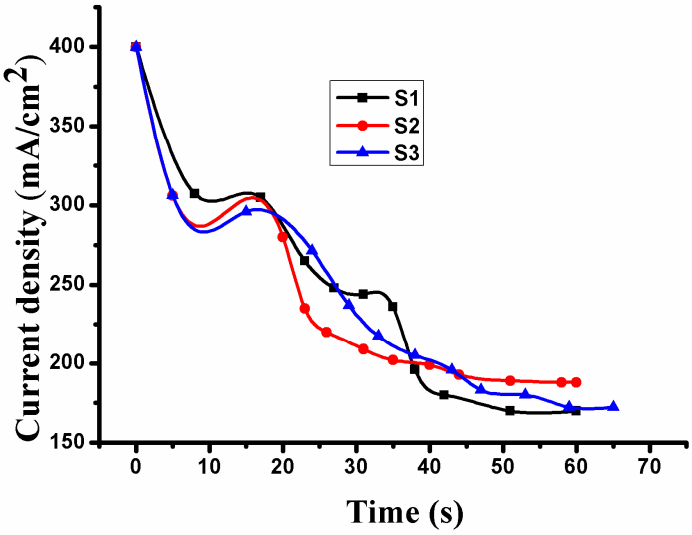

Fig. 4.2 Current density characteristics curve of Al surface at 20 V DC for 60 s.

4.2.2 Anodization of the electropolished samples

The porous anodic aluminium oxide type layer of hexagonal order was developed by the anodization process. Anodization parameters were (i) the current density (ii) concentration and the type of electrolyte solution and (iii) the anodization time. Initial resistance of the Al sheet is also important. For the anodization, 60 mL of oxalic acid of different molar concentration was prepared in 100 mL beaker and placed in a polysterene container filled with grated ice. Ice cubes were used to reduce the temperature of the electrolyte. The temperature of the electrolyte was continuously monitored using a thermometer. As the temperature of the electrolyte reached 10°C, the platinum plate, which acts as the cathode was dipped along with the electro polished Al sheet acting as the anode into the electrolyte. The anodization was carried out at constant voltage and constant current for 1 h and 30 s. To maintain the constant voltage and the constant current, Agilent power supply was used. The size of the pore is the function of anodization voltage, choice of the electrolyte used, molar concentration of electrolyte, anodization temperature and anodization time [191-193]. Fig. 4.3 shows the schematic diagram of the experimental setup for the anodization. Three samples of Al sheet under three different anodization parameters were anodized to obtain the different morphology of the samples. The anodization parameters of the three samples are shown in Table 4.1. The pre-treated sample and the platinum plate were separated by a distance of approximately 3 cm as shown in Fig. 4.3.

Sample (S1) was anodized in 0.20 M oxalic acid solution at 40 V, 5.5 mAa/cm^2 for 1 h and 30 s. Sample (S2) was anodized in 0.3 M oxalic acid solution at 40 V, 4 mA/cm^2 for 1 h and 30 s. Sample (S3) was anodized in 0.3 M oxalic acid solution at 60 V, 15 mA/cm^2 for 1 h and 30 s. The rinsing of the samples was done by deionised water. As the Al sheet was immersed in the electrolytic solution, it was anodizedon both sides. Hence, a porous Al_2O_3 film was formed on both sides of the sheet.

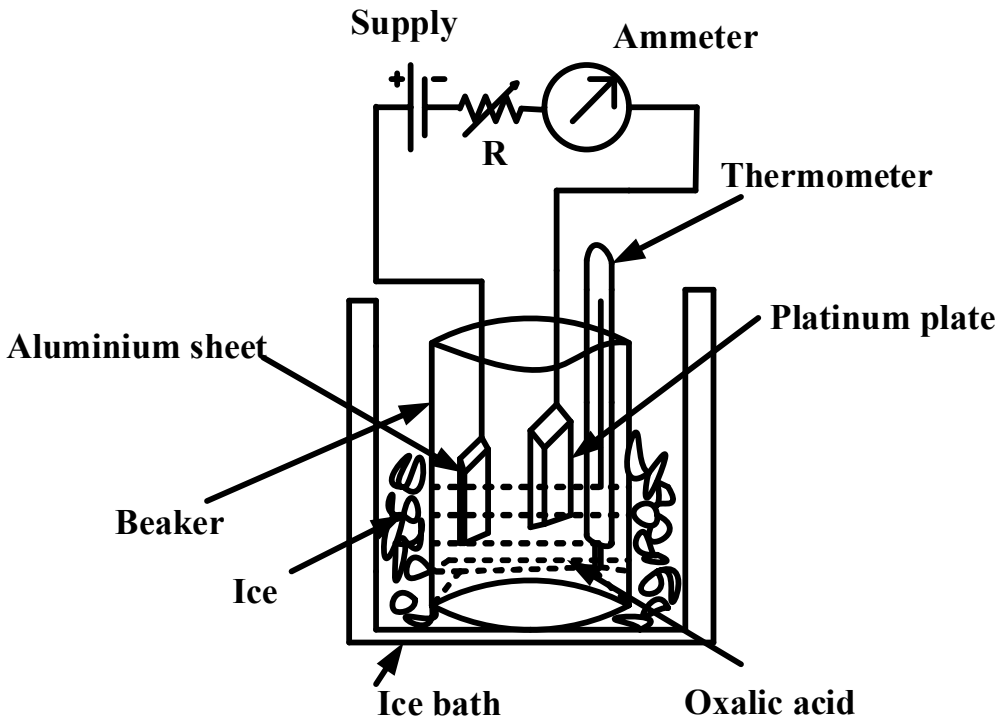

Fig. 4.3 Schematic diagram of the experimental setup for the anodization.

Table 4.1

Anodization Parameters

Sample	Electrolyte	Molar Concentration	Time (s)	Anodizing Voltage (V)
S1	Oxalic Acid	0.20 M	90	40
S2	Oxalic Acid	0.3 M	90	60
S3	Oxalic Acid	0.3 M	90	40

After anodization, deep pores of almost uniform distribution were created on each side of the Al sheet. A thin barrier type film over the metallic surface at the bottom of each pore was formed. Thickness of the metal oxide film on each side was approximately 0.3 µm. Between these two oxides films, there was bulk metal sheet of approximately 200 µm, which was

remained unoxidized. This unoxidized Al sheet used as the common electrode of the two capacitors fabricated on each side. The size of the anodized sample was 10 mm × 10 mm. The porous film and the pore wall are made of amorphous aluminum (Al_2O_3) [108-109].The oxide film in acid electrolyte grows due to local chemical dissolution at the oxide/electrolyte interface due to the presence of high electric field. During anodization, the Al^{3+} ions migrate from the Al surface at the metal/oxide boundary to the barrier oxide layer at the bottom of the pores. The stoichiometry equation is given by (4.1).

$$Al(s) \rightarrow Al^{3+}(oxide) + 3e \qquad (4.1)$$

Due to the presence of water in the solution at the interface, O^{2-} ions are formed as the O^2 (oxide) and these ions migrate to the barrier layer. The stoichiometry equation is given by (4.2).

$$\frac{3}{2}H_2O(l) \rightarrow 3H^+(aq) + \frac{3}{2}O^{2-}(oxide) \qquad (4.2)$$

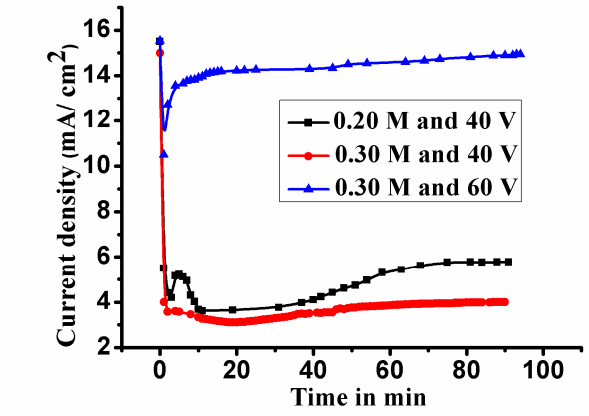

Fig. 4.4 Variation of current density with time in anodization.

In the presence of electric potential, when the size of the pores is small, electrolyte penetrates into the pores, then the pores growth become self-catalyzing. The ordering of the pores is hexagonal and it is achieved by the horizontal mobility of the ions at the barrier layer [90]. Variation of the current density with time for different samples is shown in Fig. 4.4. It shows that within very short period (Ò 5 min), the current density reaches the minimum value. Due to the fast rate of oxide formation, the resistance of the aluminium sheet increases rapidly. Once the current reaches to the minimum value, it then increases slightly due to dissolution of part of the oxide layer causing reduction of the resistance by small value. The current value then becomes almost constant. At this period, the rate of formation of the oxide layer is

almost equal to the dissolution of the oxide layer. At the bottom of the pores, local temperature of the sample rises that leads to non-uniform dissipation of heat and consequently, fluctuation of the anodizaton current occurs. The dissolution process is acid catalyzed. The protons for the dissolution are liberated from the electrolyte and splitting of the water molecules at the oxide-electrolyte interface. The chemical equation for the dissolution is given by (4.3).

$$\frac{1}{2}Al_2O_3(s) + 3H^+(aq) \rightarrow Al^{3+}(aq) + \frac{3}{2}H_2O(l) \tag{4.3}$$

Migration of the hydronium ions also occurs towards the cathode to complete the electrochemical circuit. It can be represented by (4.4).

$$3H^+(aq) + 3e \rightarrow \frac{1}{2}H_2(g) \tag{4.4}$$

The electrochemical anodization of the metallic sheet leads to the formation of the nanoporous structure of aluminium oxide.

4.2.3 Pore Morphology of the Sensing Film

Porous layer formed by the anodization is used to fabricate the capacitive sensor for humidity measurement over wide range. Pore morphology is important for the desire response parameters of the sensors. Pore morphology of the porous oxide layer was studied by Xray diffraction (XRD) study and the scan electronic microscopic image (SEM). The X-ray diffraction pattern of three different anodized aluminium samples are shown in Fig. 4.5. From the diffraction pattern, it is observed that Al_2O_3 and Al phases are present in the anodized samples. It conforms that after anodization, the porous Al_2O_3 layer was formed on both side of the Al sheet. Xôpert high score plus (version 2.0) software was used to identify the peaks. Fig. 4.5 indicates that the aluminium peaks appeared at 2ɗ = 44.48º, 64.88º and 78.03º and Al_2O_3 peaks were observed at 2ɗ =38.29º. The locations of the occurrence of the phases of Al and Al_2O_3 in three anodized samples are consistent.Pore morphology of the oxide film such as the pores size, the distribution of the pores and the thickness of porous layer depend on the anodization parameters. The scan electron microscopes image of the aluminium oxide film obtained after the first stage anodization of Al sheet at different anodization parameters are shown in Fig. 4.6.The anodization parameters are shown in table 4.1.

The image shows that the grown pore is not regular and some of the pores are combined together to form the bigger size pores.

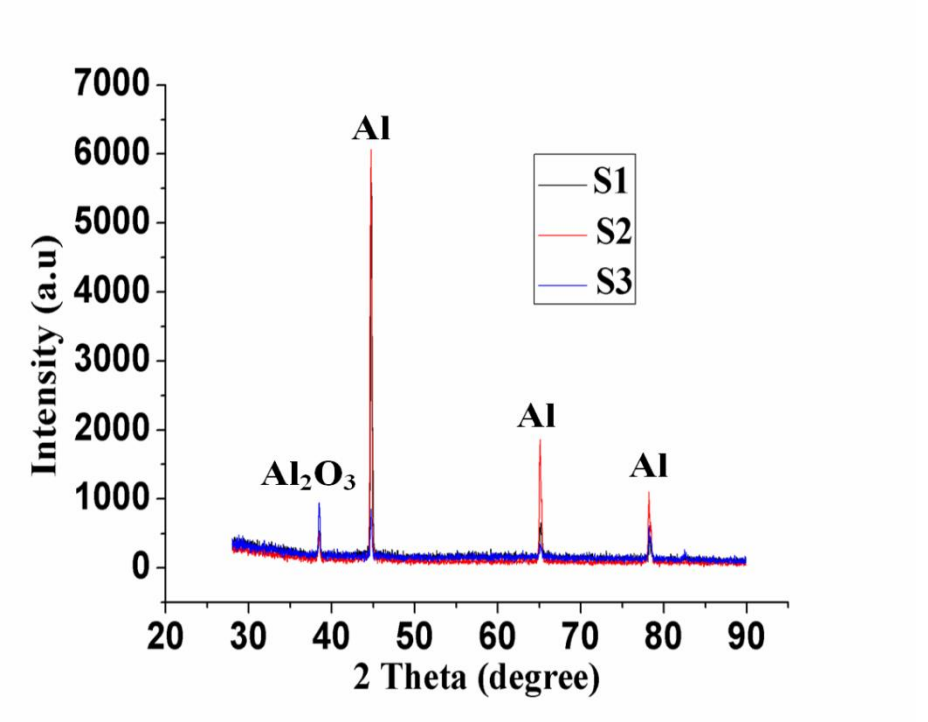

Fig. 4.5 The X-ray diffraction pattern of three different anodized aluminium samples.

The average pore diameter of the grown Al_2O_3 through the anodization of 0.2 M oxalic acid at 40 V, 5.5 mA/cm^2 for 90 minutes is 262 nm. The average pore diameter of the Al_2O_3 was noticed 20 nm, when anodization was carried out at 0.3 M oxalic acid at 60 V, 15.5 mA/ cm^2 for the duration of 90 min. The average pore diameter of Al_2O_3 was obtained 10 nm, when anodization was carried out through 0.3 M oxalic acid at 40 V, 4 mA/cm^2 for the duration of 90 min. The pore diameter of the grown Al_2O_3 highly depends upon the molar concentration of the electrolyte and anodization voltage. As the molar concentration of the electrolyte decreases, the average pore diameter of the Al_2O_3 increases. The average pore diameter also depends upon the applied electric field during the anodization. As the anodization voltage increases, the average pore diameter of the Al_2O_3 increases. The thickness of the Al_2O_3 on the Al sheet depends upon the duration of the anodization [90]. The duration of anodization for the three samples are considered same. EDAS spectra with the table of composition of element present in the developed layer of oxide (Al_2O_3) is shown in Fig.4.7.

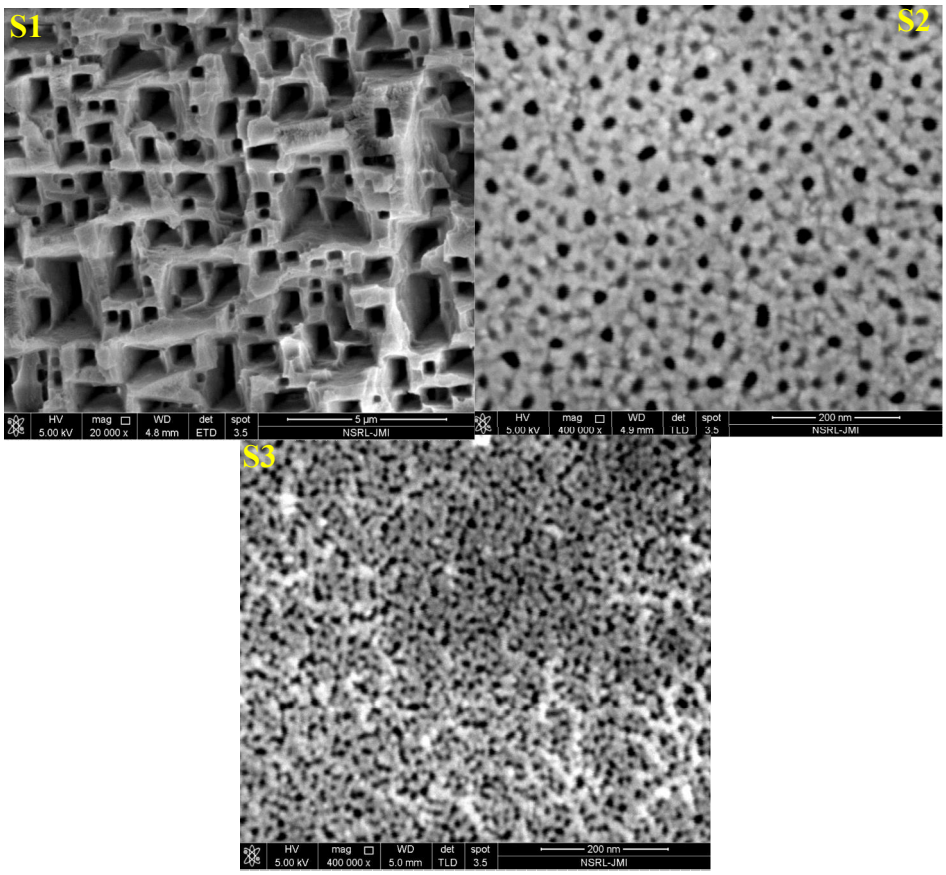

Fig. 4.6 scanning electron microscope (SEM) image of three anodized samples.

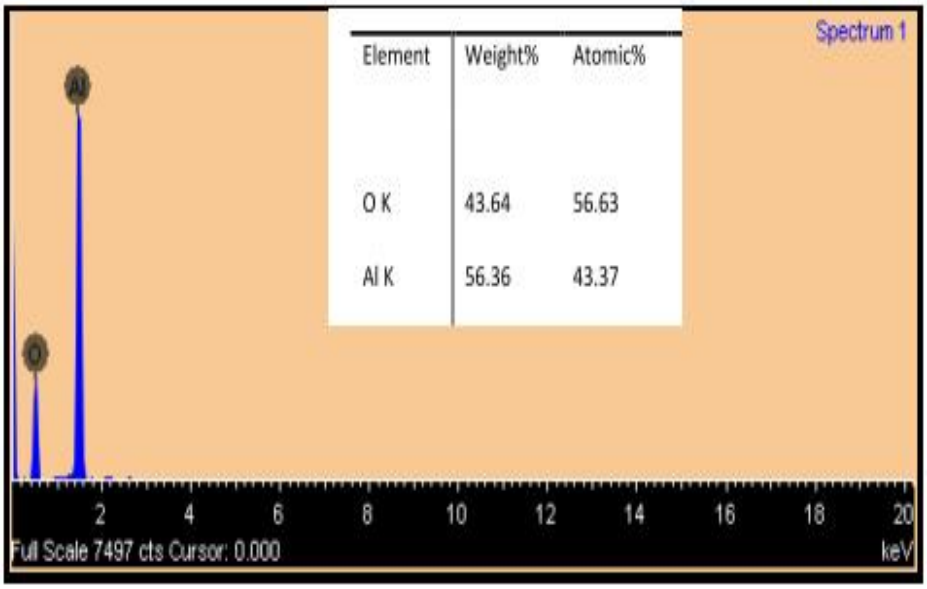

Fig. 4.7 EDAS spectra with table.

4.2.4 Design of the sensor and its fabrication

Fig. 4.8 shows the schematic diagram of the capacitive sensor for humidity measurement. The size of the pure alumina sheet on which the metal oxide layer formed was 10 mm X 10 mm. The size of the anodized oxide film was 5 mm × 5 mm. The oxide layer was formed on each side of the Al sheet.

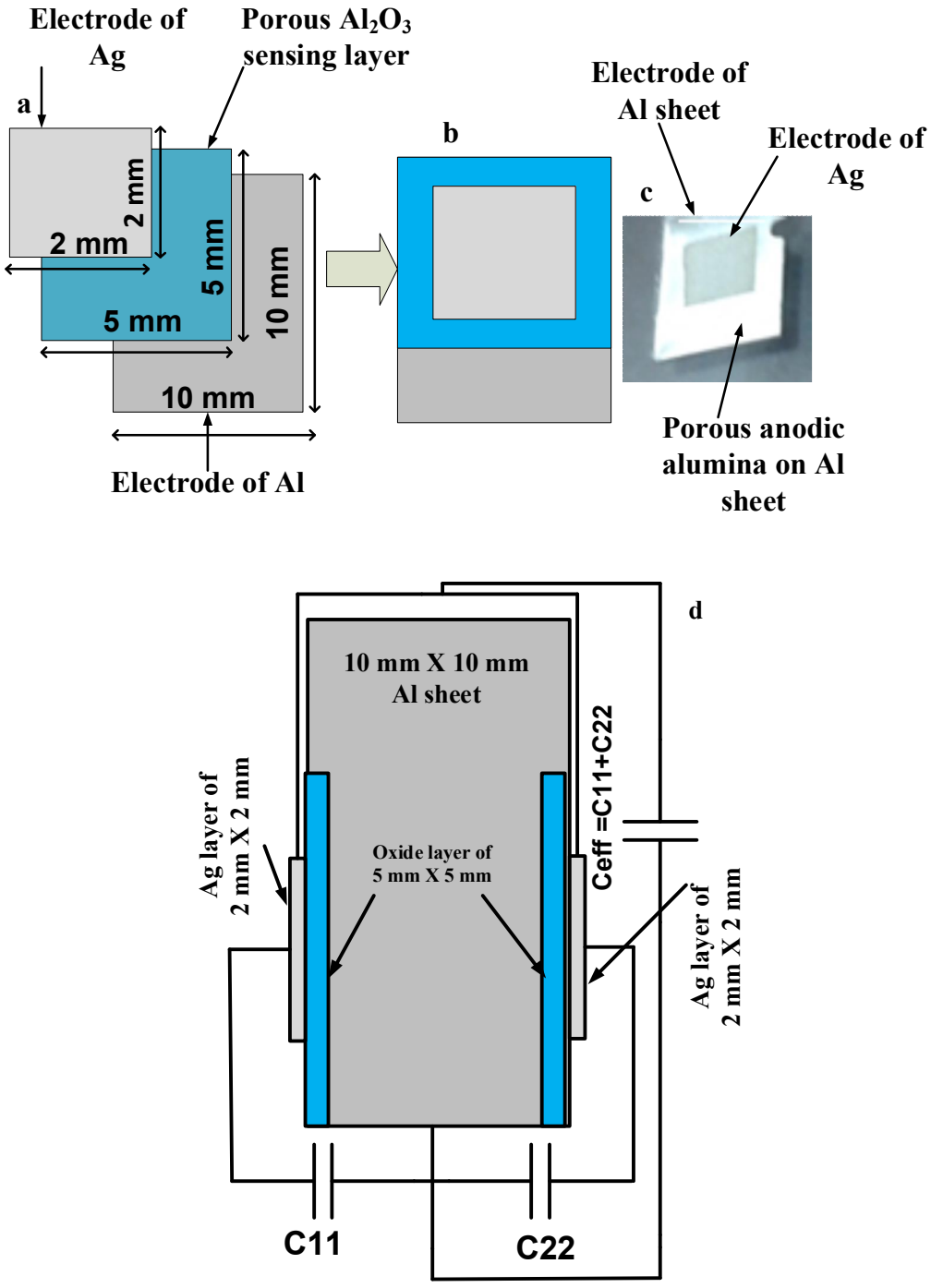

Fig. 4.8 Schematic diagram of the fabricated sensor, (a) lateral view of a sensor fabricated on one side (b) its top view,(c) its photograph (d) when two capacitors are connected in parallel.

The silver metal plates of size 2 mm × 2mm were deposited on the oxide surfaces by manual screen printing method**.** The silver (Ag) electrodes were then sintered at 350°C for 2h. The unanodized Al sheet in the middle of the oxide layers was used as another electrode. Two parallel plate capacitors (C11 and C22) of effective cross-sectional area 2 mm × 2 mm were formed on the oxide surfaces with middle electrode as the common electrode of each capacitor. The size of each capacitor sensor was 2 mm x 2 mm. Finally, the capacitors C11 and C22 were connected in parallel to form the actual capacitor C_{eff} (= C11+C22) to enhance the sensitivity. Coaxial shielded wires were then connected to the three electrodes using silver glue to form the terminal of the capacitor. Fig. 4.8 (b), and 4.8 (c) show the top view and the photograph of the sensor respectively. Fig. 4.8 (d) shows the schematic diagram of the actual sensor when both the capacitors are connected in parallel.

4.3 Experimental setup to determine the response characteristics of the sensor

Experiments were conducted to determine the response characteristics of the sensor with the variation of relative humidity (RH) from 3-97% RH. The sensor was placed in 50 cc steel chamber, which was connected in series to the reference moisture meter [208] through SS pipe. The sensor was then connected to the impedance analyzer (4294A) through the shielded cable.

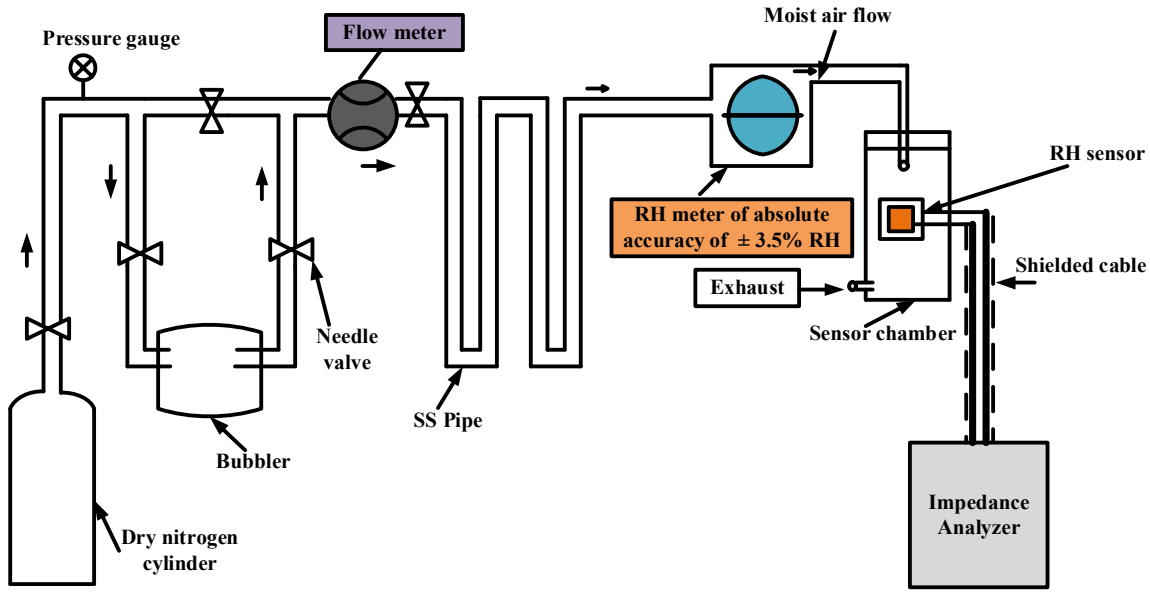

Fig. 4.9 Schematic diagram of the experimental setup.

The impedance analyzer was interfaced to the PC through data acquisition card for the acquisition of the measurement data. The moist air was generated by mixing the dry nitrogen gas (N_2) with distilled water stored in the bubbler. The RH levels were varied by adjusting the

flow rate of wet N_2 and dry N_2 air with the help of precision dialled needle valves. The schematic diagram of the experimental set up is shown in Fig. 4.9. Photograph of the experimental setup is shown in Fig. 4.10.

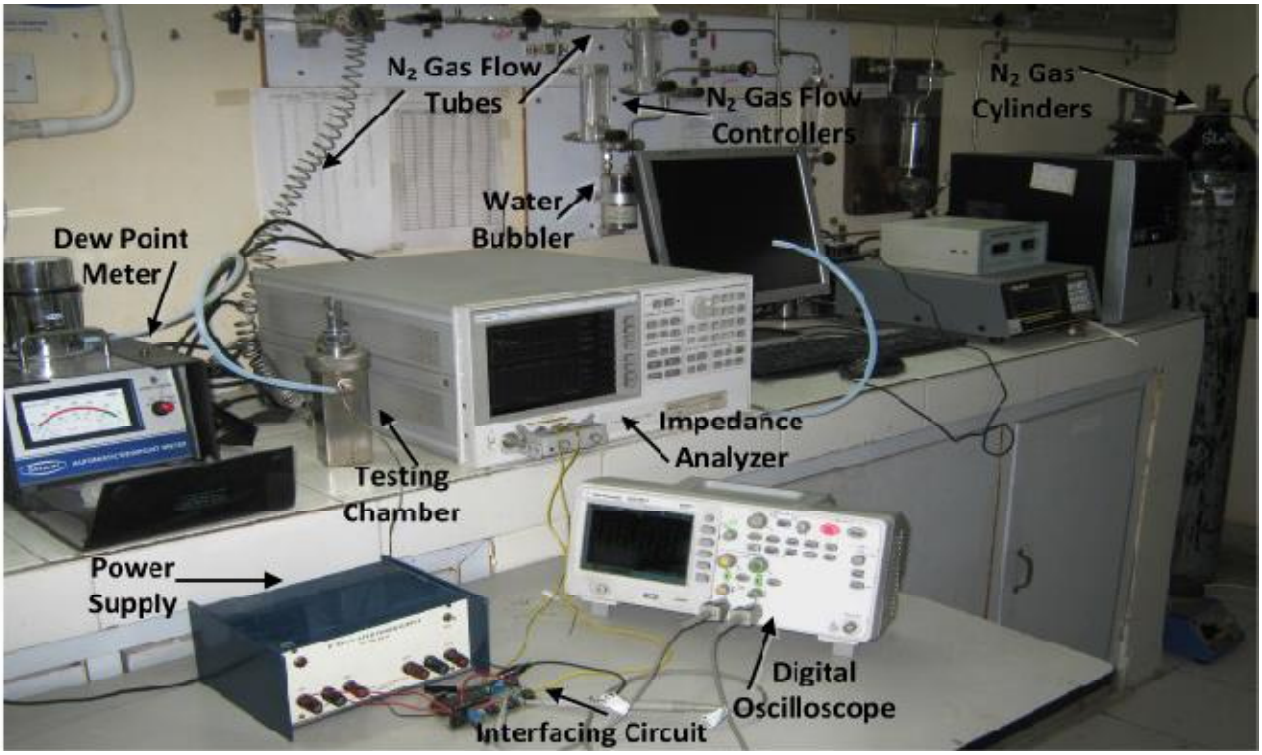

Fig. 4.10 Experimental setup for testing the sensor in different humidity level.

4.4 Electrical Characteristics of the Fabricated Sensor

4.4.1 Capacitive response of the sensor with the variation of relative humidity (%RH)

The capacitance value of the sensor with the variation of humidity was measured with the help of Keysight impedance analyzer (4294A) with the frequency variation in the range of 1-100 kHz. The capacitance value was measured when the RH level in the chamber reached to the steady-state condition for 10 min. The temperature and the pressure of the environmental condition were maintained at 20℃ and 1 bar respectively. The capacitive response of the sensor depends significantly upon the excitation frequency. The change in capacitance value with the variation of humidity level from 3% to 97% RH at different signal frequency of the three sensors are shown in Fig. 4.11. The base capacitance value of the sensors highly depends upon the average pore diameter of the sensing film [123,131]. Due to the largest average pore diameter of the sample (S1) and smallest pore diameter of the sample (S3) among the three samples (S1, S2 and S3), the base capacitance value of the S1 is the smallest and S3 is largest in different excitation frequencies as shown in Fig. 4.11.

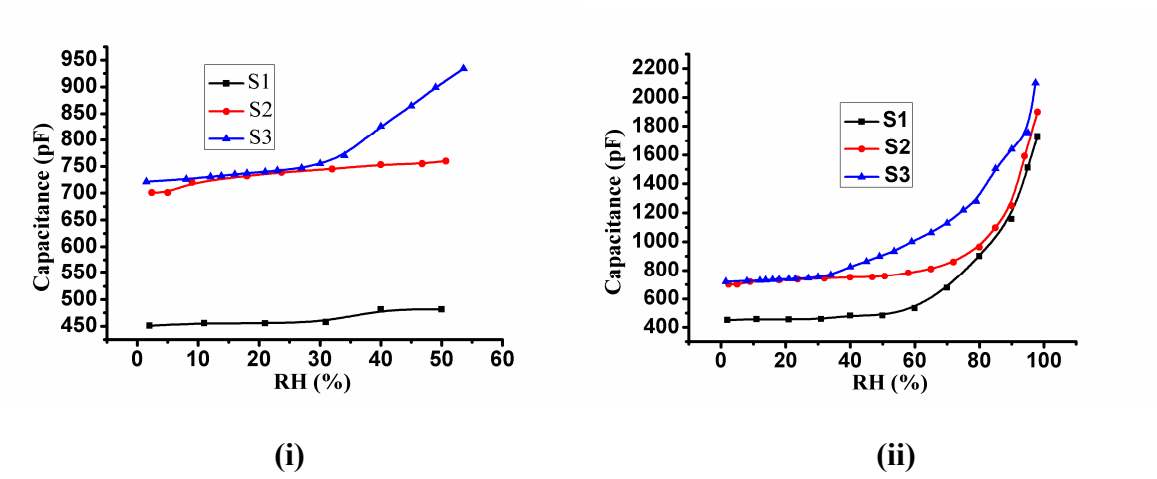

Fig. 4.11a Capacitive response at 1 kHz.

The capacitive response of the three sensors design using the samples (S1, S2 and S3) at the different excitation frequency of 1 kHz, 10 kHz and 100 kHz are shown in Fig. 4.11a, Fig. 4.11b, and Fig. 4.11c respectively. The capacitance value depends on the input signal frequency, and it decreases with increase in excitation frequency. Although, the change in capacitance value at low humidity is small but this change is still significant of the order of several tens of pF. With the help of a properly designed electronic circuit, the capacitance values for the entire humidity range can be converted into the voltage signal. The sensitivity of the designed sensors at 1 kHz excitation frequency is shown in Fig. 4.12. The sensitivity value of the sensors was estimated using (4.5).

$$S = \frac{C(pF)_{moist} - C(pF)_{dry}}{Full\ scale\ RH\ (\%)} \qquad (4.5)$$

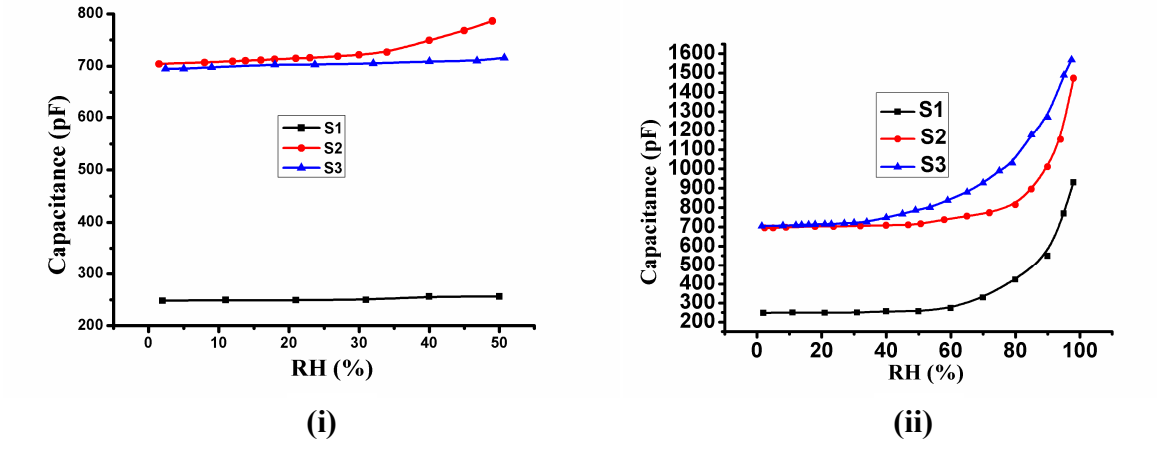

Fig. 4.11 (b) Capacitive response at 10 kHz.

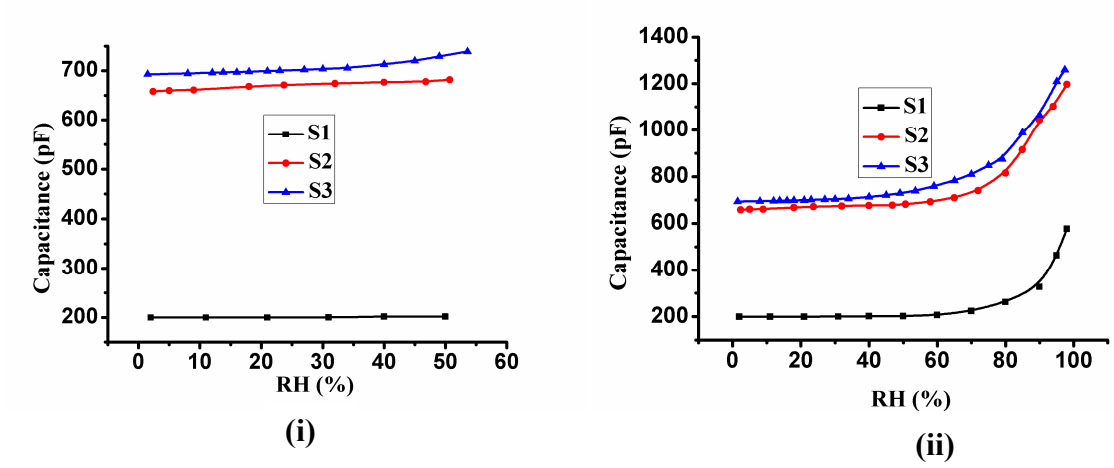

Fig. 4.11 (c) Capacitive response at 100 kHz.

From Fig. 4.12, it is noticed that the sensitivity of the sensor (S1) is zero below 20% RH. It indicates that there is no change in capacitance value below 20% RH. It means that the sensor is not suitable for the measurement of humidity below 20% RH. The sensitivity between 20% RH to 30% RH and 40% RH to 50% RH decreases; it indicates the smaller change in capacitance value of the sensor with respect to the change in humidity level. Sensitivity between 50% RH to 98% RH increases continuously. It shows that the sensor is highly sensitive above 50% RH.

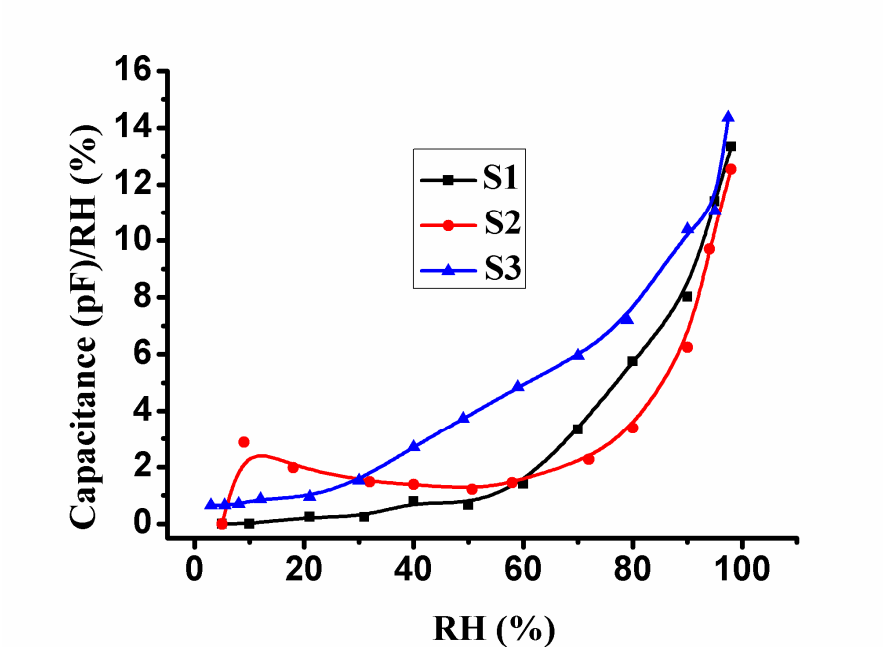

Fig. 4.12 Sensitivity of the sensors at 1 kHz excitation frequency.

The sensitivity of the sensor fabricated using the sample (S2) decreases between 10% RH to 50% RH. It indicates the smaller change in capacitance value as the humidity level increases

in the air till 50% RH. Above 50% RH, it increases continuously upto 98% RH. It shows that the sensor is sensitive in the range of 10% RH to 98% RH. However, the sensitivity below 50% RH is smaller than that of above 50% RH. The sensor is not suitable for detection of humidity level below 5% RH as it shows flat response. The sensitivity value of the sensor (S3) increases from 3% RH to 98% RH continuously. It indicates that it is highly sensitive in the range of 3% RH to 98% RH. The sensor was found sensitive from dry conditions to 98% RH.

4.4.2 Hysteresis error

Hysteresis is considered as an important phenomenon of the humidity sensor. It occurs due to the incomplete adsorption and desorption of the water molecules in the sensing layer. When a sensor is used for the detection of the humidity in any environment, the humidity level can increase or decrease with time. Ideally, the capacitive response of the sensor should be same in the same humidity level for both increase and decrease in %RH. To study the hysteresis error of the sensor, the sensor was explored to both increase and decrease in %RH. Humidity level was initially increased from low to high value gradually, then decreased from the high value to the initial low value. The capacitance value was noted for increase and decrease in humidity. The hysteresis effect was studied with the variation of humidity from 3 %RH to 97 %RH. The variation of the capacitance value of the three sensors S1, S2 and S3 at 1 kHz frequency are shown in Fig. 4.13

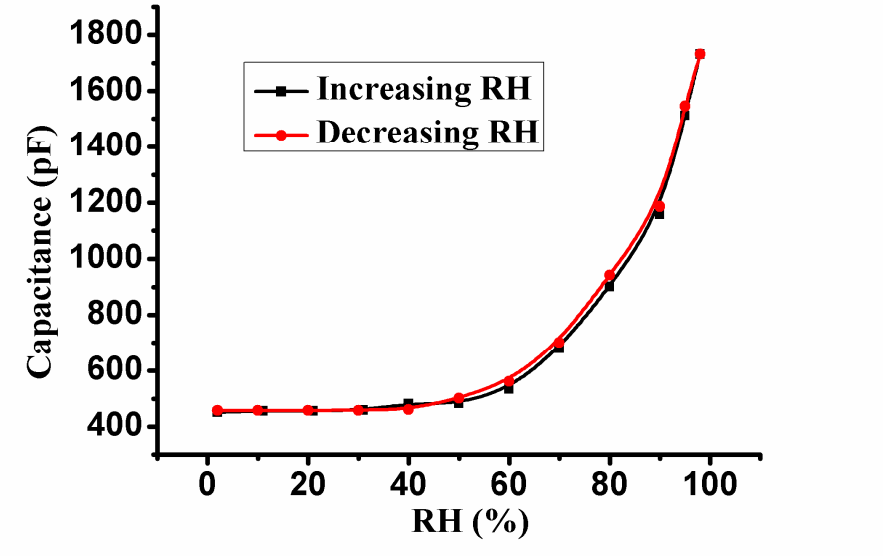

Fig. 4.13a Hysteresis curve of sensor (S1) for increase and decrease in RH level.

. The results show the negligible hysteresis errors in the responses of the sensors. The maximum deviation in the capacitive response in forward and reverse direction of humidity change in the range of 3% to 97% RH is approximately 3.5%. The hysteresis error was calculated using the expression (4.6).

$$Hysteresis\ error = \frac{C_{increase\ in\ RH} - C_{decrease\ in\ RH}}{C_{increase\ in\ RH}} * 100 \quad (4.6)$$

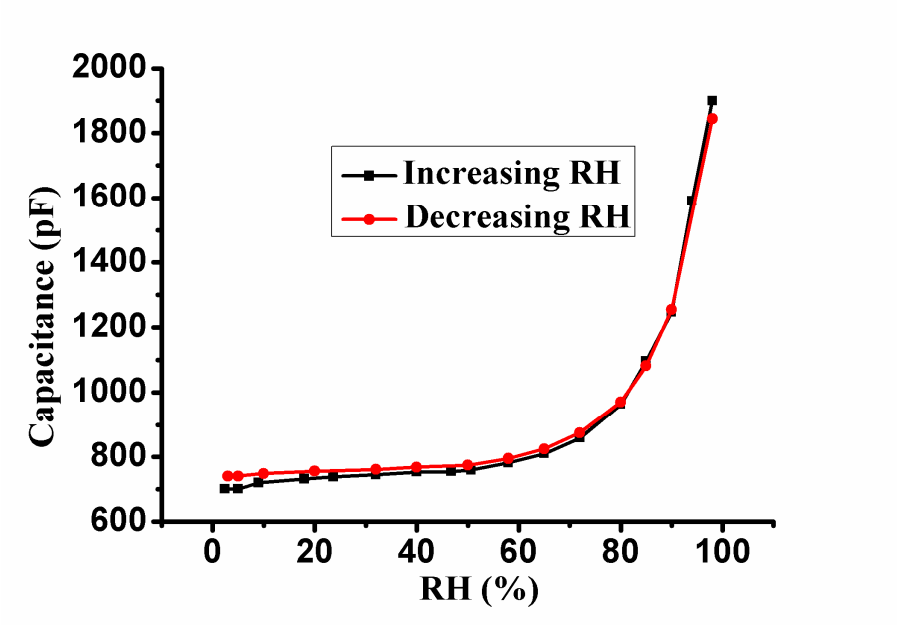

Fig. 4.13b Hysteresis curve of sensor (S2) for increase and decrease in RH level.

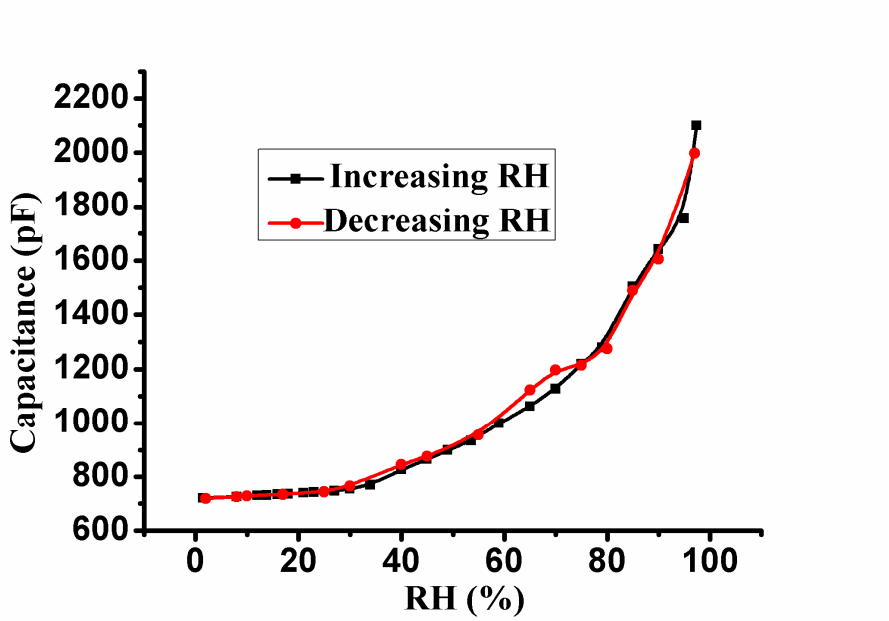

Fig. 4.13c Hysteresis curve of sensor (S3) for increase and decrease in RH level.

The hysteresis error of the sensors S1, S2 and S3 at 40% RH were found to be 3.52%, 1.99% and 2.30% respectively. Small hysteresis may be due to large pore size in the film. Water molecules are easily adsorbed during increase in humidity and desorbed during decrease in humidity. The response characteristics of the sensor S3 was found suitable for the breather application.

4.4.3 Transient response

Response and recovery time are important parameters of the humidity sensor. It is determined from the dynamic response of the senor in sudden step change in the humidity level. The response time indicates the time required for the sensor to change the output from 10% to 90% of its maximum value. Recovery time is the time required for the sensor to return from the maximum value to 10% of its initial value. Fig. 4.14 is the transient response of the sensor (S3) prepared through the anodiaztion in 0.3 M oxalic acid at 40 V. The response and recovery time of the sensor at 1 kHz frequency for detecting the humidity level from 20% to 50% RH is 27 s and 40 s respectively. The sensor was exposed to the step change in humidity from 20 to 50% RH repeatedly. The capacitive response of the sensor at 1 kHz frequency measured through the impedance analyzer is shown in Fig. 4.15. The designed sensor was found to be highly reproducible. The maximum deviation from the successive peaks was found to be less than 0.5%. Fig. 4.16 is the response of the sensor (S1) prepared through the anodization in 0.2 M oxalic acid.

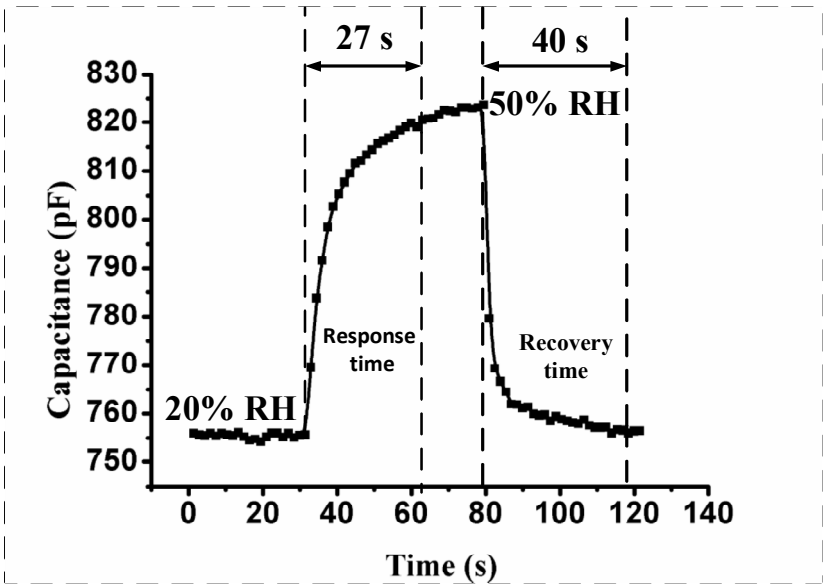

Fig. 4.14 Transient response curve for step change of humidity from 20% to 50% RH.

The response of the sensor for detection of humidity in the range of 40% RH to 65% RH is found to be 12 s and recovery time is 16.5 s. The response was measured at 1 kHz frequency through the impedance analyzer (4294A). The response and recovery time of the sensor is smaller at higher humidity level. It indicates that the sensor is highly sensitive at higher humidity level. The sensor was exposed to the step change in humidity from 45 to 65% RH repeatedly. The reproducibility of the sensor at 1kHz is shown in Fig. 4.17. The maximum deviation in successive peak was found to be less than 0.3%.

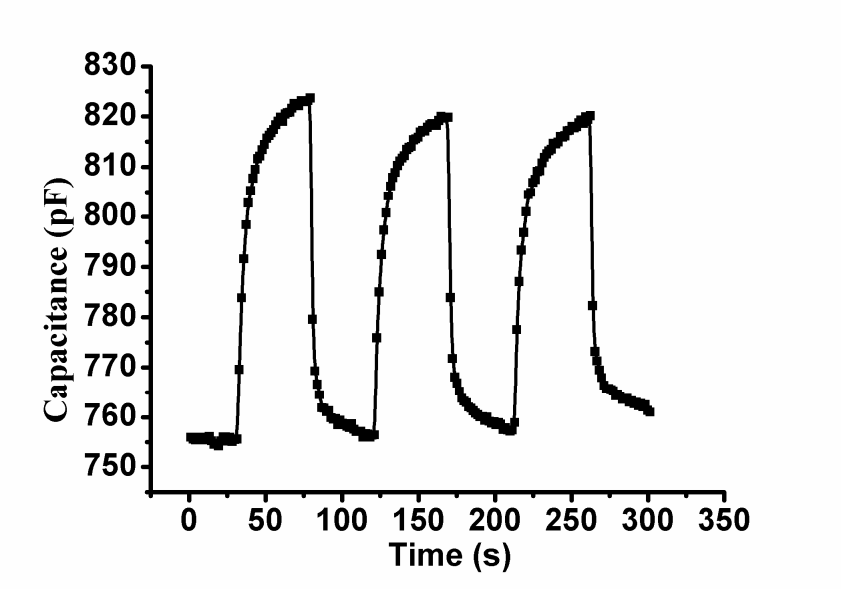

Fig. 4.15 Dynamic response of sensor (S3) to determine the reproducibility of the output from 20% to 50% step change in humidity.

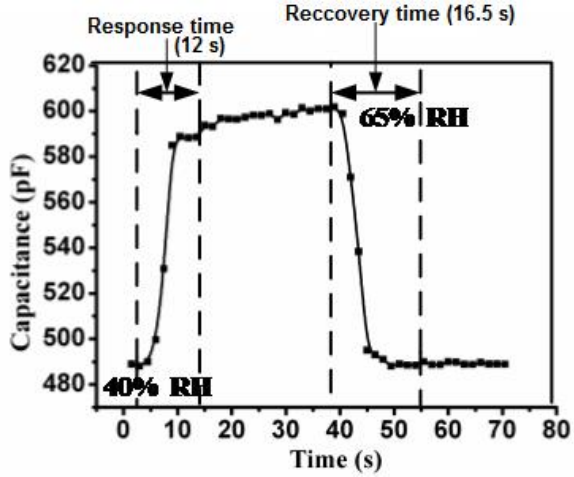

Fig. 4.16 Transient response curve for step change of humidity from 40% to 65% RH.

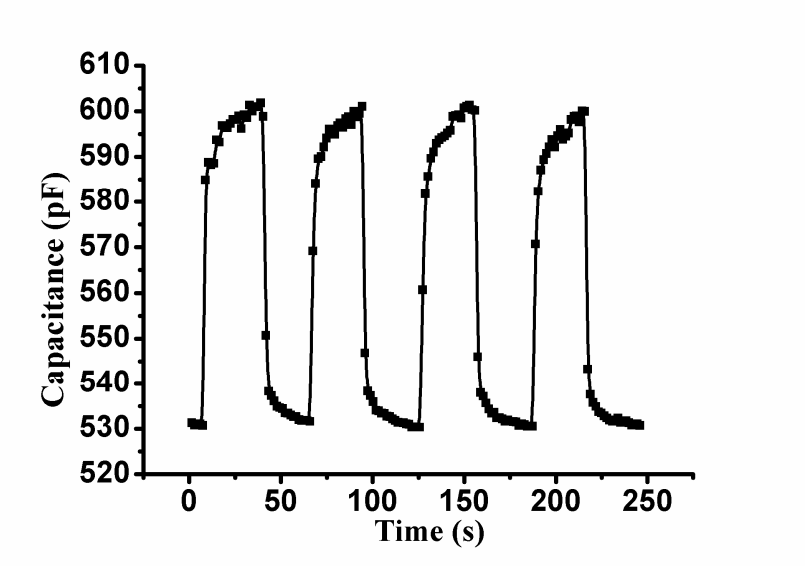

Fig. 4.17 Dynamic response of sensor (S1) to determine the reproducibility of the output from 40% to 65% step change in humidity.

Table 4.2

Electrical characteristics parameters of the designed sensor

Sensor	Molar concentration	Average pore size of film (nm)	Response time (s) @ 1 kHz	Recovery time (s) @ 1 kHz	Hysteresis (%) @ 1 kHz	Measuring range (%RH)
S1	0.20	262	12	16.5	3.52	30-98
S2	0.30	20	-	-	1.99	20-98
S3	0.30	10	27	40	2.30	05-98

4.5 Detection of Moisture in Transformer Oil using Designed Sensor

The sensor fabricated using sample (S3) was used for the measurement of moisture in ppm level. Purpose of this experiment was to measure moisture in T/F oil. The moisture molecules are dissolved in the oil. The concentration may vary but the presence of moisture in the oil is ppm range. In the beginning, the sensor was used to measure moisture in the wet N_2gas with variation of moisture from 0 to 800 ppm. The moisture level in dry N_2 was 3 ppm. The experiment setup shown in Fig. 4.10 was used. Moisture in the range of 3 ppm to 800 ppm was generated by the use of N_2 as a carrier gas. Dry N_2 was mixed with water vapour for generation of different level of moisture in ppm. Water vapour was generated by mixing the dry N_2 in water bubbler. A commercial dew point meter (Model SADP (R), SHAW, U.K.) (range 0-1000 ppm, absolute accuracy= ±1 ppm moisture) was employed to monitor the moisture concentration of the moist gas. Sensor was placed inside the chamber. The moisture level inside the chamber was precisely controlled through the precision valve.

The capacitance change of sensor with moisture (ppm) was recorded with the help of LCR meter at different frequency. The capacitive response of the sensor with different moisture level at different frequencies (1 kHz, 10 kHz and 100 kHz) are shown in Fig. 4.18.

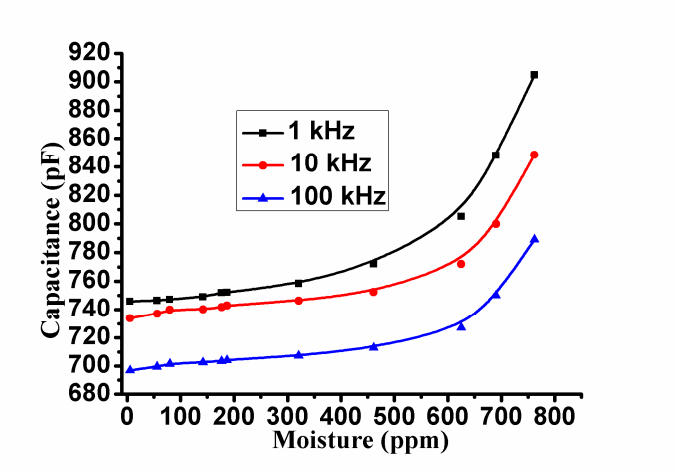

Fig. 4.18 Capacitive response of sensor with respect to moisture (ppm).

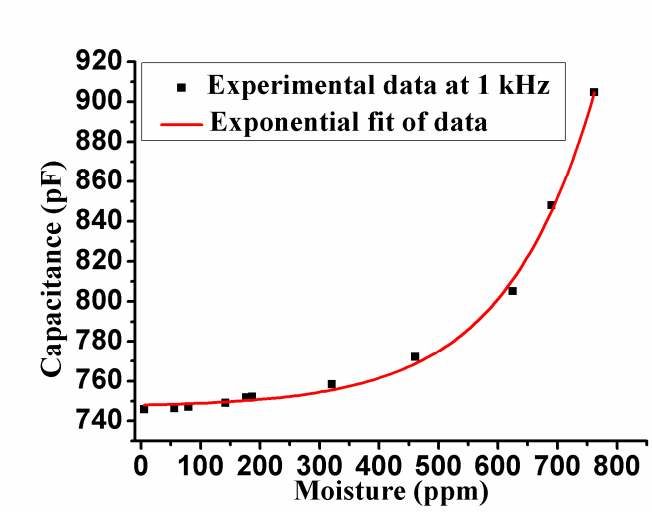

Fig. 4.19 Exponential fit of capacitive response with moisture at 1 kHz frequency.

The capacitance value increases with increase in ppm but the response decreases as the excitation frequency increases. The exponential fit of the capacitive response of sensor with the moisture at 1 kHz frequency was obtained using curve fitting method. The equation of the exponential fit is given by (4.7).

$$C_m = 1.05 \exp\left(\frac{M_{ppm}}{152.283}\right) + 746.82 \qquad (4.7)$$

Where, C_m is the capacitance value and M_{ppm} is the moisture level in ppm.

The exponential fit of the response is shown in Fig. 4.19. The correction coefficient of the curve is 0.9964. Further, the sensor was used for the measurement of moisture generated from the transformer oil at different temperature.

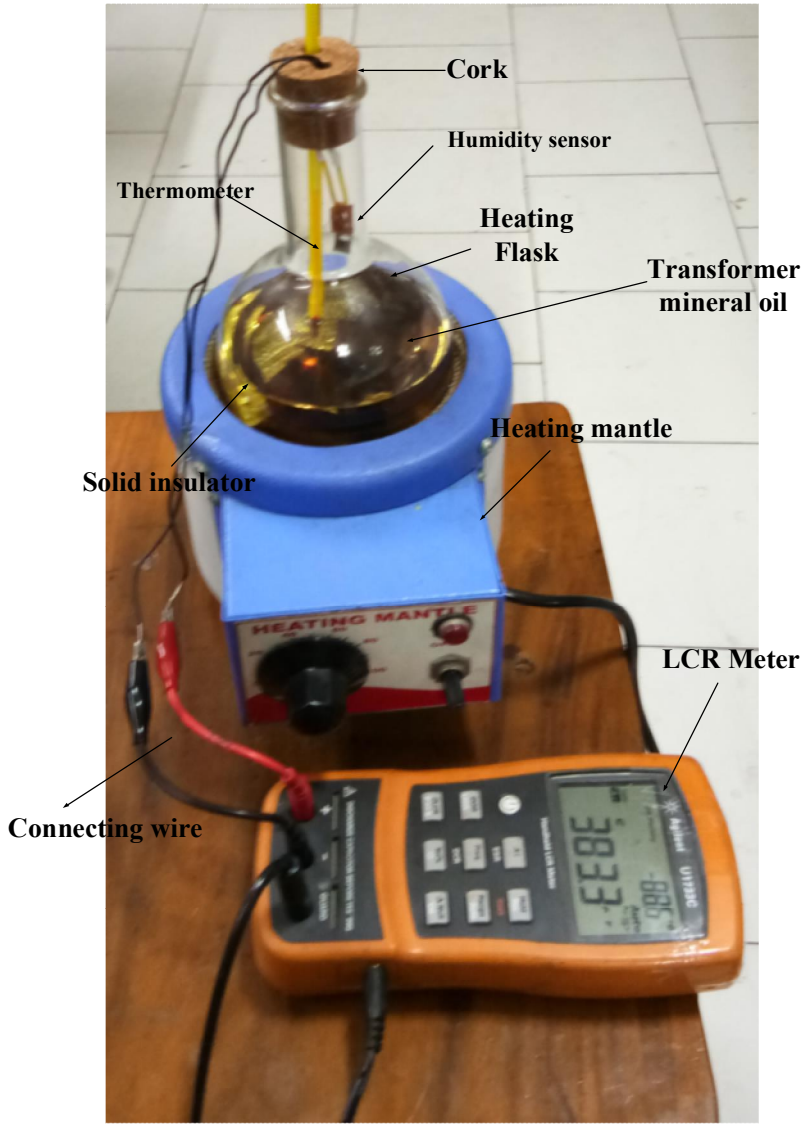

Fig. 4.20 Experimental setup for detection of moisture generated from transformer oil through sensor at different temperature.

The photograph of the experimental setup is shown in Fig. 4.20. The oil was aged for six months. 500 ml of ten years aged mineral oil containing 20 g of dry solid cellulose insulator was taken in a flask. On each day, the oil with paper insulation was heated at 100°C for 12 min. Moisture will distribute between the paper and the oil in a definite ratio at steady state. At equilibrium, the moisture content of the paper is much more than that of the oil. After six months, the sensor was placed in the empty space of the flask having T/F oil. The oil was

heated from 30ŰC to 110ŰC. When the flask was heated, the moisture molecules in vapour form occupy the free space of the flask, where the sensor was placed. Some amount of moisture in the space depends upon the heating temperature or the temperature of the oil. The capacitance change of the sensor was noted with the variation of the temperature of the oil. The oil temperature was measured by the mercury thermometer. The capacitance value was noted only when the temperature of the oil is fixed. The variation of the capacitance with the increase in temperature is shown in Fig.4.21. The curve shows that the capacitance value increases with the increase in oil temperature. From the capacitance value, the amount of moisture in the free space of the flask was determined using (5.7). Due to non-availability of the reference meter to measure in the moisture in oil, moisture concentration was determined indirectly. The variation of moisture with temperature is shown in Fig. 4.21. The sensor successfully measures the moisture present in the oil. Experiment may be conducted by immersing the sensor in the oil, but it was avoided to protect the sensor from sticky oil.

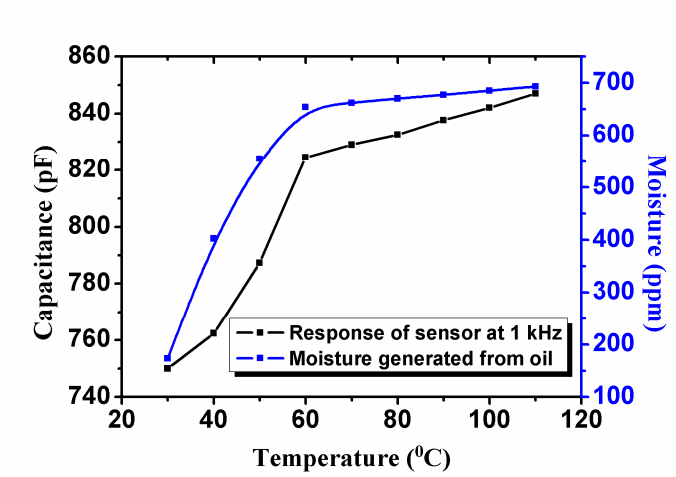

Fig. 4.21 Measurement of moisture in vapour generated through the transformer oil.

5.6 Conclusion

Parallel plate capacitive humidity sensors using electrochemical anodization method were developed. Hexagonally ordered porous Al_2O_3 moisture sensing thin film were developed by the anodization of Al sheet. Poremorphology of the films depends upon the anodization parameters. Grown of Al_2O_3 through anodization was conformed through the XRD pattern of the anodized samples. The pore morphology of the film was studied using scanning electron microscopy of the anodized sample. Average pore size depends upon the molar concentration of electrolyte and applied electric field for anodization. Film thickness depends upon the anodization time. Sensitivity of the designed sensors depends upon the poremorphology of the films. By controlling the poremorphology, different types of humidity sensors for the

detection of different level of relatve humidity (RH) were fabricated. Experiments have been conducted to determine the capacitive response and the hysteresis errors. Maximum hysteresis in the response of the sensor was 3%. The designed sensor was used for absolute measurement of moisture in the range of 172 ppm to 800 ppm. The designed sensor was found to be suitable for the measurement of moisture generated from the transformer oil at different temperature.

Chapter 5

Design and Implementation of an Electronic Circuit for Controlling the Humidity Level of the Breather

5.1 Introduction

To improve the operating life of a T/F, the insulating oil is protected from the excess moisture ingress. Two types of the T/F such as the air breathing type and the hermetically sealed type are used in normal practice. The hermetic type offers more moisture protection over the air breathing type as long as it is properly sealed from air. Due to certain mechanical limitations in the hermetic type, 90% of the transformers across the world are of free breathing type [8, 15-16]. Free breathing T/F having no conservator has the headspace having mixture of gasses above the oil level. This type of the T/F during breathing inhales the differential volume of air from the atmosphere, which contains different percentage relative humidity. Humidity level varies from around 20% RH (on sunny day) to around saturation level (on rainy day) across the world. To protect the oil from the direct contact of air moisture, a conservator tank connected in series with the silica gel breather is placed on the top of the tank. A rubber bladder inside the conservator of the high rated T/F protects oil from the direct contact to the ambient air. However, over the time of the service, the bladder material degrades and gets ruptured and goes undetected due to difficulty in inspection. During breathing, the silica gel crystals inside the breather serve to remove the moisture from the air and transfers the dry air to the transformer. In low rated air-breathing T/F of less than 500 kVA, the conservator has no rubber bladder, so there is a moisture leakage inside the conservator [10, 16, 25, 154]. The size of the breather in liquid cool T/F depends on its rating (MVA), maximum oil content (liters), maximum air space (liters), daily breathing rate (liters) and charge life (days).The daily breathing rate is based on the assumption that the temperature of T/Fdrops twice upto 8°C in 24 h [4]. Types of the silica-gel in the breather depend on the local environmental conditions throughout the year. The silica gel has the finite capacity to absorb the moisture, so, it is saturated and it requires frequent replacement [6]. Due to unpredictable weather condition and transformer loading, it is very difficult to predict the replacement timing of silica gel inside the breather. To avoid the need of frequent replacement and for condition monitoring of silica gel, an auto regenerative dehydrating breather may be an advanced solution. When the humidity in the breather is high, it is isolated from the conservator tank. The silica gel in this breather will be refreshed automatically by the heating process.

To isolate the breather from the conservator tank during the non-breathing period, a dual column breather is required. In this dual column breather, one column always contains dry silica gel available through the auto regeneration principle. In chapter 4, the response characteristics of the three sensors fabricated by anodization method are reported. For better response in the range of 10 to 90 % RH another sensor is fabricated to monitor and control the humidity inside the breather. The designed sensor was found to be sensitive in the range of 10 to 97% RH. The sensor was then interfaced with a phase detection electronics circuit. The output voltage of which varies with the variation of humidity. Another signal conditioning circuit was designed and realized to control the power of the heater, which was used to refresh silica ï gel to maintain the moisture in the breather. Power available to the heating element for dehumidification is controlled using integral cycle control technique. This eliminates the visual monitoring, and the regular replacement of the silica gel. The detail of experimental setup for monitoring and controlling the moisture in the breather is shown in Fig. 5.1.

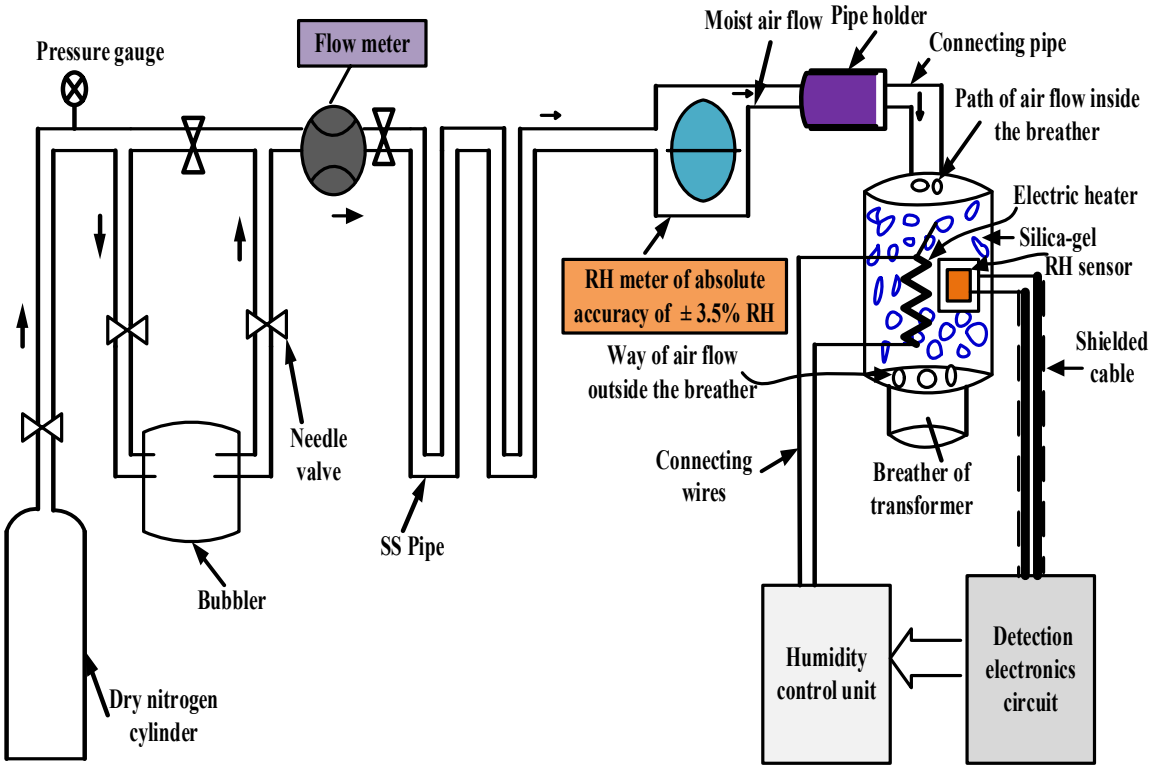

Fig. 5.1 Block diagram of the proposed sensor based experimental set up to measure and control humidity in the breather.

5.2 Fabrication and determination of the response of the sensor

The size of the anodized oxide film was 10 mm × 10 mm. The oxide layer was formed on each side of the Al sheet. The silver metal plates of size 4 mm × 4 mm were deposited on the oxide surfaces by manual screen printing method**.** The silver (Ag) electrodes were then sintered at 350°C for 2h.The unanodized Al sheet in the middle of the oxide layers was used as another electrode. Two parallel plate capacitors (C11 and C22) of effective cross-sectional area 4 mm × 4 mm were formed on the oxide surfaces with middle electrode as the common electrode of each capacitor. The size of each capacitor sensor was 4 mm x 4 mm. Finally, the capacitors C11 and C22 were connected in parallel to form the actual capacitor C_{eff} (= C11+C22) to enhance the sensitivity. Coaxial shielded wires were then connected to the three electrodes using silver glue to form the terminal of the capacitor. Fig. 5.2 (a) shows the schematic diagram of lateral view of the sensor formed on each side of the Al sheet. Figures 5.2 (b), and 5.2 (c) show the top view and the photograph of the sensor respectively. Experiments were conducted to determine the response characteristics of the sensor with the variation of relative humidity (RH) from 3-97% RH. The sensor was placed in 50 cc steel chamber, which was connected in series to the reference moisture meter [24] through SS pipe. The moist air was generated by mixing the dry air with distilled water stored in the bubbler. The RH levels were varied by adjusting the flow rate of wet air and dry air with the help of precision dialled needle valves. The photograph of the experimental setup is shown in Fig. 4.10

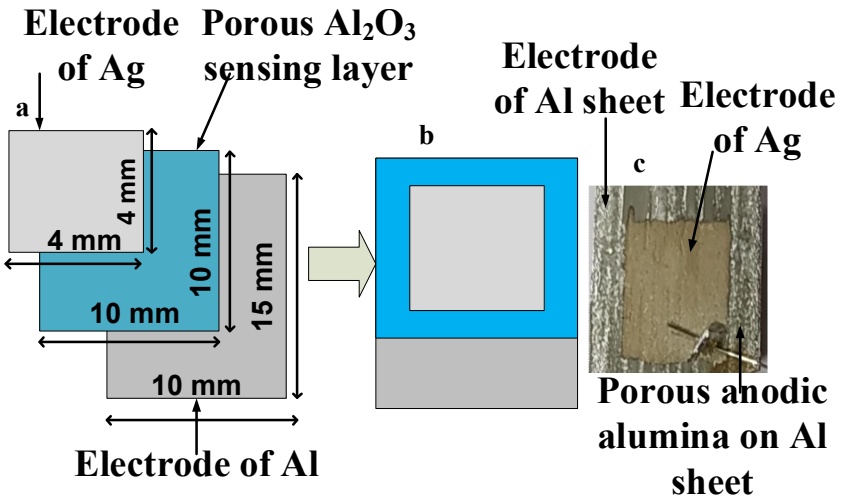

Fig. 5.2 Schematic diagram of the fabricated sensor, (a) lateral view of a sensor fabricated on one side (b) its top view,(c) its photograph.

The capacitance value of the sensor with the variation of humidity was measured with the help of Keysight impedance analyzer (4294A) in the range of 1-100 kHz frequency. The accuracy of the capacitance measurement in the range of 0.5 nF to 460.0 nF is ~ 0.08%. The capacitance value was measured when the RH level in the chamber reached the steady-state condition for 10 min. The temperature and the pressure of the environmental condition were maintained at 20°C and 0.1 bar respectively. The capacitive response of the humidity sensor depends significantly upon the excitation frequency. The change in capacitance value with the variation of moisture level from 3% to 97% RH at different signal frequency is shown in Fig. 5.3. Capacitance change below 40% RH is much smaller than the capacitance change above 40% RH. Fig. 5.3 (a) shows the capacitance variation with humidity from 3 to 40% RH and Fig. 5.3 (b) shows the capacitance variation for the full scale humidity range. The sensor is highly sensitive in the range of 20 to 97% RH. Although, the change in capacitance value at low humidity is small but this change is still significant of the order of several tens of pF. With the help of a properly designed electronic circuit, the capacitance values for the entire humidity range can be converted into the voltage signal. However, the capacitance value depends on the input signal frequency, and it decreases with increase in excitation frequency**.** When the concentration of water vapor increases at high humidity, the clusters size of water molecules increases. Now, it becomes difficult for the clusters to follow the alternately changing electric field. So, the effective dielectric constant of the sensor reduces.

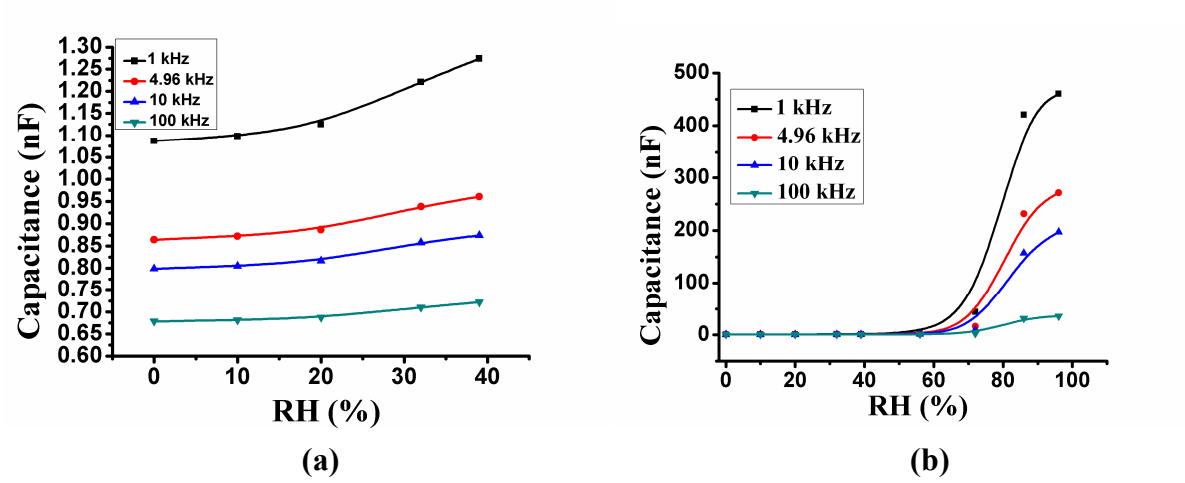

Fig. 5.3 The change in capacitance of the sensor with the variation of humidity.

In addition to this, the dielectric constant of water molecules decreases with increase in frequency.

Relatively high excitation frequency of several kHz is suitable as some of the performance parameters such as nonlinearity and hysteresis are improved at high frequency [61].

5.3 Proposed Electrical Circuit for Controlling the Moisture inside the Breather

The interfacing electronics circuit was used to monitor the response of the moisture sensor in terms of voltage and frequency [163, 179-180]. Complete schematic diagram of the proposed electrical circuit is shown in Fig. 5.4. The circuit was hardware implemented on PCB. The circuit consists of five functional units such as (i) the phase detection circuit, (ii) the signal conditioning circuit, (iii) Arduino microcontroller board for controlling the power of heating element in breather, (iv) the phase-controlled driver circuit and (v) a heater placed in the breather. The heater was connected to an ac supply via a triac. The phase detection circuit was used to generate pulse width modulated (PWM) signal in response of humidity using the capacitive moisture sensor in the breather. As shown in Fig.5.4, the circuit consists of two timer circuits which are implemented by the timer ICs (7556) and one XOR gate (IC 74LS136). One timer IC (7556) contains two CMOS timers (555). One 555 timer is configured as an astable multivibrator circuit and the other one as the monostable multivibrator circuit. In an astable circuit, the output voltage alternates between V_{cc} and zero (0) continuouslyand produces the pulse train in order to trigger the other 555 timer, which operates in PWM mode.The excitation frequency for the sensor in the phase detection circuit was generated using the astable configuration of the timer circuit. Equation (5.1) indicates the frequency of the pulse train obtained from the astable configuration.

$$F_{out} = 1/T = 1.44/\{(R_1 + 2R_2) \times C_1\} \quad (5.1)$$

The component values were selected to generate the oscillating signal of 1 kHz or 42 kHz frequency. The on time period (T_{on}) of the PWM signal was generated through the monostable configuration of the 555 timer circuit. Two PWM signals were generated from dual timer IC (7556).PWM 1 signal was the response of the moisture sensor in the breather at different humidity level and PWM 2 signal was the response at dry condition of the breather. The on time (T_{on}) of the PWM1 signal was proportional to the ambient humidity and the PWM2signal had the fixed T_{on} period. Equation (5.2) can be used to obtain the change in T_{on} period of the PWM 1 signal due to ambient humidity, when exposed to the sensor.

$$T_{on} = 1.1 \times R_3 \times C_{RH} \quad (5.2)$$

The component values of both the timer circuits were selected such that at dry humidity, the duty cycles of both the waves were identical. Therefore, the phase difference between the two output signals was zero. The phase difference between two these PWM signals was detected by the XOR gate. The output of the XOR gate (IC 74LS136) was a pulse wave signal, the width of which is proportional to the ambient humidity. The discrete ceramic capacitance value (C_r), which was equal to the capacitance value of the humidity sensor at dry condition was selected for generating the PWM2 signal. The duty cycle (DC_0) of the PWM 1 signal is given by (5.3).

$$DC_0 = 1.1 \times R_3 \times C_{RH}\left(R_{1`} + 2R_2\right) \times C_{1} \frac{1}{1.44} \tag{5.3}$$

For the PWM1 wave, the conduction period should be greater than the ON time period ($T > T_{on}$). The ON time period changes due to change in the capacitance value of the moisture sensor. The main purpose of this scheme was to control the input power applied to the heater. It has been reported by some work that the response of the oxide sensor is independent of temperature and pressure for certain range [68]. The sensing layer of the sensor is porous aluminium oxide (Al_2O_3). Metal oxide is stable material. Therefore, it isexpected that there will be no influence of the altitude for the response of the sensor**.** The block diagram of the experimental setup is shown in Fig. 5.1. In the breather, the sensor was exposed to the humidity, the capacitance value of the sensor changed. The change in capacitance value caused the change in pulse width of the PWM1 signal. Humidity dependent PWM1 wave was compared with the reference PWM2 wave at dry humidity with the help of digital XOR gate. The XOR output was then converted into DC voltage signal using a low pass filter. Thus, the DC output voltage of the signal conditioning unit varied due to variation of humidity. The obtained DC voltage was applied to the differential amplifier circuit through a unity gain buffer. It was then applied to pin A3 of the Arduino microcontroller (model 2560) board. Equation (5.4) gives the magnitude of the analog DC signal applied to the A3 of the controller. The firing pulses applied to the triac via driver circuit were generated by Arduino mega 2560.

$$V_{out} = \frac{R_7}{R_6} \times V \times \frac{R_7}{\left(R_6 + R_7\right)} - V_{cc} \times \frac{R_8}{\left(R_v + R_g\right)} \tag{5.4}$$

The microcontroller was programmed to generate the PWM signal having fixed conduction period ($T = T_{on} + T_{off}$) at pin 8.

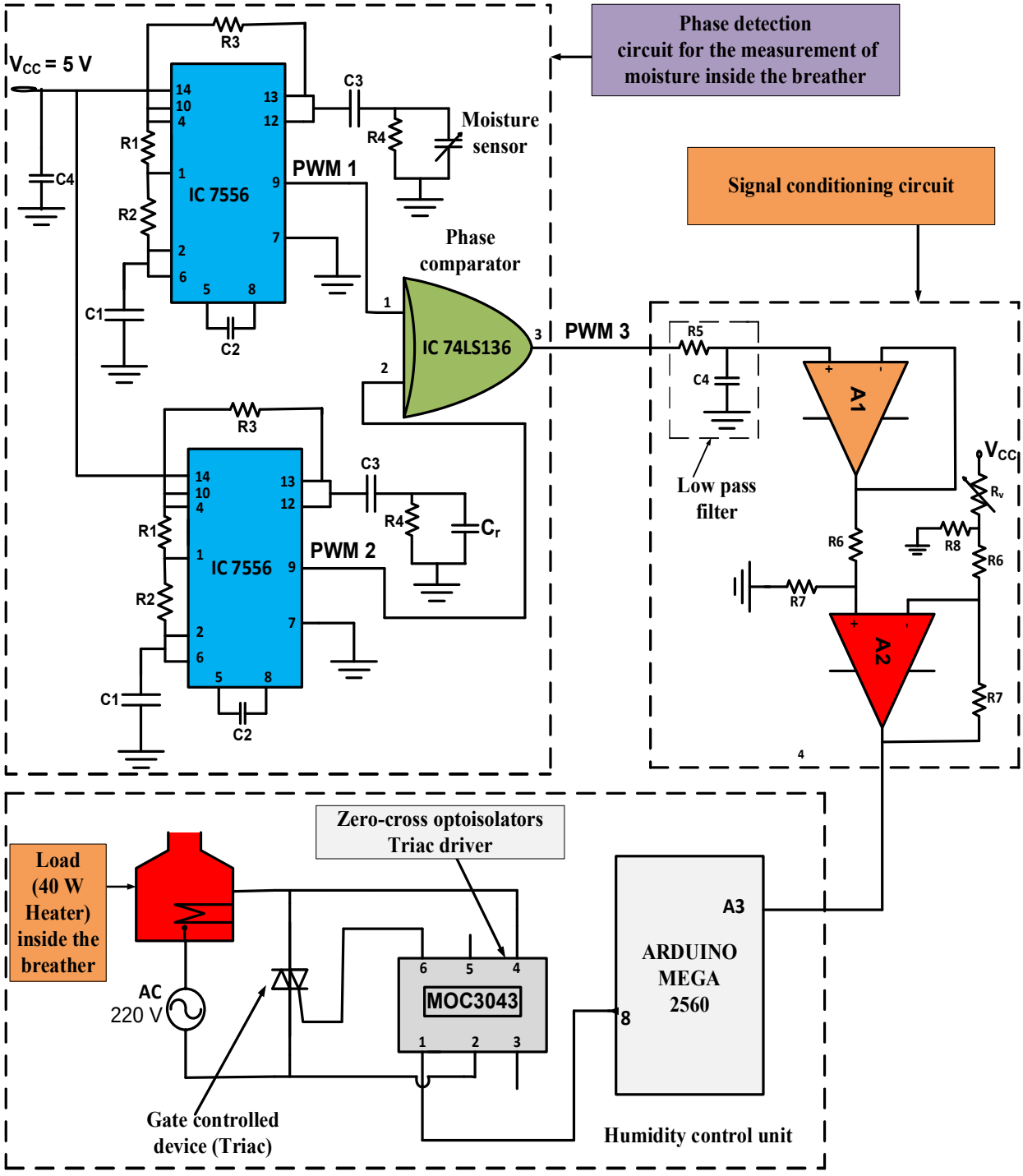

Fig. 5.4 Schematic diagram of microcontroller based integral cycle control dehydrating electrical circuit.

The controller unit produced pulses with duration (T_{on}) equal to the number of ON cycles required for controlling the heater power according to the magnitude of the input analog signal atA3.

The output of the controller at pin 8 was kept low, when the analog input at bit 3was beyond the range of controlled humidity inside the breather. A zero voltage crossing, the bilateral triac driver (MOC3043) was interfaced with the controller and the heater via 220 V AC supply. It provided the desired level of firing pulses to the triac at pin 6 after receiving the input signal at pin 1 from the controller. As T_{on} time of the generated PWM from the controller increased, the number of ON cycles across the load increased. This was the basic phenomena of the integral cycle control [181-183]. Thus, the number of ON cycles of the supply across the load changes according to the ambient humidity. Since, the input power available to the load depends on the number of ON and OFF cycles of the supply voltage, the load will vary according to the humidity. By varying the number of ON and OFF cycles, the output voltage, the load current and power delivered to the load will be regulated as desired. The rms values of voltage (V_{or}), current (I_{or}) and power (P) are given by (5.5), (5.6) and (5.7) respectively.

$$V_{or} = \frac{V_m}{\sqrt{2}}\left(\sqrt{\frac{n}{n+m}}\right) \tag{5.5}$$

$$I_{or} = \frac{V_{or}}{R} \tag{5.6}$$

$$P = \frac{V_s^2}{R}\left(\frac{n}{n+m}\right) \tag{5.7}$$

5.4 Experimental Results of Electrical Circuit

The voltage response of the moisture sensor with humidity was determined in the range of 3 to 97% RH. Fig. 5.1 shows the schematic of the experimental setup to generate the desired humidity level. The fabricated sensor was placed in the test chamber connected in series with the commercial moisture meter. Terminals of the sensor were connected to the interfacing circuit as shown in Fig.5.4. At each humidity level, the voltage signal was measured at least for three times and the average voltage output was plotted. Fig. 5.5 shows the change in output voltage of the circuit with the variation of percentage relative humidity at two signal frequencies. Deviation of the maximum output voltage from the average voltage for three successive measurements at 1 kHz and 42 kHz frequencies are also shown in Fig. 5.5. Two excitation frequencies were generated by the phase detection circuit realized using timer IC 555. The maximum percentage error obtained from the experiment results is 0.5%.

It shows in Fig. 5.5 that as the humidity level increases, the amplitude of the voltage signal increases. However, the sensitivity of the output response depends upon the excitation frequency and it decreases with increase in excitation frequency.

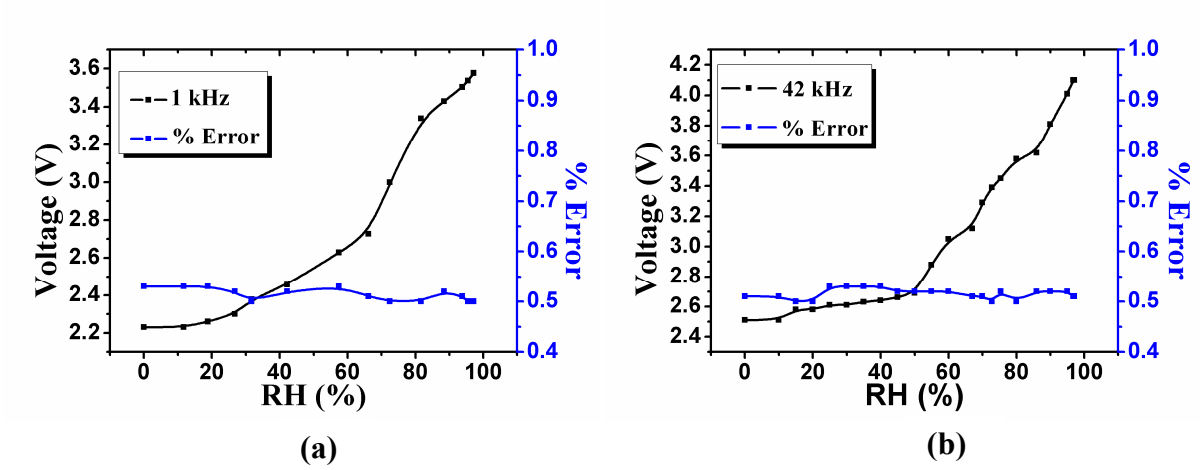

Fig. 5.5 Voltage response of the phase detection circuitwith humidity at two excitation frequencies.

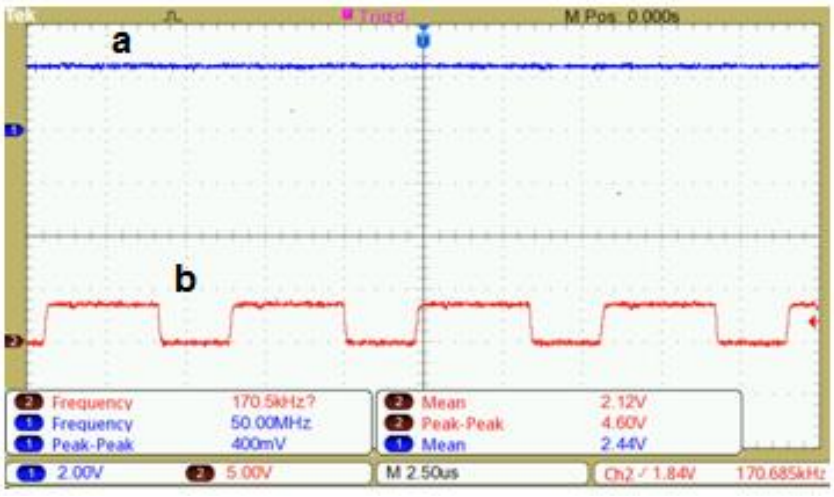

Fig. 5.6 Waveforms at terminals 2 and 4 of the phase detection circuit (Fig.5.4).

But, the decrease in output voltage at 42 kHz frequency compared to the value at 1 kHz is small because of relatively small change in capacitance value. This behaviour confirms that the capacitance value as shown in Fig. 5.3 decreases with increase in signal frequency. The output response is nonlinear, which is mostly observed for the humidity sensors working on adsorption and desorption principle [131]. At high frequency, although the change in voltage is reduced marginally but some parameters such as nonlinearity is also improved.

Fig. 5.6 shows the signal waveforms at terminals 2 and 4 of the circuit, when the sensor was exposed to 60% humidity in the breather.

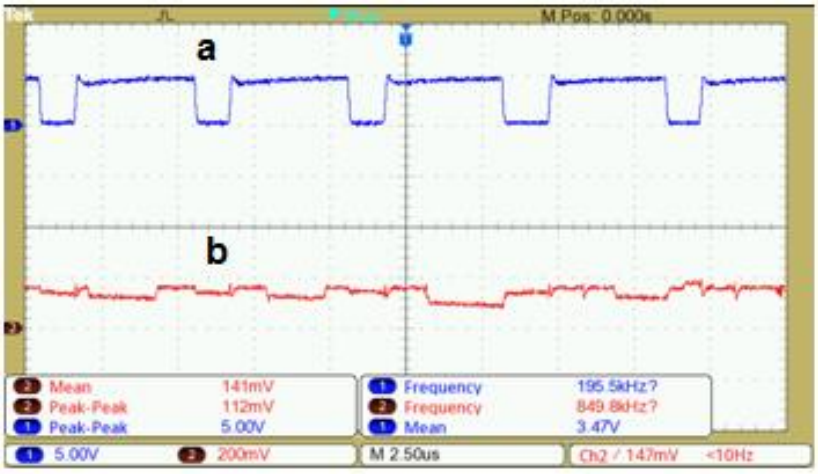

Fig. 5.7 Waveforms at terminals 1 and 3 of phase detection circuit (Fig. 5.4).

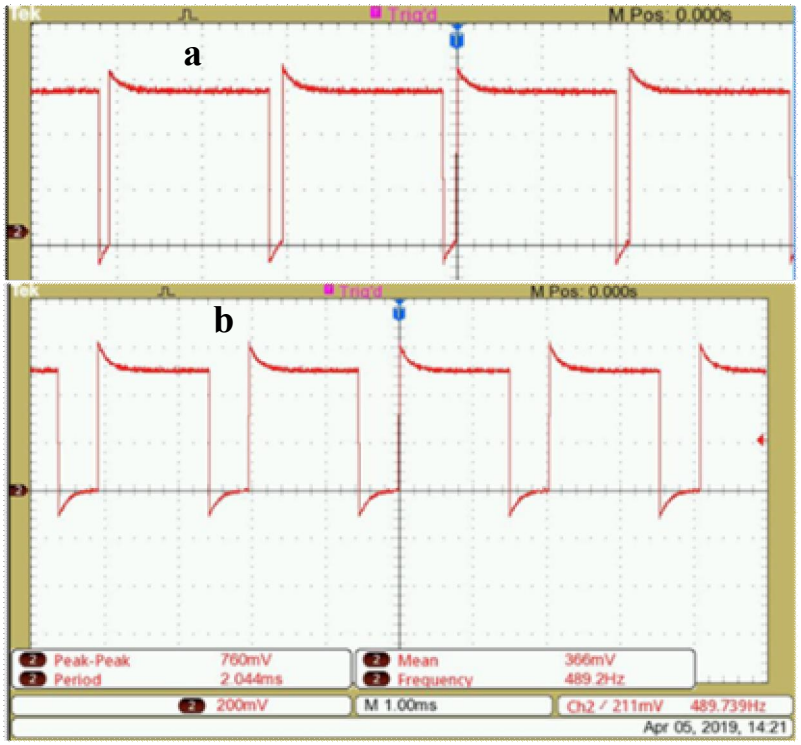

Fig. 5.8 The generated PWM waveforms through the microcontroller at (a) 80% RH (b) 60% RH.

The PWM 2 signal at dry condition of the breather (fresh silica gel ~ 5% RH), at 200 kHz excitation frequency is shown in Fig. 5.6b.

The capacitive value of the sensor measured by the Impedance analyzer at dry condition at 200 kHz frequency was used as the reference value (C_r) for the timer circuit to generate the PWM 2 signal. The PWM 1wave obtained when the sensor was exposed to 60% RH is shown in Fig. 5.7a. When both the signals PWM 1 and PWM 2 were applied to the inputs of the XOR gate, the pulse wave modulation signal PWM 3 was obtained. The PWM 3 signal is shown in Fig. 5.7b. The duty cycle of the PWM 3 signal depends upon the moisture level in the breather. The PWM 3 was converted into dc voltage and properly conditioned and applied to the microcontroller. As the moisture level in the breather increases, the on time (T_{on}) of PWM signal generated through the pin 8 of the arduino 2560 microcontroller also increases. Consequently, the power across the load increases as the number of ON cycles increases and will be obtained by (5.7). The PWM wave generated at 80% RH and 60% RH through the microcontroller is shown in Fig. 6.8a and Fig. 6.8b respectively. The signal across the gate of the triac at 40% RH is shown in Fig. 5.9. The triac is conducting in both of the positive and negative half cycle of the supply. Therefore, triggering signal during the continuous conduction of the triac in both of the positive and negative cycle is available.

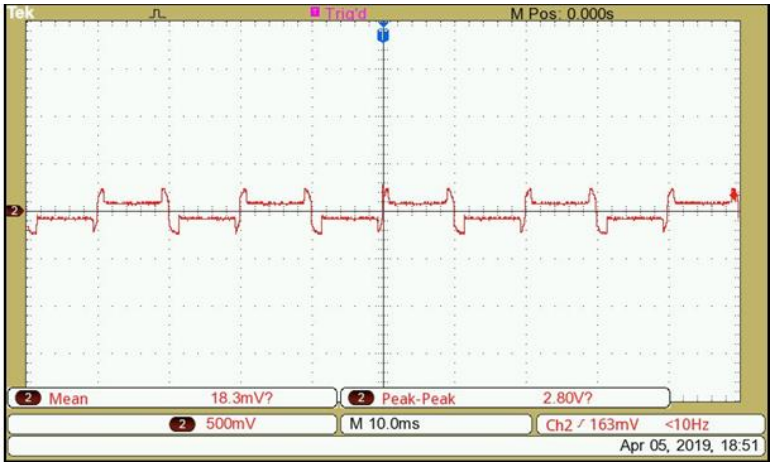

Fig. 5.9 Waveform of the triggering signal across the gate of the Triac at 40% RH.

The microcontroller based integral cycle controlled voltage waveforms at different humidity are shown in Fig. 5.10. Fig. 5.10a, Fig. 5.10b, Fig. 5.10c and Fig. 5.10d shows the voltage waves corresponding to humidity levels of 40%, 60%, 80% and 90% RH respectively. The available power across the 40W heater at different %RH is shown in Fig. 5.11.It shows that as the humidity level increases, the power available to the load increases significantly. During the non - conduction cycles, the voltage is available across the device (Triac) and there is no power across the load.

The waveform of voltage across the device at 80% RH during the non - conduction cycle is shown in Fig. 5.12. At 80% RH device is conducting for four cycles and non-conducting for one cycle. For the validation of the proposed electrical circuit in the high voltage transformer, a breather of 0.5 kg silica gel capacity was used. It is generally used in the distribution transformer of rating up to 200 kVA.

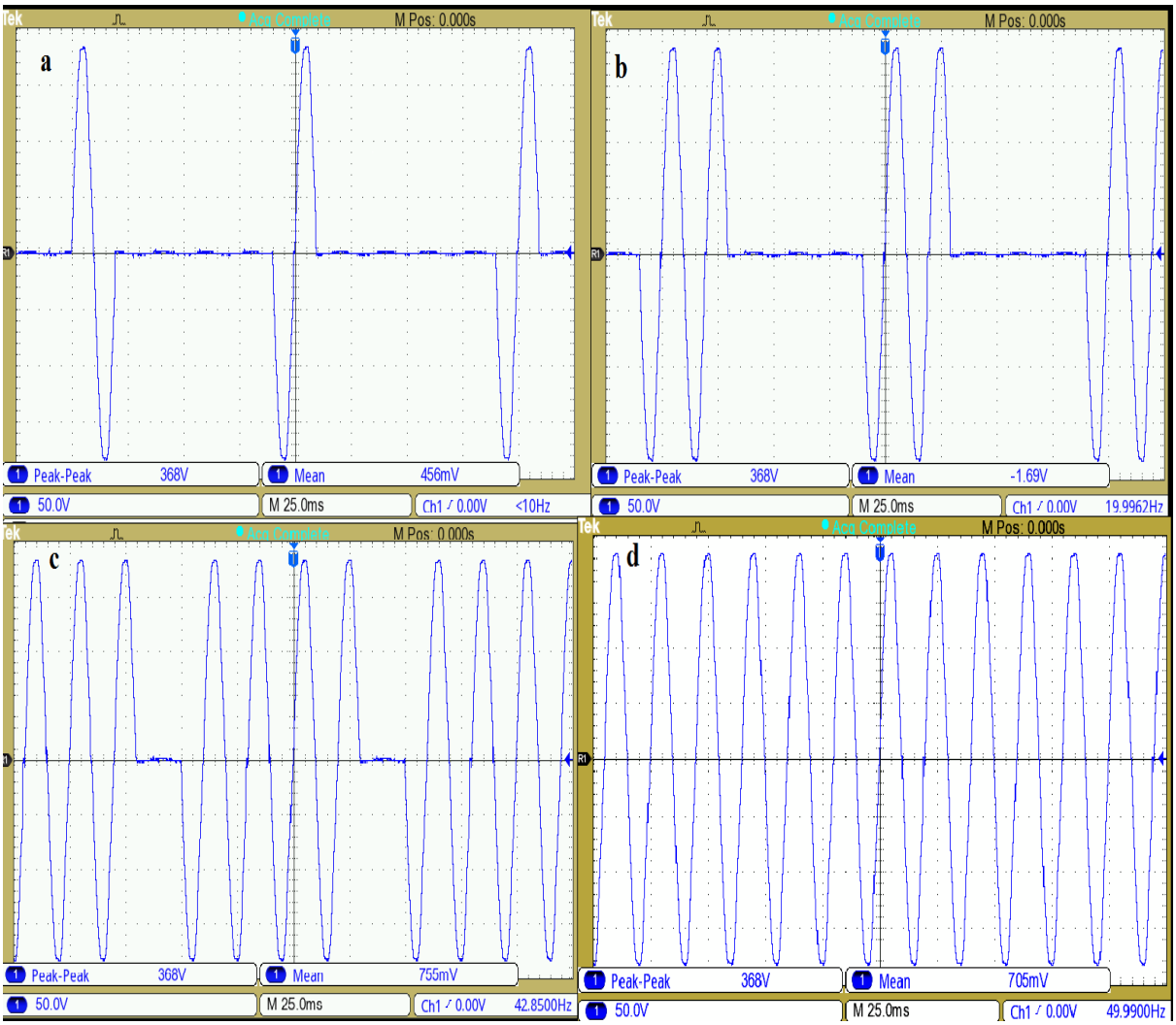

Fig. 5.10 Integral cycle-controlled voltage waveforms at different humidity (%RH).

To measure and control humidity in the breather, the experimental set up shown in Fig. 4.10 was used. The output pipeline of moist air was connected to the inlet pipe of the breather. Moist air of 80% RH was continuously passed to the breather at the rate of 2 l/min at 2 bar pressure. The experimental setup of self-dehydrating breather is shown in Fig. 5.13. The RH level at the inlet of the breather was monitored with the help of commercial moisture meter [178].

The fabricated sensor along with the commercial sensor (HIH 4000-003l, Honeywell) was placed in the breather towards the outlet leading to the conservator. The RH level of filtered air at the outlet of the breather was monitored continuously for 44 h. The drying efficiency ($\tilde{E}_{dry}$) of the breather was estimated using (5.8) continuously for 45 h. The drying efficiency is shown in Fig. 5.14. The drying efficiency of the dehydrating breather deteriorates with time.

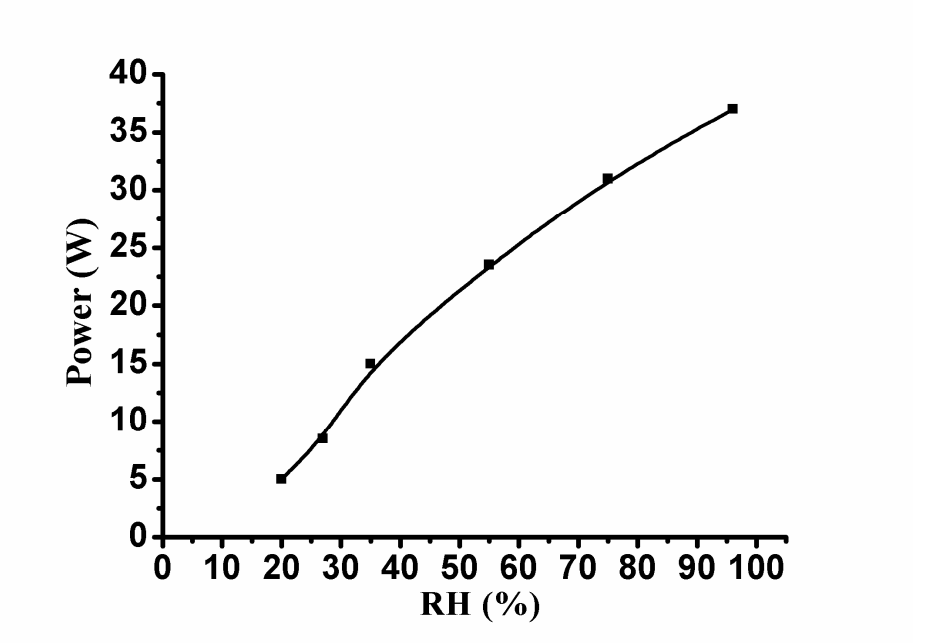

Fig. 5.11 Variation of the load power with change in % RH.

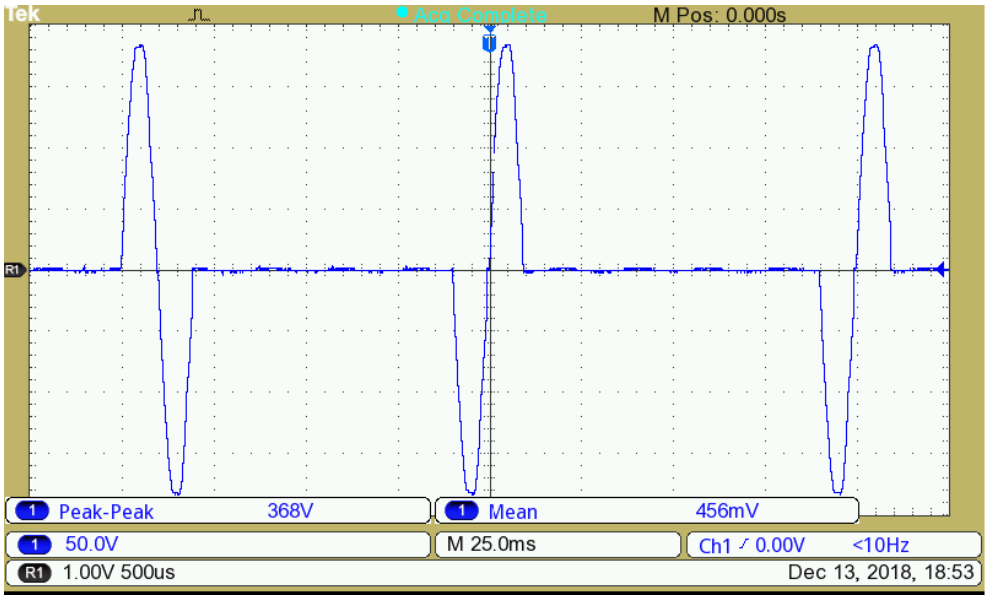

Fig. 5.12 Waveform of voltage across the Triac at 80% RH.

$$\eta_{dry} = \frac{\left(RH_{in} - RH_{out}\right)}{RH_{in}} \times 100 \qquad (5.8)$$

The steady state response of the sensor was considered to estimate the moisture content in the silica gel.At steady state, the moisture level indicated by the sensor in the breather air is equal to the moisture adsorbed by the silica gel crystals. As the moisture content within the silica gel increases, its moisture adsorbing capacity decreases. Consequently, the relative humidity (RH) monitored by the sensor will also increase.

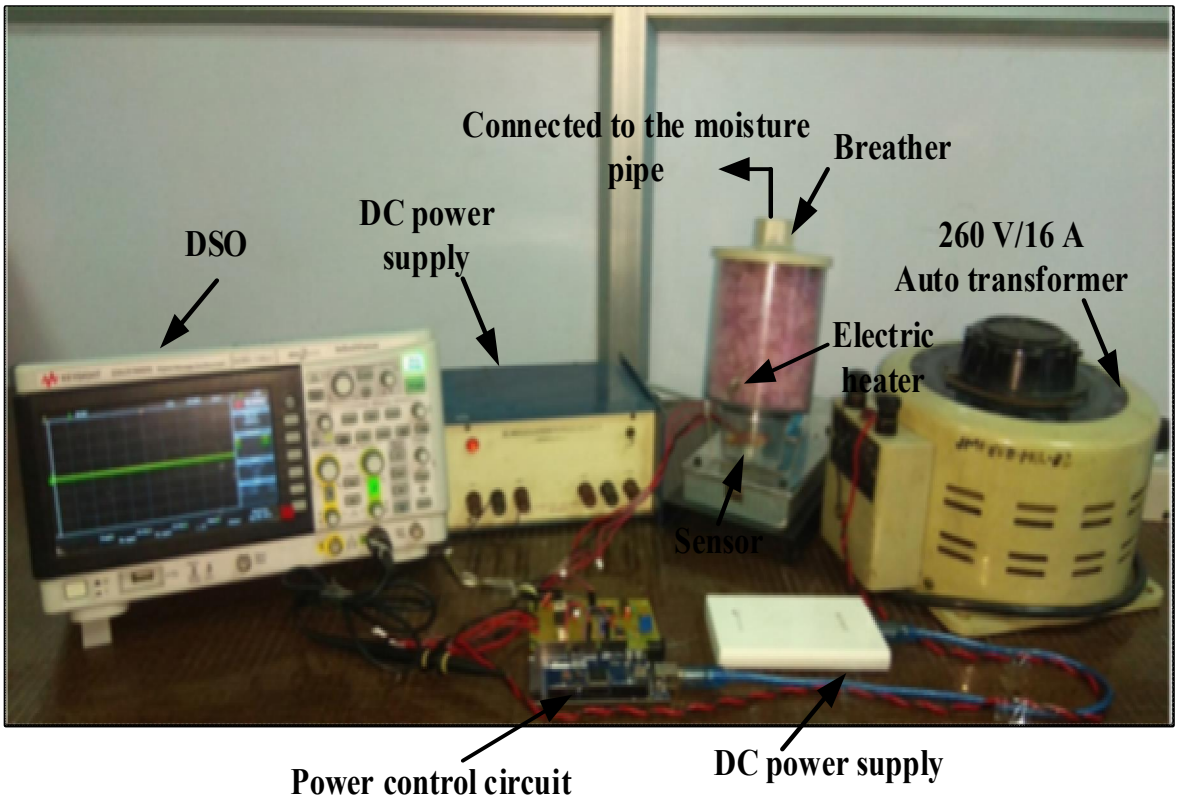

Fig. 5.13 Experimental setup of self-dehydrating breather.

Due to slow process of moisture migration between moist air and silica gel, several hours required to reach the moisture to steady state condition. The response of the sensor for the duration of 48 h is shown in Fig. 5.15. It shows that as the moisture content in the silica gel increases with time, the capacitance value of the sensor increases. Equation (5.9) gives the model for forecasting the moisture equilibrium concentration in the breather with time. Experimental data points were fitted by polynomial equation available in MATLAB software. The order of the polynomial equation was found to be second order with correlation coefficient 0.99.

$$RH_{st} = 5.18 + 0.43 \times t + 0.01 \times t^2 \quad (5.9)$$

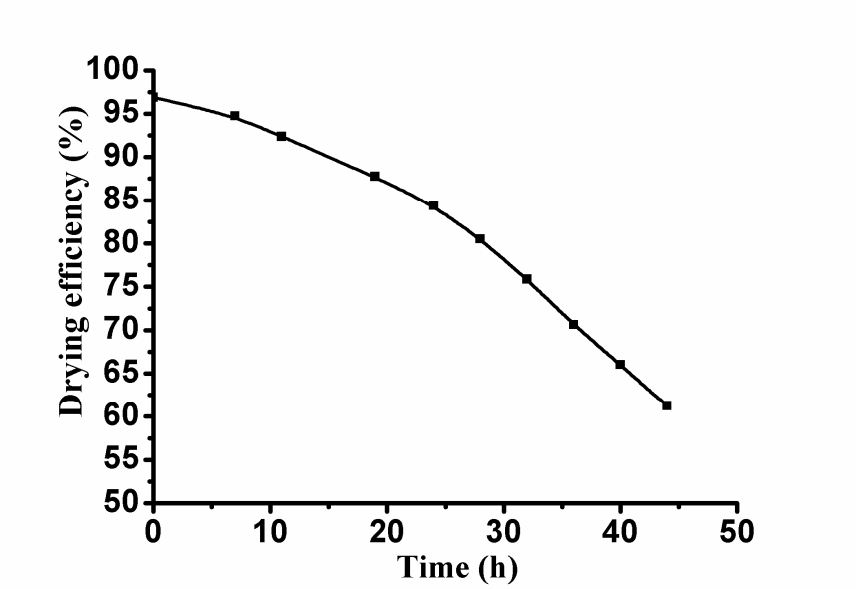

Fig. 5.14 Drying efficiency of the conventional dehydrating breather.

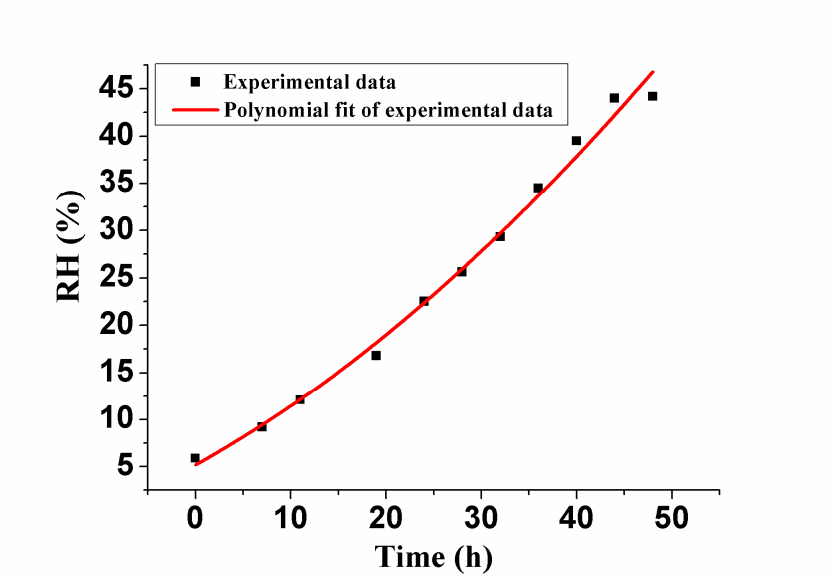

Fig. 5.15 RH level inside the breather at steady-state condition.

The color of the silica gel after the absortion of moisture in different time is shown in Fig. 5.16. In initial stage, when the gel was fresh its color is light blue as shown in Fig. 5.16a. The image of the silica gel after the absortion of moisture from the moist air flow at the rate of 2 litre per minute at 80 % RH at 2 bar pressure inside the 0.5 kg capacity of breather for 10 hours, 20 hours, 30 hours, 40 hours and 44 hours are shown in Fig. 5.16b, Fig.5.16c, Fig. 5.16d, Fig. 5.16e and Fig. 5.16f respectively.

The color of the silica gel changes from blue to dark pink with time. Consequently, its moisture absortion capacity also deteriorates with time. Consequently, the moisture content inside the silica gel also increases. The % RH indicated by the sensor inside the breather increases with time.

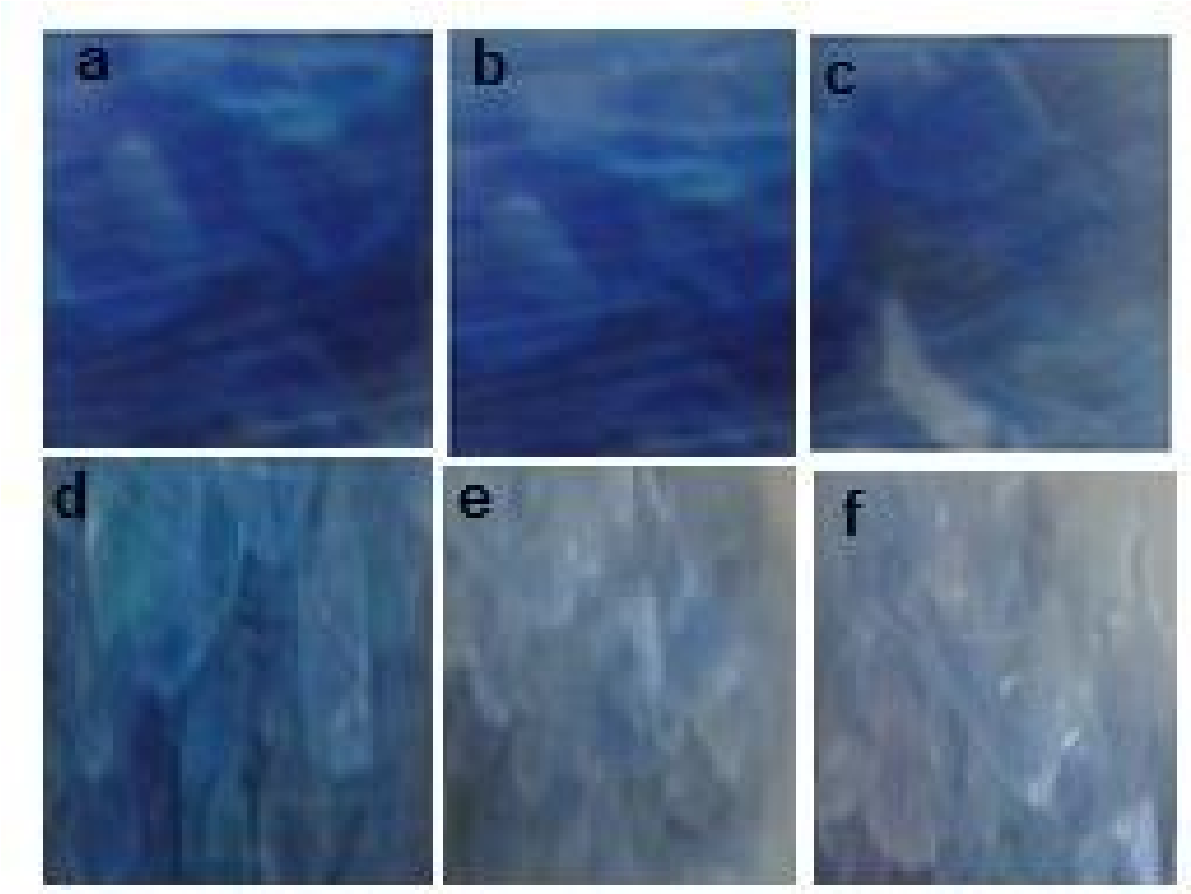

Fig. 5.16 Image of variation of colour of silica gel inside the breather in the duration of 44 h continious flow of moist air at 80% RH at the rate of 2 lit/min.

5 Conclusions

A moisture sensor interfaced with phase detection electronics circuit was designed for monitoring the moisture in the breather of T/F. The sensor was fabricated by the electrochemical anodization of the Al sheet. The sensor was found to be highly sensitive above the 20% RH. Although, the capacitance change below the 20% RH was small, but it is sufficient for measurement. The phase detection electronics circuit was interfaced with the Arduino microcontroller board for generating the moisture dependent PWM wave. The PWM was further applied to the gate of the triac for controlling the power across the heating load. Moisture inside the breather was controlled, when its pre-set value for dehumidification wasachieved. The waveforms at different operating points of the electronics circuit were

recorded. The mathematical equations at different operating points of the electronics circuit were developed. Drying efficiency of the breather was tested through the experimental setup developed in the laboratory. The image of silica ï gel after the adsorption of moisture at different time within the duration of 45 days was recorded. It deteriorates with time. The proposed method of moisture control using heater via moisture sensor in the breather will reduce the visual inspections of the degree of moisture level in the drying agent (silica gel), regular replacement of drying agent. Finally, the operational reliability of the transformer will increase due to automatic moisture control of the breather.

Chapter 6

Moisture Measurement in ppm using Aluminium Oxide Capacitive Sensor and its Drift Study

6.1 Introduction

Moisture measurement below 100 ppm is important for different applications including the moisture measurement in transformer oil. A capacitive parallel plate sensor with moisture sensing film made of aluminium oxide has been fabricated by sol-gel method. The sensor shows significant capacitive change with the variation of moisture from 0 to 100 ppm. The sensor may be suitable to measure moisture in the oil being thermally and chemically stable. However, the drift in the sensor output is an important phenomenon of the capacitive humidity sensor, the most vital device in the commercial dew point meter. Table-6.1 shows the drift behaviour of some humidity sensors reported in literature. Due to drift in the output, most of the meters for critical applications require costly and time-consuming recalibration. Modelling of drift phenomenon for RH humidity sensors including the sensor fabricated by electrochemical anodization of aluminium sheet is reported in the literatures. But, to the best of our knowledge, there is no work reported so far about the modelling of drift of the sensors used for trace level moisture detection. In the previous chapter, alumina metal oxide sensors have been fabricated to measure moisture of the breather as well as the transformer oil. The sensor for breather application measures moisture in high humidity range but the sensor with suitable pore morphology can measure moisture in ppm in T/F oil. The sensors were fabricated by the anodization method. This chapter presents the mathematical model, the electrical equivalent circuits and the long-term drift analysis of the capacitive sensor for T/F moisture fabricated by sol-gel method. The proposed modelling may also be used for the modelling of alumina sensor fabricated by the anodization method. The sensors were having porous alumina oxide thin film for detecting moisture in the range of 3 to 100 ppm. To study the long-term drift, experiments were performed under different operating conditions over a period of nearly one year. Drift behaviour was studied when the sensor (i) was stored in drying agent (ii) was stored in open atmospheric condition of laboratory. The response behaviours of the sensors were simulated with the help of the model. To develop a model, the actual pore morphology of the sensor obtained experimentally using Bruner Emmet and Teller (BET) and Electron Microscopy (FESEM) analysis was used. Comparing the model response with the experimental results, the proposed model can be used for drift analysis for an aged

sensor, determination of hydration level and moisture condensation in the pores. Experimental results showed that when a sensor was kept in drying agent, the maximum average drift of only 1.5% was observed but when a similar sensor was kept in open high humidity atmosphere, the maximum long-term drift was found to be ~ 11.20%.

6.2 Structure and Electrical Equivalent Circuit of an Aged Metal Oxide Humidity Sensor

The schematic diagram of the fabricated sensors to perform the experimental work is shown in Fig. 6.1. The porous alumina humidity sensor comprising porous Al_2O_3 thin film sandwiched between two gold electrodes on an alumina substrate (alpha). The gold electrode has macro pores and the macro pores are open ended. The pore size of the sensing film is of nano meter order, while the size of the pores of the gold electrode is of macrometer (μm) order [83-84, 163]. The longer size pores of the gold electrode provide easy passage to the vapour molecules to condense in the micro pores of the metal oxide sensing film.It was fabricated by depositing thin film of aluminum hydroxide sol solution on the gold electrode by dip coating technique. The sol solution was prepared by hydrolyzing aluminum sec. butoxide precursor in excess water by Yoldas method. The film was sintered at 450°C for three hours. For capacitive structure another gold electrode was deposited on top of the oxide film. Details of the sensor fabrication were reported in [84, 163]. The sensitivity of the sensor for detection of ppm level of moisture depends on the pore size of the sample and the mean free path (MFP) of the vapor molecule. For adsorption to occur on the pore walls, the Brownian energy of the vapor molecules should be minimum. For the minimum energy, the value of MFP should be minimum. Therefore, the pore size of the sample should be comparable to the MFP of the vapor so that it provides the entry to the vapour molecules and adsorb on the pore walls [77]. The surface of the pores gradually attains the wet bulb temperature of the air and a continuous water layer will stretch over the pore surface. The layer of the water slowly stretches away from the solid surface as more vapour condensed and becomes a continuous phase. Wetting and formation of the water layer on pore surface causes variation in dielectric constant from lower to higher values. Consequently, the capacitive response of the sensor changes with the change in the moisture concentration. Fig. 6.2 shows the cross-sectional view and the electrical equivalent circuit of one pore cell of the designed sensor S1. The sensor S1 was stored inside the drying agent. The drying agent utilized was molecular sieves. The electrical equivalent circuit of the sensor consists of a parallel connected structural capacitance (C_{sc}) and a resistor (R_{sc}), a humidity dependent capacitor

(C_{hd}) and a resistor (R_{hd}).The components of the structural capacitance and the resistance are the capacitance of air pore (C_{ap}) and the resistance of air pore (R_{ap}), the capacitance of dry pore wall (C_{dw}) and the resistance of dry pore wall (R_{dw}).

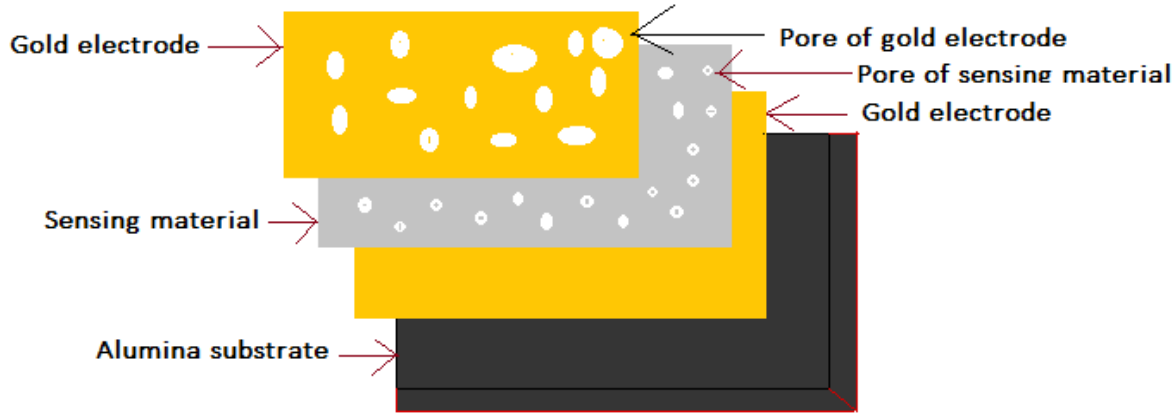

Fig. 6.1 Schematic diagram of the moisture sensor.

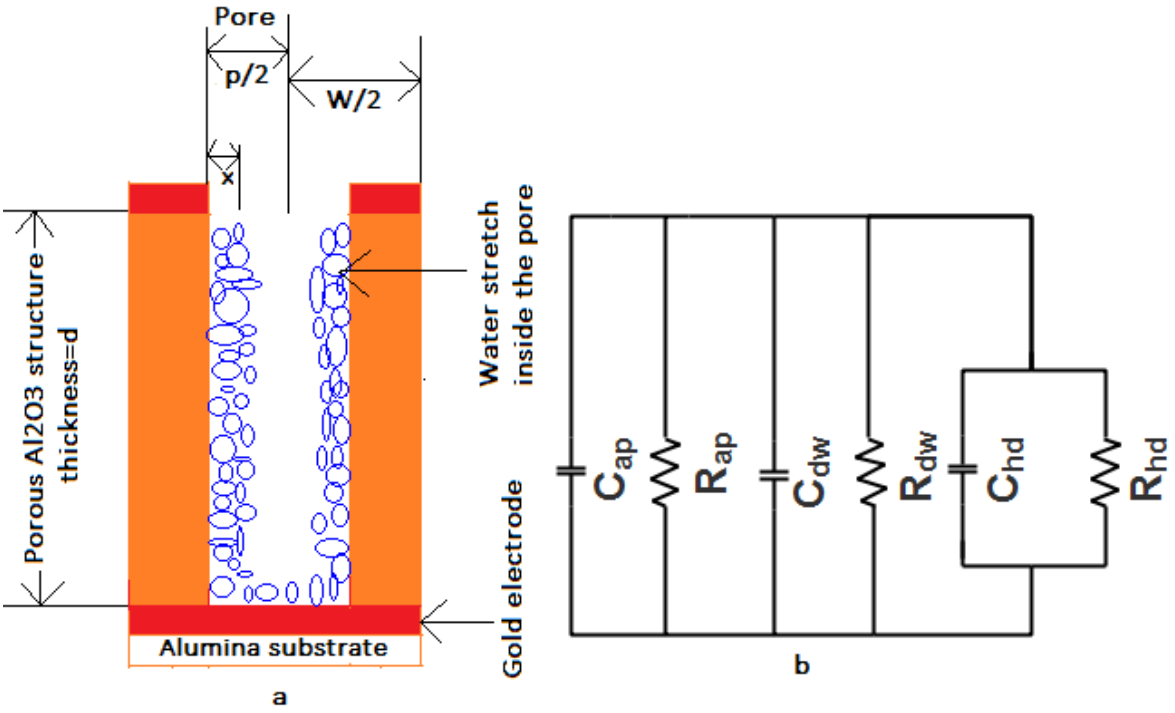

Fig. 6.2 Schemetic diagram of one pore cell of the sensor S1 kept in drying agent (a)Cross-sectional view (b)Equivalent electrical circuit.

Fig. 6.3 shows the cross-sectional view and the electrical equivalent circuit of one pore cell of aged humidity sensor S2. The sensor S2 was stored in an open environment of laboratory at high humidity. The electrical equivalent circuit of S2 consists of one additional component in structural capacitance due to the formation of hydrated wall stretched horizontally inside the

air pore and the dry wall of the cell. The capacitance and the resistance of the hydrated pore wall are C_{hw} and R_{hw} respectively.

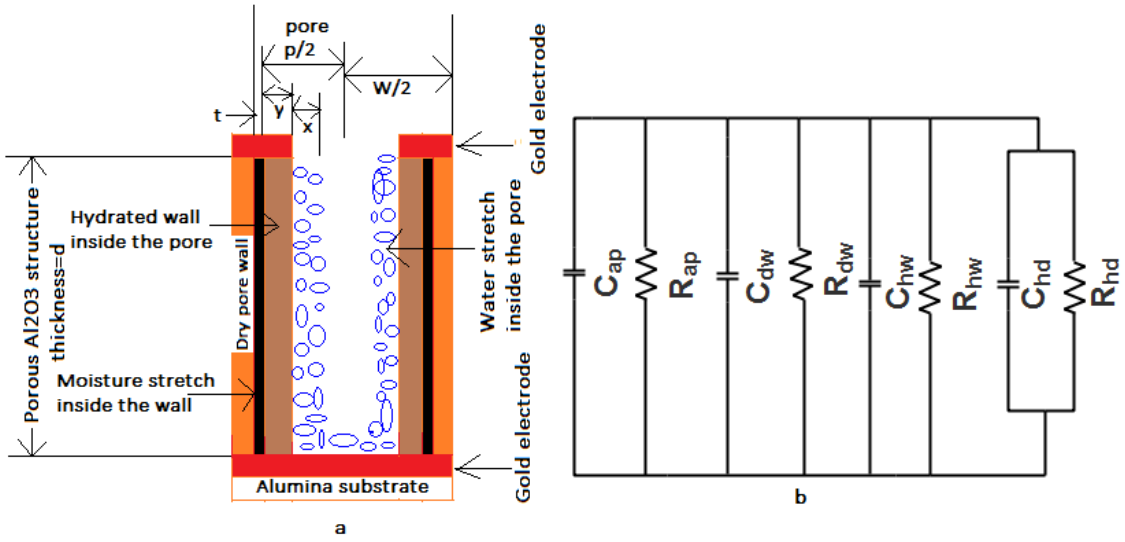

Fig. 6.3 Schemetic diagram of one pore cell of the sensor S2 kept in open environment (a)Cross-sectional view (b)Equivalent electrical circuit.

The equivalent capacitance of the sensor can be given by

$$C_{sensor} = C_{sc} + C_{hd} \tag{6.1}$$

For the sensor kept in drying agent, the structural capacitance of the cell is given by

$$C_{scn} = \frac{k(p/2)^2}{d} + \frac{8k((w/2)^2 - (p/2)^2)}{d} \tag{6.2}$$

For the aged sensor kept in open environment, the structural capacitance of the cell can be given by

$$C_{sco} = C_{ap} + C_{dw} + C_{hw} \tag{6.3}$$

To investigate the aging effect of the sensor, each circular cell of the sensor enclosing one pore is considered. Due to prolong exposure of the sensor at any humidity level, a part of the dry wall of the cell becomes hydrated and a layer of hydrated alumina is formed inside the pore. The water condensation stretches horizontally inside the pore.

Table-6.1

Comparison of average percentage drift of different humidity sensors in the literature

Prior art	Operating range (%RH/ppm)	Average drift (%RH/ppm)	Duration and condition for drift	Technologies	Estimated modelling errors
[117]	10-90% RH	Marginal below 45% RH but 15% above at 90% RH	30 days, stored in 75% RH	Al_2O_3 capacitive sensor	No drift model
[118]	40-98% RH	(2±1.9)% RH at 60% RH and (2.9±2)% RH at 90% RH	200 days, stored in open atmosphere	Polymer capacitive Sensor	No drift model
[121]	20-98% RH	Maximum 49% at 98% RH	10 days, freshly prepared sensor	Porous silicon capacitive sensor	No drift model
[133]	1-15 ppm	12% at 2 ppm 25% at 15 ppm	274 h, stored at 15 ppm 167 h stored below 1 ppm	Al_2O_3 capacitive sensor	No drift model
[134]	10-90% RH	1-20% at 10-90% RH	28 days, 85% RH	Polymide capacitive sensor	No drift model
[152]	10-97% RH	Not available	Not available	Al_2O_3 capacitive sensor	Sensor was not experimentally validated
Reported Work	3-100 ppm	11.20% at 3-100 ppm	10 months at 60% RH	Sol-gel based capacitive sensor	Experimentally validated model

Equations (6.4) and (6.5) indicate the structural capacitance of the aged sensor due to the formation of hydrated alumina wall inside thepore and the dry wall respectively.

Table- 6.2

Explanation of terms of equations 6.4, 6.5 and 6.6

Equation	Terms	Capacitance of	Area of
6.4	$\frac{k(p/2-y)^2}{d}$	air pore (Ů= 1)	air pore = $\pi(p/2-y)^2$
6.4	$\frac{2.5k((p/2)^2-(p/2-y)^2)}{d}$	hydrated alumina wall inside the pore (Ů= 2.5)	hydrated wall = $\pi((p/2)^2-(p/2-y)^2)$
6.4	$\frac{8k((w/2)^2-(p/2)^2)}{d}$	dry wall (Ů= 8)	dry wall = $\pi((w/2)^2-(p/2)^2)$
6.5	$\frac{k(p/2)^2}{d}$	air pore	air pore = $\pi(p/2)^2$
6.5	$\frac{2.5k((p/2+t)^2-(p/2)^2)}{d}$	hydrated alumina wall inside the pore	hydrated wall = $\pi((p/2+t)^2-(p/2)^2)$
6.5	$\frac{8k((w/2)^2-(p/2+t)^2)}{d}$	dry wall	Dry wall = $\pi((w/2)^2-(p/2+t)^2)$
6.6	$\frac{k(p/2-x)^2}{d}$	air pore	air pore = $\pi(p/2-x)^2$
6.6	$\frac{79k((p/2)^2-(p/2-x)^2)}{d}$	Moisture dependent capacitance, when water condenses inside the pore (Ů= 79)	water condense = $\pi((p/2)^2-(p/2-x)^2)$
6.6	$\frac{8k((w/2)^2-(p/2)^2)}{d}$	dry wall when water stretches inside the pore	dry wall when water stretches inside the pore = $\pi((w/2)^2-(p/2)^2)$

The capacitance of the new sensor due to the condensation of moisture inside the pore is given by (6.6).

$$S_{sco1}=\frac{k(p/2-y)^2}{d}+\frac{2.5k((p/2)^2-(p/2-y)^2)}{d}+\frac{8k((w/2)^2-p/2)^2)}{d} \quad (6.4)$$

$$C_{sco2}=\frac{k(p/2)^2}{d}+\frac{2.5k((p/2+t)^2-(p/2)^2)}{d}+\frac{8k((w/2)^2-(p/2+t)^2}{d} \quad (6.5)$$

$$C_{new\ sensor}=\frac{k(p/2-X)^2}{d}+\frac{79k((p/2)^2-(p/2-X)^2)}{d}+\frac{8k((w/2)^2-(p/2)^2)}{d} \quad (6.6$$

Where,

$k = \pi\varepsilon_o$

The parameter $\mathring{U}_0$ is the permittivity of the vacuum and $\mathring{U}_0$ = 8.854 X 10^{-12} F/m. The dielectric constant of air ($\mathring{U}_a$) is unity, the dielectric constant of dry alumina wall (C_{dw}) is 8, the dielectric constant of the hydrated wall (C_{hw}) is 2.5 and the dielectric constant of (C_{hd}) is 79 [153]. Explanations of each term in the expression of (6.4), (6.5) and (6.6) are given in Table 6.2. The sensor S1 having area of 115.5 mm^2 contains approximately 266 x 10^9 cells. The sensor S2 having area of 107.12 mm^2 contains approximately 227 x 10^9 cells. The capacitance values of S1 and S2 are obtained by multiplying the capacitance of per unit cell by the factor 266 x $10^9$and 227 x 10^9 respectively. The geometrical parameters of the sensors are shown in Table ï 6.3. For y = t = 0, (6.4) and (6.5) yield the capacitance values of the un-hydrated sensor. The effective dielectric constant of the sensor includes the dielectric constant of the hydrated alumina, the dry alumina, the water condensed inside the pore and the air pore. Capacitance C_{sco1}, C_{sco2} and $C_{new\ sensor}$ are computed by (6.4), (6.5) and (6.6) respectively.

Table 6.3

Geometrical parameters of fabricated sensors

Sensors of different dimension	Upper electrode Dimension	Cross-sectional area of sensing film (mm^2)	Thickness of the film (ε m)	Average pore diameter of the film (nm)	Average diameter of the cell (nm)	No of cells in the film of the sensor (Sensing area of the sensor/Area of the one cell)
S1(Kept in drying agent)	10.5 mm X 11 mm	115.5	10.5	10.5	23.5	266x$(10)^9$
S2(Kept in open environment)	10.3 mm X 10.4 mm	107.12	12	10.5	24.5	227x$(10)^9$

6.3 Simulation of the Aged Sensor Characteristics using Equivalent Circuit Model

The response of the moisture sensor is the combination of its structural and humidity dependent capacitances. The structural response of a capacitive sensor is the result of dielectric material surroundings the air pore. The aged sensor has lower structural capacitance than the new sensor due to the lateral seepage of the moisture inside the dielectric material surrounding the pores. Simulation of the responses of the new and aged sensors was carried out using the Matlab software. The structural response of the sensor was simulated considering all possible conditions of formation of the hydrated alumina wall inside the pore and dry wall of the cell as indicated in (6.4) and (6.5) respectively. The effective dielectric constant of the sensor decreases as the hydrated layer formed inside the dry wall and increases when it is formed inside the pore. Consequently, the capacitance value of the sensor decreases due to formation of hydrated layer inside the dry wall and increases for the air pore as shown in Fig. 6.4. Similarly, the capacitive responses of the freshly fabricated sensors S1 and S2 were simulated by (6.6). The simulated response of the sensors is shown in Fig. 6.5. As the level of moisture condensation inside the pores increases, the effective dielectric constant of the sensors increases consequently, the capacitance value of the sensors also increases. However, the capacitance values of the sensor S1 are different from the values of the sensor S2. This difference in capacitive response is due to their different geometrical parameters and pore morphology.

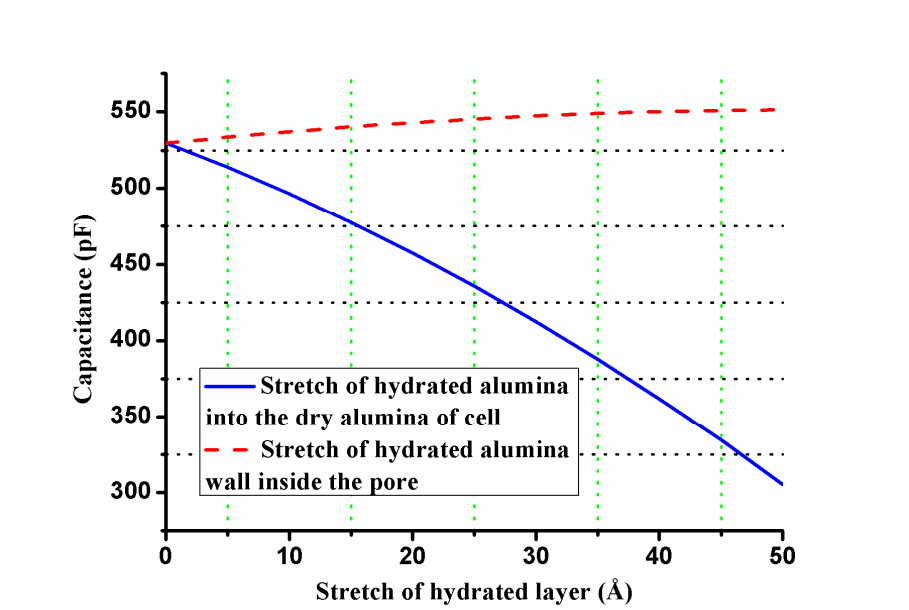

Fig. 6.4 Simulation results of the structural capacitance of the sensor S2 with the variation of hydrated alumina wall thickness.

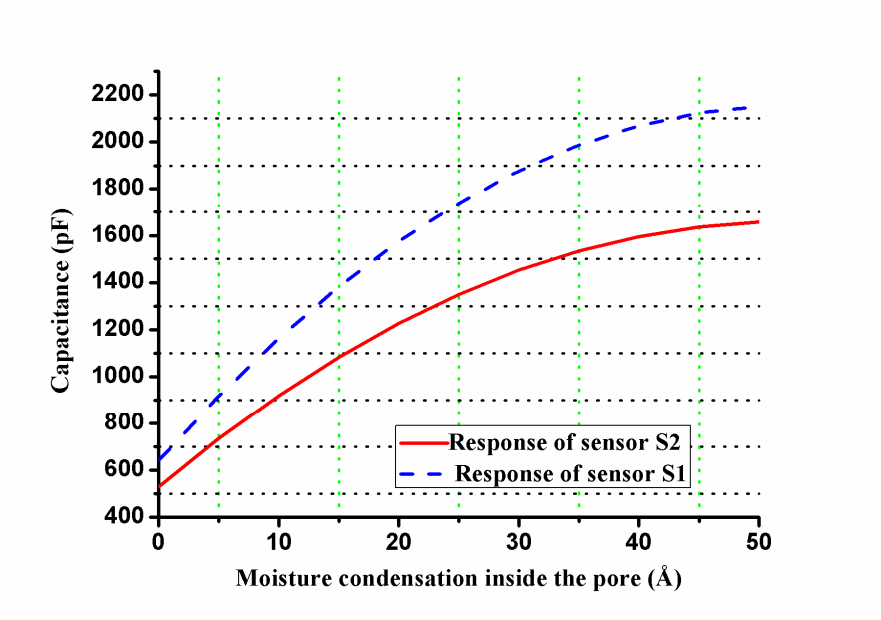

Fig. 6.5 Simulation results of new fabricated sensors with the variation moisture condensation inside the pores.

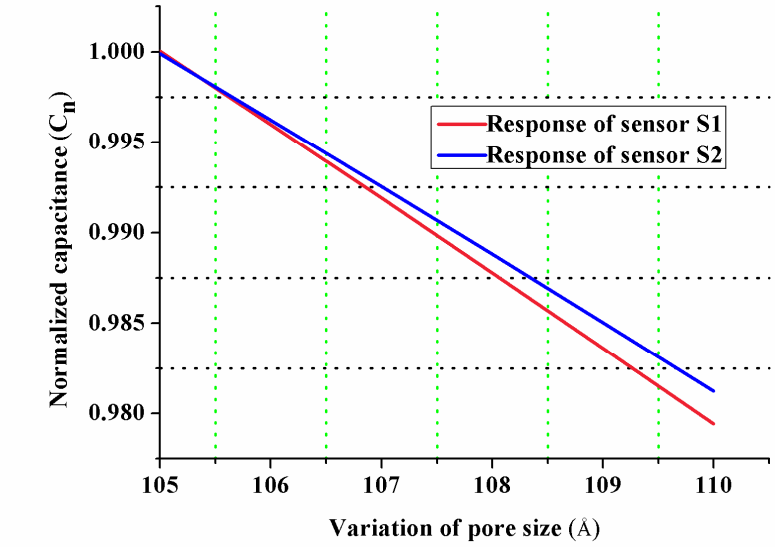

Fig. 6.6 Simulation results of the structural capacitive response of the sensors with the variation of air pore size.

The normalized structural capacitive response $\left(C_n = \frac{C_p}{C_m}\right)$ of the sensors with the variation of the pore size (p) is simulated by (6.2) and the responses are shown in Fig.6.6.Where,C_p is the capacitance value for different pore sizes and C_m is the maximum capacitance value of the sensors. It is observed in Fig. 6.6 that the response of the sensors decreases with the increase

in the pore size. The pore size plays an important role for sensing humidity [191]. It is governed by Kelvin equation of pore radius. It is established by (6.7).

$$r_k = \frac{2\gamma M}{\rho RT \ln(P_S / P)} \tag{6.7}$$

With the increase in pore size, less number of water molecules gets condensed in the pores causing a smaller change in effective dielectric constant.

6.4 Simulation of response of the sol-gel based (γ-Al_2O_3) humidity sensor using the dielectric theory

For cross-verification of the equivalent circuit model developed using the actual response, the effective dielectric constant ($\mathring{U}_{effective}$) of mixture of dielectrics A and B is given by (6.8) [133].In equation (6.8), $\mathring{U}_A$ and $\mathring{U}_B$ are the relative permittivity of the dielectrics A and B respectively. Dielectric B is suspended in the supporting dielectric.

$$\varepsilon_{effective} = \left(1 + \frac{\lambda\alpha(\varepsilon_B - \varepsilon_A)}{(\lambda - 1)\varepsilon_A + \varepsilon_B}\right) \tag{6.8}$$

Where,

$$\alpha = \frac{(\pi p^2 / 4)d - (\pi(p - 2x)^2 / 4)d}{(\pi p^2 / 4)d} \tag{6.9}$$

$$\lambda = \frac{(\mathrm{d}/\mathrm{p})^2}{(\ln(2\mathrm{d}/\mathrm{p}) - 1)} \tag{6.10}$$

Fig. 6.7 shows the effective dielectric constant of the sensor with the hydrated alumina layer thickness stretched into the air pore. Here, $\mathring{U}_B$ is the dielectric constant of the hydrated layer and $\mathring{U}_A$ is the dielectric constant of the air. Fig.6.8 shows the response of the dielectric constant when the hydrated layer spread into the dry alumina wall. There is a good agreement between the response of the sensor obtained from the equivalent circuit model and dielectric theory.

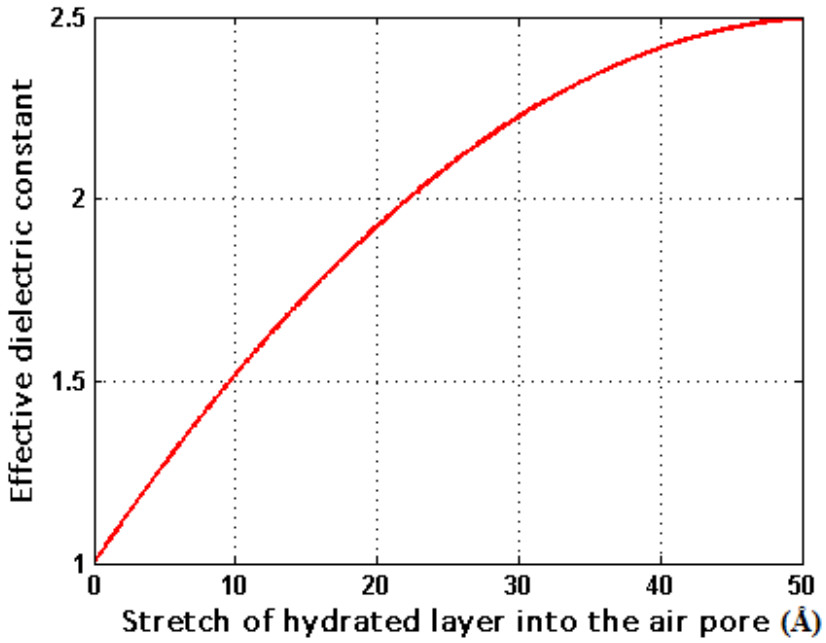

Fig. 6.7 simulation response of the sensor when hydrated alumina layer spread into the air pore.

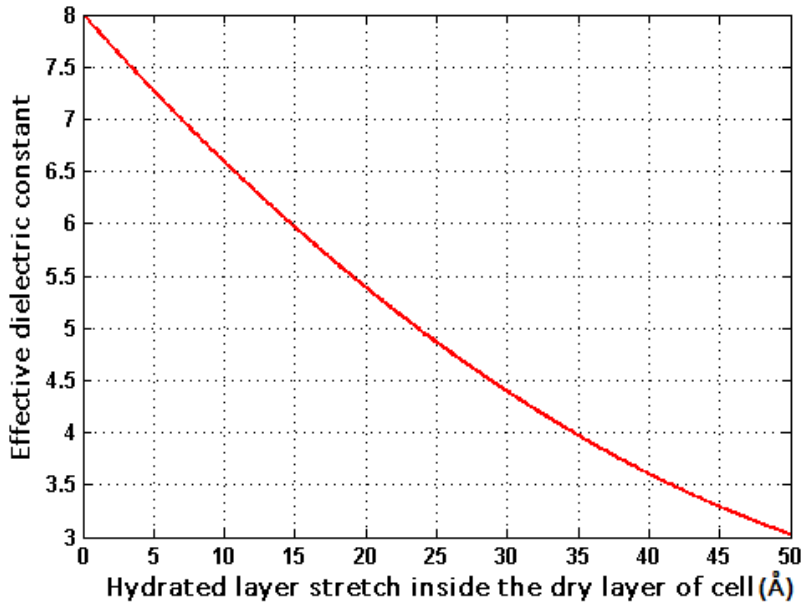

Fig. 6.8 Simulation response of the sensor when hydrated alumina spread into the dry wall of the cell.

6.5 Experimental methods of drift study of the fabricated sensor

To study the drift and sensitivity at different environment, the sensor S1 was kept in desiccator with drying agent and the sensor S2 was put in open clean laboratory environment. The room temperature and the relative humidity of the environment were 25°C ± 2°C and 65%

± 5% RH respectively. The desiccators was having a sealed environment with drying agent of 3 Å molecular sieves. The molecular sieves absorb water and maintain the desiccator environment of constant RH of nearly 3% at room temperature, as practiced by commercial dew point meter [173]. For maintaining the constant humidity level inside the desiccator, the condition of the drying agent was monitored regularly and replaced by fresh drying agents when the humidity level deviated from the actual value. The humidity level of the laboratory environment was monitored by Honeywell sensor based digital hygrometer (10-98% RH, ± 5% accuracy) but the humidity of the desiccators was measured by the dew point meter. The level of humidity in the room was maintained around 65% RH. Therefore, the sensor with drying agent had minimum exposure to high humidity causing less change in surface area as well as morphology. But the sensor S2, which was kept in atmospheric humidity, the humidity level was very high around 65% RH. In high humidity, the chemisorbed water layer causes the formation of aluminum-oxy hydroxide ((AlO(OH)) called boehmite, and then a mixture of aluminiumtri hydroxides (Ŭ-Al(OH)3) called a bayerite and a more stable gibbsite (ɔ-Al(OH)3) [124]. The result of these oxides formation is the modification of the morphology of the sensors. Initially, just after fabrication, the sensor S1 was exposed to different moisture in the range of 3 to 101 ppm, the capacitive response was determined and then it was stored in the drying agent. After five months, the sensor S1 was again tested in the same moisture range and then stored in the drying agent. The experiment was repeated every five months. Schematic of the test set up is shown in Fig.6.9. The moisture content in the range of 3 to 101 ppm inside the test chamber was created by using N_2 as the carrier gas. The testing chamber was made of steel with 50 cc volume. The chamber is having ¼ò inlet and outlet gas pipe connectors. Dry N_2 gas was mixed with water vapour for creating the different level of moisture. To obtain water vapour, dry N_2 gas was allowed to pass through a water bubbler. The moisture concentration was varied precisely with precision dialed needle valve. A commercial dew point meter (Model SADP(R), SHAW, UK) (range 0-1000 ppm, absolute accuracy = ±1 ppm moisture) was employed to monitor the moisture concentration of the moist gas. The sensor was placed in the chamber and the capacitance values were noted with the help of Agilent 4294A Impedance analyzer at 1 kHz signal frequency. The temperature and pressure were controlled and remained constant throughout the experiment at various moisture levels. Experiments were conducted at room temperature (25ŬC) and at a pressure of 1 bar. The response of the aluminum oxide moisture sensor was independent of temperature and pressure. Since the sensor was an oxide material and the sensing film was fabricated at high temperature (450ŬC), the variation of the ambient temperature of the sensor did not affect

the response. This was also previously observed and reported in [68]. For online data acquisition, the impedance analyzer was interfaced with a PC with the help of data acquisition card (82357B USB/GPIB).The sensor was connected to the impedance analyzer through the test fixture, 1604E and a short coaxial shielded cable. The shield of the cable was grounded. To avoid electromagnetic and electrostatic noise, the sensor was placed inside a metallic grounded sample holder. Since, the present sensor was an oxide material, so the resistance value in ppm moisture was very high of the order of MÝ, so the contact resistance was negligible. Fig. 4.10a, Fig.4.10b and Fig. 4.10c show the capacitive response of three samples of same geometrical parameters of the sensor S1. The variation of the capacitance values among the three samples is in the range of 2 to 6% for moisture in the range of 3.5 ppm to 101 ppm. The response of the sample 1 in the first five months, shows the maximum drift of only 11 pF (base capacitance and sensitivity drift) but in the next five months, the sensor shows negligible drift and the output becomes stable. The maximum drift of the base value including the sensitivity at 3 ppm in the first five months after the fabrication is 11 pF.

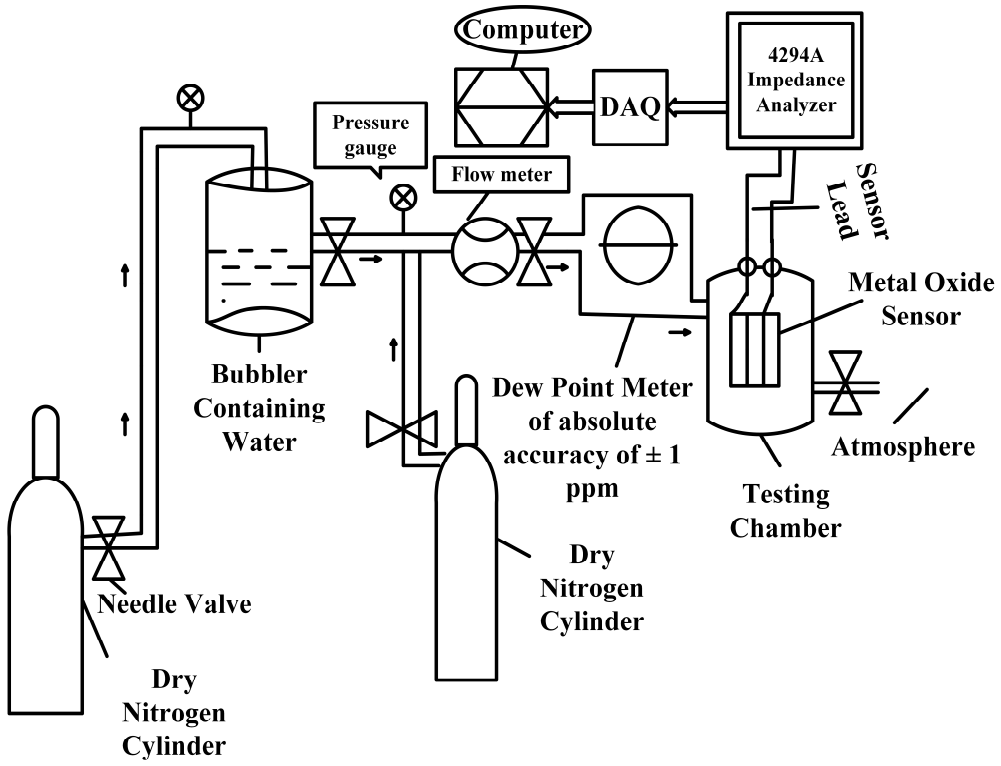

Fig. 6.9 Schematic diagram of the experimental setup.

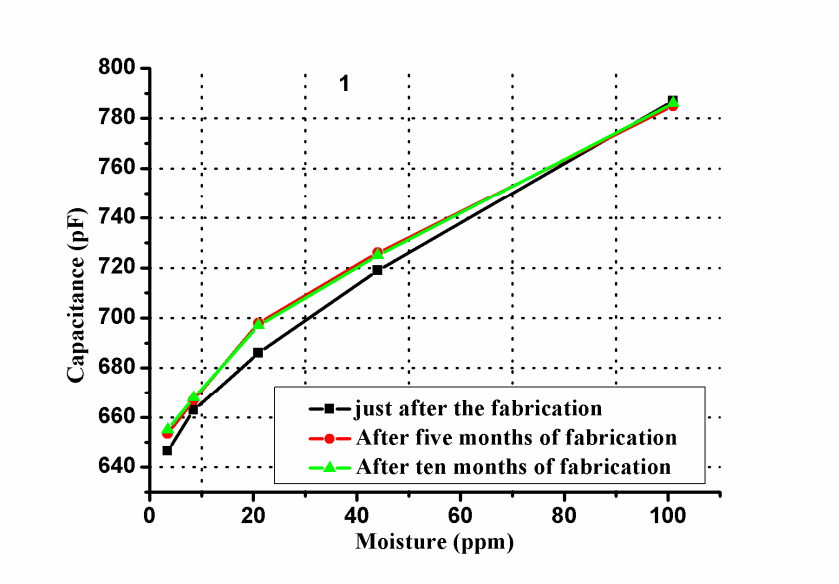

Fig. 6.10a Capacitive response of sample 1of sensor S1 kept in drying agent.

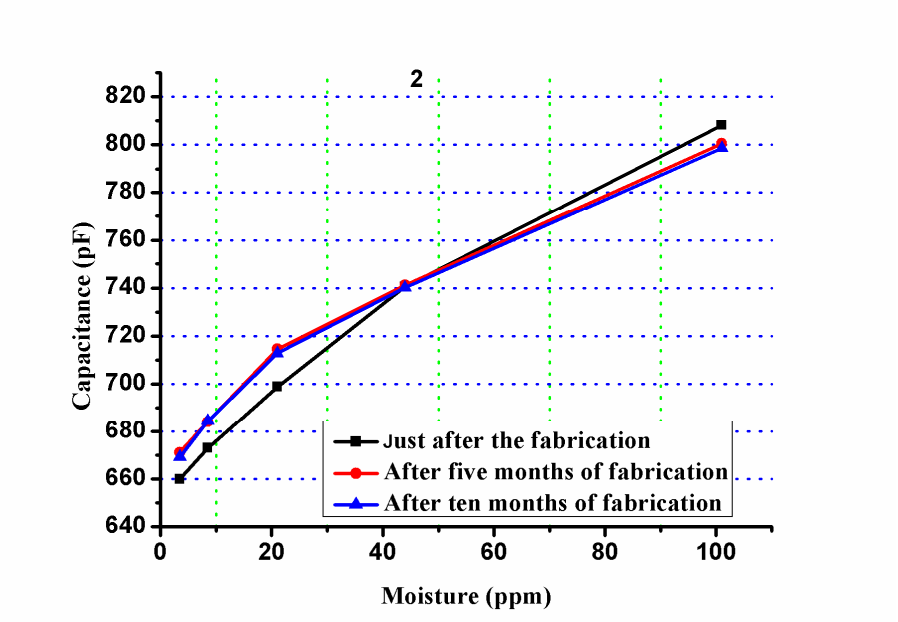

Fig. 6.10b Capacitive response of sample 2 of sensor S1 kept in drying agent.

However, it is to be noted that it is very difficult to measure and maintain the 0ppm moisture concentration in environment around the sensor. Therefore, the base value of the sensor was estimated with the curve fitting of the experimental data shown in Fig. 6.10a.The base value of the sample 1of the sensor S1 just after the fabrication, in the first five months and in the next five months are 636.9 pF, 649 pF and 650.5 pF respectively. The maximum sensitivity drift (without offset value) in the first five months at 3 ppm and 101 ppm are 1.56 pF and 14.1 pF respectively.

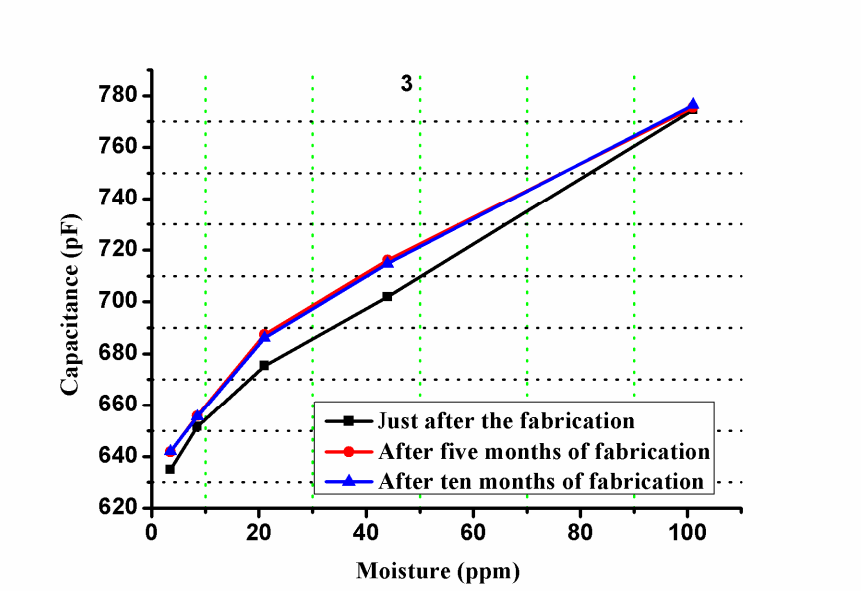

Fig. 6.10c Capacitive response of sample 3 of sensor S1 kept in drying agent.

But in the next five months, the sensitivity drift is negligible. Similar response is observed for the other two samples of the sensor S1 as indicated in Fig. 6.10b and Fig. 6.10c. Table ï 6.4 shows the average sensitivity of three samples at different time. The drift in sensitivity is small. The experiment was then performed with the sensor S2. The capacitive response of three samples of same geometrical parameters of the sensor S2 stored in open laboratory environment is shown in Fig. 6.11a, Fig. 6.11b and Fig. 6.11c. Fig. 6.12 shows the sensitivity drift of the sensor S2 at different time. It shows that there is a significant drift in sensitivity of S2 with time and the sensitivity decreases continuously as the moisture level increases. The average sensitivity of three samples of sensor S2 at different time is also shown in Table-6.4. The estimated base line value of sample 1 of S2 at 0 ppm just after the fabrication, in the first five months and in the next five months were 526.4 pF, 536.31 pF, and 527.4 pF respectively. In the first five month, the base value of sensor S2 increases. It indicates the higher effective dielectric constant of the sensing material than fresh prepared sensor due to the formation of hydrated layer inside the air pore and dry wall, increment in the pore size and a layer of residual water in the pores. However, the base capacitance decreases after ten months. It indicates that the effective dielectric constant of the sensing material decreases due to the large stretch of hydrated wall inside dry wall of the pore cell with time. The base values of the sample 1 of the sensor S2 after ten months aging obtained from the experimental data, when heated at 450ŰC, and without heating are 474.5 pF and 527.4 pF respectively. The change in base value after heating indicates the increased pore size due to aging of the sensor S2 in ten months, because after heating the sensor at 450ŰC the hydrated wall was dried and the residual

water layer inside the pore was completely destroyed. The estimated pore size obtained using model (6.2) after ten months of aging was 13.04 nm. The drift in base value after ten months with and without heating at 450°C is 52.9 pF. It indicates the drift is mainly due to the stretch of hydrated alumina inside the dry wall and residual water layer inside the pore. The base value after ten months without heating is still lesser than base value after five months, which indicates the further stretch of hydrated alumina inside the dry wall with time but the layer of residual water and hydrated layer inside the pores remain more or less constant. The maximum drift in the estimated base value after first five months is 9.91 pF. The maximum sensitivity drift of the sample 1of S2 after ten months at 15 ppm moisture was 1.25 pF/ppm. The sensitivity just after the fabrication, in the first five months and in the next five months at 15 ppm moisture concentration were 1.57 pF/ppm, 0.5492 pF/ppm and 0.3141 pF/ppm respectively. Similar response is observed for the other two samples of S2 as shown in Fig. 6.11b and Fig. 6.11c respectively. The sensitivity was estimated using (6.11).

$$S = \frac{C_{moist}(pF) - C_{dry}(pF)}{Full\,scale(ppm)} \tag{4.11}$$

Experiments were also conducted to observe the effect of heating of the sensor S2 at high temperature but the response of the sol-gel based ɔ-Al_2O_3 moisture sensor was temperature independent [68]. The sensor was tested at the step change in moisture from 3 to 100 ppm and the sensor produced repeatable results [83-84, 163]. After 10 months, the sensor S2 was then heated at 450°C to refresh it and then the experiment was again repeated to determine the capacitance values with variation of humidity in ppm. Results of three samples are shown in Fig. 6.11a, Fig.6.11b and Fig. 6.11c (green color). It is observed that the sensitivity of S2 was recovered almost completely. When S2 was stored in open atmosphere, the un-hydrated alumina surface undergoes phase transformations during the hydration process and the surface morphologies vary due to lateral seepage of moisture with time. As the pore size increases, the capacitance value of the sensor decreases as shown in simulation results in Fig. 6.6 for the model of S2 represented by (6.6). However, heating the sensor at 450°C after ten months, the sensor is completely dried (formation of hydrated layer inside the dry wall and pore is considered negligible)but the pore size increases. Therefore, the sensitivity of the sensor is similar to the new designed sensor but lower base capacitance value.

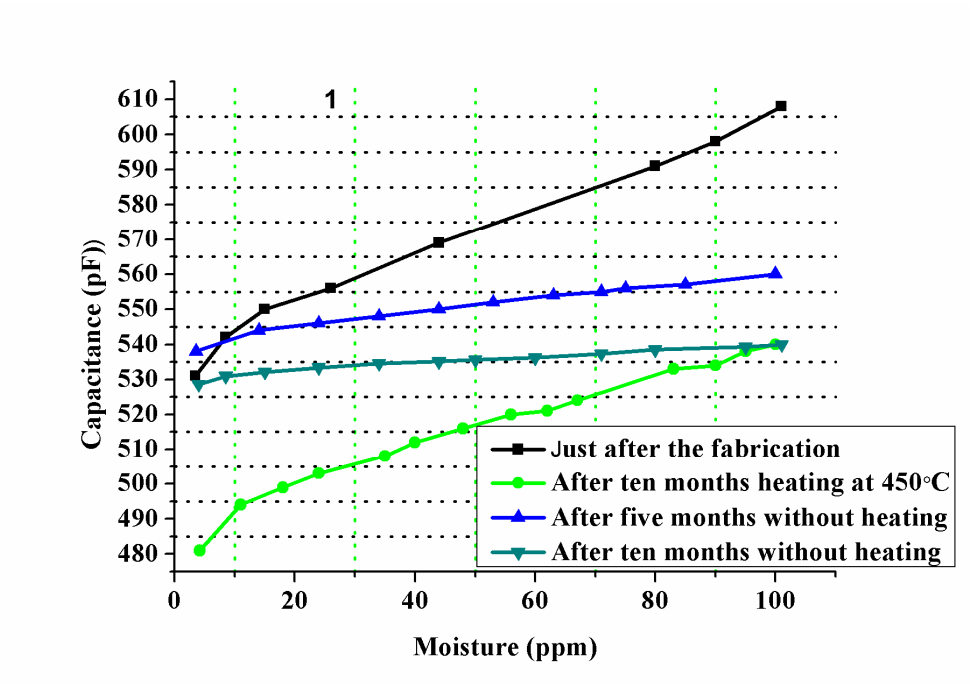

Fig. 6.11a The capacitive response of the sample 1of the sensor S2 kept in atmospheric humidity of laboratory.

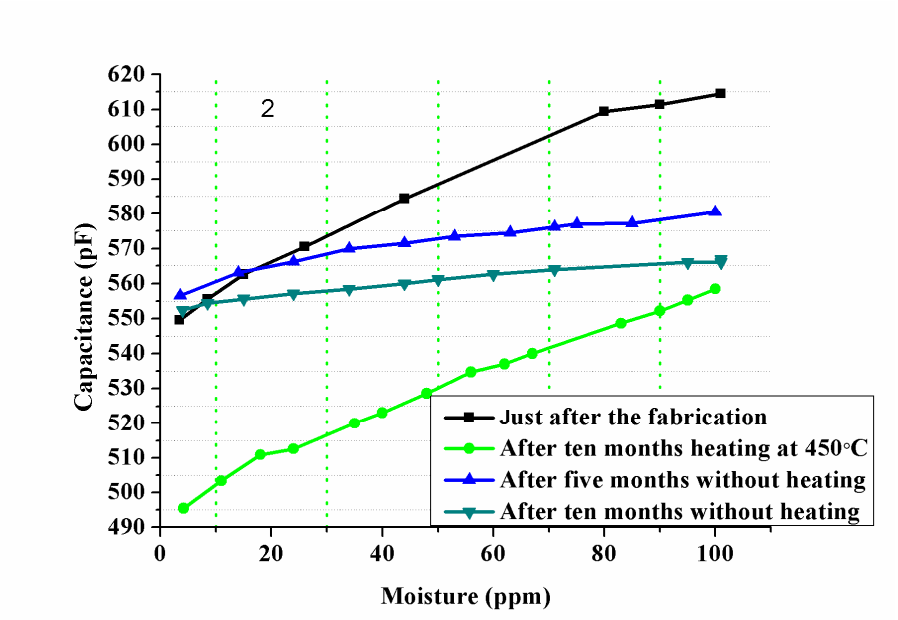

Fig. 6.11b Capacitive response of sample 2 of sensor S2 kept in atmospheric humidity of laboratory.

Thus, the drift can be reduced to a great extent by heating the sensor. Since the sensor S1 having negligible drift even after ten months, study of the drift after heating the sensor at 450ŰC was not performed.

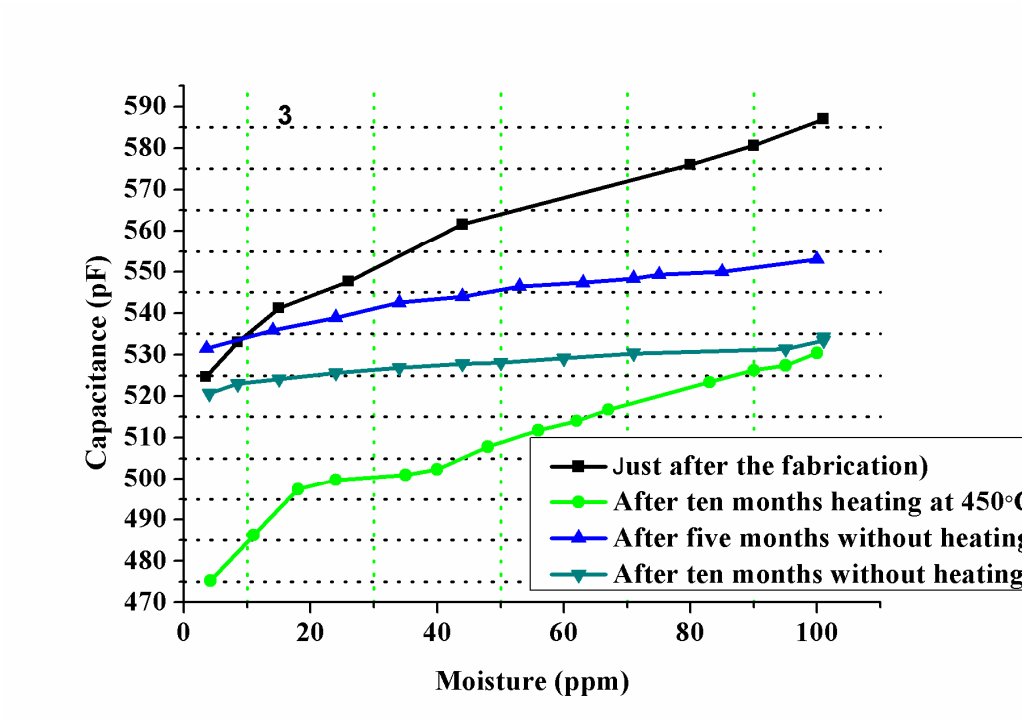

Fig. 6.11c The capacitive response of the sample 2 of the sensor S2 kept in atmospheric humidity of laboratory.

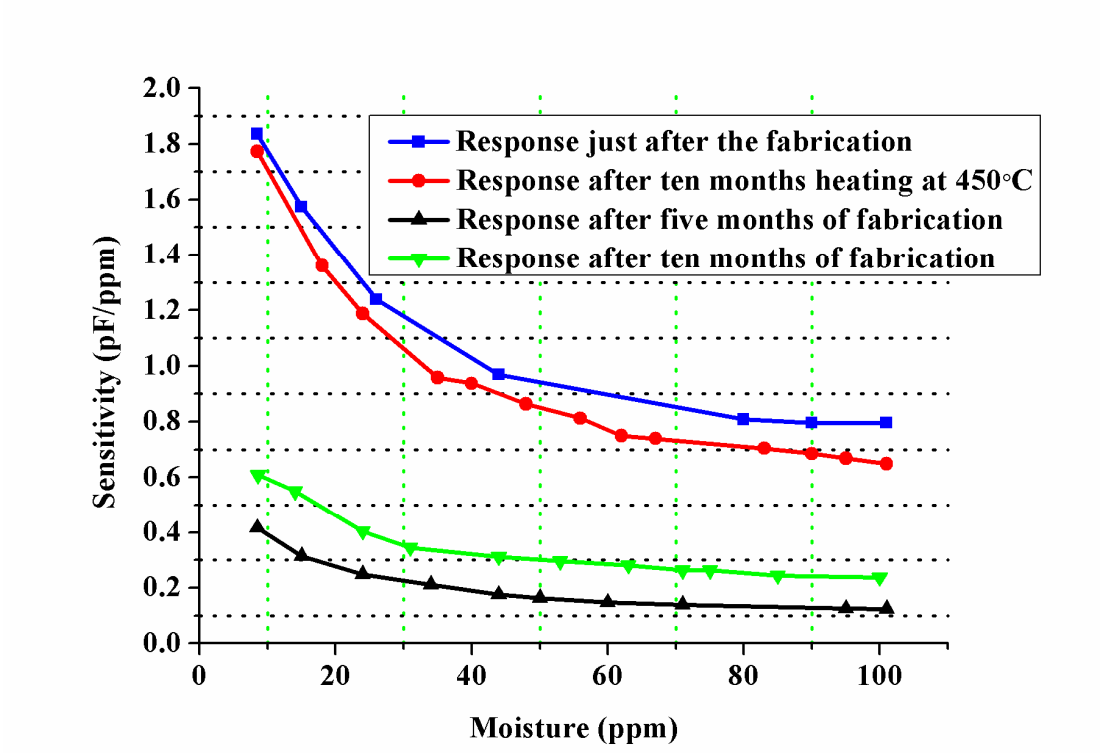

Fig. 6.12 Variation of the sensitivity of sample 1 of sensor S2 at different moisture level and different time.

Table-6.4

Average sensitivity in different time for S1 and S2

Sensor	Sample No.	Fresh sensor (pF/ppm)	After five months (pF/ppm)	After ten months (pF/ppm)	After ten months heating at 450°C (pF/ppm)
S1 (In drying agent)	1	2.068	1.895	1.822	Not studied
	2	2.06	2.01	2.12	-
	3	2.17	2.14	2.09	-
S2 (In open environment)	1	1.10	0.329	0.209	0.988
	2	0.89	0.361	0.215	0.780
	3	0.97	0.296	0.212	0.871

6.6 Validation and suitability of the developed model

The normalized simulated response of the sensors S1 and S2 obtained using models (6.2) are shown in Fig. 6.6.The experimentally determined pore size and predicted pore size using model (6.2) of the sample 1 of the sensor S1 were 10.5 nm and 10.69 nm and for the sample 1 of the sensor S2 were 10.5 nm and 10.76 nm respectively. The estimated values were close to the actual values obtained experimentally. Maximum deviation of pore size of both S1 and S2 were 1.80% and 2.47% respectively. The base capacitance value of the sample 1 of the sensors S1 and S2 just after the fabrication obtained using curve fitting of the experimental data as shown in Fig. 6.10a and Fig. 6.11a are 636.9 pF and 526.4 pF respectively and the computed value from the model (6.6) are 641.7 pF and 529.7 pF respectively. Maximum deviation of the estimated capacitance value for S1 and S2 were 0.75% and 0.62% respectively. Thus, there is a close agreement between the experimental and predicted models values. The structural response of the aged sensor S2 obtained with the help of model. (6.4) is shown in Fig. 6.4. The capacitance value increases as the hydrated layer formed inside the pore and decreases as the layer formed into the dry alumina wall. The base values of sample 1 of sensor S2 after ten months aging obtained from the experimental data, when heated at 450°C and without heating are 474.5 pF and 527.4 pF respectively. The change in base value after heating at 450°C indicates the increased pore size due to aging of the sensor S2 with time. The estimated pore size obtained using model (6.2) after ten months of aging was 13.04 nm. An increment in the pore size of the sample with time was due to the lateral seepage of

moisture into the dry alumina wall of the cell. The level of hydrated alumina into the dry wall corresponding to the increased pore size of 13.04 nm, which was determined using model (6.5), was estimated to be 0.291 nm. Similar type of response was also found for rest of the two samples of sensor S2 as shown in Fig.6. 11b and Fig. 6.11c. The condensation of moisture and layer of residual water inside the pores of the sensor will be computed with (6.6) using the experimental capacitive response of the sensors. Formation of hydrated alumina wall in S1 kept in drying agent was considered negligible. The capacitive response of sensors S1 and S2 with condensation of moisture inside the pore are shown in Fig. 6.5.The area of the pores filled with moisture has higher effective dielectric constant than the pores filled with air and consequently, the capacitance values of the sensors increase as the level of the moisture condensation inside the pores increases. The condensation of moisture inside the pores increases due to the increase in moisture level around the sensor environment. At higher concentration, when the pores are completely filled, the capacitance value reaches to the saturation level.

6.7 Conclusion

In this chapter, two capacitive sensors were fabricated to study the offset capacitance and the sensitivity drifts for measuring moisture in ppm in different environments. The electrical equivalent circuits to show the drift behaviour of the aged sensors for the measurement of trace moisture were developed. Modelling of drift of the sensors was done using the actual pore morphology of the porous layer obtained from the experimental data. The response of the sensors was simulated using a mathematical model obtained from the electrical equivalent circuit. The moisture condensation inside the pores, level of hydrated layer into the dry alumina and inside the pore of the sensor was computed using the model equations. The sensitivity of the sensor S2 kept in the open atmosphere decreases continuously with time as the moisture level in the atmosphere around the sensor increases. But the sensitivity of the sensor was recovered after ten months when the sensor was heated at 450°C. The sensitivity of the sensor S1 kept in the drying agent remains more or less constant for the whole duration of ten months of the experiment. A close agreement between the simulated and the experimental responses in the sensors was found. The models can be used to estimate the level of moisture condensation and the drifts in any capacitive humidity sensor working at ppm level. The main objective of this chapter is to study the drift of the sensor with respect to time. So that the accuracy of moisture measurement in real time application can be ensured and the calibration of the sensor can be planed.

Chapter 7

Summary, Conclusions and Future Scope

7.1 Summary and Conclusions

Moisture is the key impurity in high voltage transformers. It accelerates the aging of the insulation. Ambient air moisture is considered as the major source of moisture contamination. For the protection of the transformer from the excess ingresses of atmospheric air moisture, self dehydrating silica gel breather required. For the health assessment of insulation, there is a need to continuously monitor the humidity level of the T/F breather and oil.

For estimating the moisture content of the silica ï gel inside the breather, mathematical models are developed. Models are developed considering the real time operation of the high voltage transformer. Model was analysed using the steady state operation of moisture transfer between breather air to the silica - gel. The models were validated with the experimental results. The model has capability to predict the failure of the silica - gel.

A state of art to develop different levels of moisture sensitive capacitive humidity sensors by controlling the pore morphology of anodic aluminium oxide (AAO) and by optimizing the structure of the sensor has been developed. The minimum and maximum sensitivity of the designed sensor was 0.8 PF/RH and 15 PF/RH in the range of 1-97% RH. The designed sensor was used for absolute measurement of moisture (172- 796 ppm) in transformer oil at different temperature (30-110℃).

A microcontroller based electronics circuit works on the principle of phase detection to monitor and control the moisture in the breather of T/F has been designed. The possible mathematical equations at different operating points of the electronic circuit were developed. The proposed method of moisture control using a heater via moisture sensor in the breather will reduce the visual inspection of the degree of moisture level in the drying agent (silica gel), regular replacement of drying agent. Finally, the dehydrating capacity of the proposed breather has been improved by 42.85%. The operational reliability of the transformer will increase due to automatic moisture control of the breather.

A mathematical model indicating the drift phenomena of the sol-gel based capacitive humidity sensor was developed and simulated. The sensor was fabricated to measure moisture from 3-100 ppm, as the anodized capacitive sensor shows the response from 172-796 ppm. Model was developed with the help of an electrical equivalent circuit of the aged humidity sensor. It can be used for the estimation of variation of pore size, level of hydration of pore

cell and level of water stretching inside the pore due to the aging of oxide layer. The maximum variation in the model response and experimental data was found 2.47%. The same model can be used for the ppm alumina sensor fabricated by the anodization method.

7.2 Future scope

The present thesis was aimed to develop the humidity sensor for the health monitoring of the high voltage transformer. For the trace level moisture measurement sol-gel techniques was used for the development of sensor. For the high level of moisture measurement (% RH), electrochemical anodization method was used for the fabrication of the sensor. Anodized sensor was also used to measure moisture in ppm in transformer oil. By controlling the pore morphology of the sensing material through electrochemical anodization, the developed sensor is used for the detection of different level of humidity in %RH.

Development of electrochemical anodization-based sensor for trace level of moisture detection in gas insulated switch gear (GIS) may be the future scope of the work.

A drift model for the sol gel-based humidity sensor was developed. Drift is due to aging of the porous structure of the sensing material. Anodic aluminium oxide developed through the electrochemical anodization has also porous structure. Development of drift model for this sensor may be the future work.

The developed sensors were used to monitor the moisture inside the breather and oil of the transformer. This sensor can be used to measure the moisture based on Internet of Things (IoT). Data can be monitored through IoT on the smart phone. It may be future scope of the work to develop a prototype system based IoT for online condition monitoring.

A moisture model for the detection of moisture in the silica-gel breather using finite difference method may be the future scope of the work.

References

[1] Bruno Andò, Salvatore Baglio, Antonio Pistorio, Giuseppe Marco Tina and Cristina Ventura, ñSentinella: smart monitoring of photovoltaic systems at panel levelò, IEEE Transaction Instrumentation and Measurement, vol. 64, no. 4, pp. 2188-2199, Aug. 2015.

[2] Jose Ignacio Aizpurua, Stephen D. J. McArthur, Brian G. Stewart, Brandon Lambert, James G. Cross and Victoria M. Catterson ñAdaptive power transformer lifetime predictions through machine learning and uncertainty modelling in nuclear power plantsò, IEEE Transaction on Industrial Electronics, vol. 66, no. 6, pp. 4726 ï 4737, Jun. 2019.

[3] Parts of a power-transformer, 2019. Available at http://owlcation.com>STEM> Electrical Engineering.

[4] Electrical 4u: ñSilica-gel breather of transformerò, 2014. Available at http ://www.electrical4u.com/silica-gel breather

[5] Transformer breather, 2019. Available at www.brownell.co.uk.

[6] David Yu, S. A. Klein, and D. T. Reindl, ñAn evaluation of silica-gel for humidity control in display casesò, Waac News letter, vol. 23, no. 2, pp. 1-17, 2001.

[7] Messko instruments, ñMaintenance - free dehydrating breather of premium series twice as reliable and simply effectiveò, Ref. N2072/08/01 EN ï Messko® MTraB® premium series ï MS99089103 - 10/14 ï ©Messko GmbH 2014. Available at http://www.messko.com. Solution of dehydrating breather.pdf

[8] John Sabau , Fofana, A. Bouaïcha, and Y. Hadjadj , ñAn environmentally friendly dissolved oxygen and moisture removal system for freely breathing transformersò, IEEE Electrical Insulation Magazine, Vol. 26, no. 3, pp. 35-43, Jun. 2010.

[9] Annual Book of ASTM Standards Part 40, Electrical Insulation -Specifications: Solids, Liquids, Gases; Test Methods Liquids, Gases; Electrical Protective Equipment for Workers, Phila. , Pa., 1981

[10] Ivanka Atanasova-Höhlein et al.ñExperience with capacitive on-line sensors for moistur evaluation in transformer insulationò IEEE Electrical Insulation Magazine, vol. 35, no.2, pp. 18-26, Aprl. 2019.

[11] A.C.M. Wilson, ñInsulating liquids; their Uses, Manufacture and Propertiesò, Peter Peregrinus Ltd. ISBN 0 906048 23 0, pp 1-82.

[12] M. Eklund, ñMineral insulating oils; functional requirements, specifications and productionò, Conference Record, International Symposium on Electrical Insulation, 2006.

[13] Singh, J., Sood, Y. R., and Verma, P., ñExperimental investigation using accelerated aging factors on dielectric properties of transformer insulating oilò, Electrical Power Components and Systems, vol. 39, pp. 1045-1059, 2011

[14] BS EN 60156: 1996, IEC 60156:1995, Insulating liquids. Determination of the breakdown voltage at power frequency, Test method.

[15] Abdel Ouahab, M.A., Hamada, M.M., Zeitoun, A.G., Ismail G., ñA newly modiýed forced oil cooling system and its impact on in-service transformer oil characteristicò, IEEE Trans. Power Deliv., vol. 18, no. 3, pp.827-834, 2003.

[16] I. Fofana ; H. Borsi and E. Gockenbach, ñFundamental investigations onsome transformer liquids under variou outdoor conditionsò, IEEE Transactions on Dielectrics and Electrical Insulation, Vol. 8, no. 6. pp. 1040-1047, Dec. 2001.

[17] Paulapuro, Hannu , ñPaper and Board gradesò, Paper making Science and Technology-18. Finland: Fapet Oy. ISBN 952-5216-18-7, pp. 106ï 108, 2000.

[18] Ekanayake, C., Gubanski, S.M., Graczkowski, A., Walczak, K., ñFrequency response of oil impregnated pressboard and paper samples for estimatingmoisture in transformer insulationò, IEEE Trans. Power Delivery, vol. 21, no. 3, pp. 1309-1317, 2006.

[19] Katsuhko Ogata: Modern Control Engineering (Prentill Hall, 2010, 5thedn.

[20] Ernest O Doebelin: Measurement Systems (Tata McGraw Hill Education Private Limited, 2003, 6th edn.

[21] M. Butcher: ñMechanisms of charge conduction and break down in liquid dielectricsò, Ph.D. dissertation, Graduate Faculty of Texas Tech University 2005.

[22] P. Przybylek, ñThe influence of temperature and aging of cellulose on water distribution in oil-paper insulationò, IEEE Transactions on Dielectrics and Electrical Insulation, vol. 20, no. 2, pp. 552-556, 2013.
[23] Yuanwei Zhu , Shengtao Li and Daomin Min: ñOrigin of dielectric processes in aged oil impregnated paperò, IEEE Transactions on Dielectrics and Electrical Insulation, Vol. 24, no. 3, pp 1625-1635, Jun. 2017.
[24] Odríguez-Rodríguez J H, Martínez-Piñon F, ÁlvarezChávez J A, Jaramill ï Vigueras D and Robles-Pimentel E G, ñDirect optical techniques for the measurement of water content in oil-paper insulation in power transformersò, Measurement Science and Technology, vol. 22, no. 11. pp. 65706-65716, 2011.
[25] M. Koch, S. Tenbohlen, M. Rösner, ñMoisture ingress in free breathing transformersò, CMD 2008 International Conference on Condition Monitoring and Diagnosis, Beijing, China, 2008.
[26] Yi Cui ; Hui Ma ; TapanSaha ; Chandima Ekanayake ; Guangning Wu, ñMulti-physics modelling approach for investigation of moisture dynamics in power transformersò, IET Generation, Transmission & Distribution, vol. 10, no. 8, pp. 1993-2001, May 2016.
[27] Belen Garc´ëa , Rafael Villarroel, and Diego Garc´ëa, "A multiphsical model to study moisture dynamics in transformers", IEEE Trans Power delivery, vol. 34, no. 4, pp. 1365-1373, August, 2019.
[28] Abubakar Abdullkareem Suleiman et al. ñMoisture effect on conductivity of kraft paper immersed in power transformer vegetable-based insulation oilsò, IET Generation, Transmission & Distribution, Vol. 11, no. 11, pp. 2269-2274, Jul. 2017.
[29] Alhaytham Alqudsi ; and Ayman El-Hag, ñAssessing the power transformer insulation health condition using a feature-reduced predictor modeò, IEEE Transactions on Dielectrics and Electrical Insulation, Vol. 25, no. 3, pp. 853-862, Jul. 2018.
[30] IEC 60814 (1997) Insulating liquidsð oil-impregnated paper and pressboardð determination of water by automatic coulometric Karl Fischer titration.
[31] M. Koch, S. Tenbohlen, J. Blennow, I. Hoehlein, ñReliability and Improvements of Water Titration by the Karl Fischer Techniqueò, Proceedings of the XVth International Symposium on High Voltage Engineering, ISH, Ljubljana, Slovenia, 2007.
[32] V. Sarfi, S. Mohajeryami, and A. Majzoobi, ñEstimation of water content in a power transformer using moisture dynamic measurement of its oilò, High Voltage, vol. 2, no. 1, pp. 11ï 16, Jun., 2017.
[33] Ryuichi Nakane, Hitoshi Okubo; and Katsumi Kato, ñHVDC electrical insulation performance based on charge activity in oil -pressboard composite insulation structuresò, IEEE Transactions on Dielectrics and Electrical Insulation, vol. 26, no. 2, pp. 576-583, Mar. 2019.
[34] Temperatures. Part 2. Influence of Moisture and Temperature on Degree of Polymerization and Formation of Furanic Compounds in Free-Breathing Systemsò IEEE Electrical Insulation Magazine, vol. 21, no.5, pp. 20-24, Oct., 2005.
[35] A. Baral ; S. Chakravorti Prediction of moisture present in cellulosic part of power transformer Insulation using Transfer Function of modified debye modelò, IEEE Transactions on Dielectrics and Electrical Insulation, Vol. 21, no.3, pp. 1368-1375, Jun. 2014.
[36] Garcia, B., Burgos, J.C., Alonso, A.M., Sanz, J., ñA moisture-in-oil model for power transformer monitoring ï part I: theoretical foundationò, IEEE Trans. Power Deliv., Vol. 20, pp. 1417-1422, Aprl. 2005.
[37] Ruijin Liao, Yuandi Lin, Yiyi Zhang and Huanhuan Xia, ñIndependent effects of aged oil and aged paper on moistur evaluation of power transformersò, Electric Power Components and System, Vol. 44, no. 5, pp. 556-564, Mar. 2016.
[38] P.A. von Guggenberg, ñApplication of interdigital dielectrometry to Moisture and Double Layer Measurements in Transformer Insulationò, PhD Thesis, Section 6.3, Massachusetts Institute of Technology, MA, June 1993.
[39] Manoj Mandlik and T. S. Ramu, ñMoisture aided degradation of oil impregnated paper insulation in power Transformersò, IEEE Transactions on Dielectrics and Electrical Insulation, vol. 21, no. 1, pp. 186-193, 2014.

[40] Hao, J., Liao, R., Ma, Z., Yang, L., ñInþuence of natural ester onfrequency dielectric response of impregnated insulation pressboardò, IET Sci. Meas.Technol., vol. 6, no. 6, pp. 403ï 411, 2012.
[41] Garcia, B., Burgos, J.C., Alonso, A.M., Sanz, J., ñA moisture-in-oil model for power transformer monitoring ï part I: theoretical foundationò, IEEE Trans. Power Deliv., vol. 20, no. 5, pp. 1417-1422, 2005.
[42] Ivanka Atanasova-Höhlein et al., ñExperience with capacitive on-line sensors for moisture evaluation in transformer insulationò, IEEE Electrical Insulation Magazine, Vol. 35, no. 2, pp. 18-26, Aprl. 2019.
[43] Alaa Razzaq ; Hidayat Zainuddin ; Farhan Hanaffi and Radhi M. Chyad ñTransformer oil diagnostic by using an optical fibre system: a reviewò, IET Science, Measurement & Technology, vol. 13, no. 5, pp. 615-621, July 2019.
[44] Chenhu Sun , Paul R. Ohodnicki and Emma M. Stewart ñChemical Sensing Strategies for real-time monitoring of transformer oil: A Reviewò, IEEE Sensors Journal, vol. 17, no. 18, pp. 8786-5806, Sept. 2017.
[45] S. Laskar and S. Bordoloi, ñMonitoring of moisture in transformer oil using optical fiber as sensorò, Journal of Photonics, vol. 13, no.1, pp. 1-7, Jul. 2013.
[46] T. L. Yeo, T. Sun and K.T. V. Grattan, ñFibre-optic sensor technologies for humidity and moisture measurement,ò Sens. Actuators A Phys. 144, pp. 280ï 295, 2008.
[47] Daniela Lo Presti, Carlo Massaroni and Emiliano Schena, ñOptical fiber gratings for humidity measurementsò, A Reviewò IEEE Sensor Journal, vol. 18, no. 22, pp. 9065-9074, Sept. 2018.
[48] Tengpeng Sun , Weijia Wang , Jiankun Peng , Yapeng Qu , Jixiang Dai and Minghong Yang, ñEffect of different inorganics on polyimide-based bragg grating humidity sensorò, IEEE Sensors Journal, vol. 19, no. 6, pp. 2016-2022, Mar. 2019.
[49] Debdulal Saha and K Sengupta[2,ò] Trace moisture detection in oil filled transformer by ceramic sensorò, IOP Conf. Series: Materials Science and Engineering, vol. 73, no.1, pp. 1-4, 2015.
[50] Tarikul Islam, Md. Firoz A Khan and Shakeb A Khan. ñMoisture measurement of transformer oil using thin film capacitive sensorò, 6th IEEE Power India International Conference (PIICON), 2014.
[51] J. H. Rodriguez-Rodriguez, F. Martinez-Pinon, J. A. Alvarez Chavez et al., "Polymer optical fiber moisture sensor based on evanescent-wave scattering to measure humidity in oil-paper insulation in electrical apparatusò, IEEE Sensors Journal, vol. pp. 1052-1055, 2008.
[52] Deba Kumar Mahanta and Shakuntala Laskar, ñWater quantity-based quality measurement of transformer oil using polymer optical fiber as sensorò, IEEE Sensors Journal, vol. 18, no. 4, pp. 1506-1512, Feb. 2018.
[53] Tapan K. Saha, ñReview of modern diagnostic techniques for insulation condition in aged transformerò, IEEE Transactions on Dielectrics and Electrical Insulation, vol. 10, no. 5, pp.903-917,. 2003.
[54] M.C. Zaretsky , J.R. Melcher and C.M. Cooke, ñMoisture sensing in transformer oil using thin-film microdielectrometryò, IEEE Transactions on Electrical Insulation, vol. 24, no. 6, pp. 1167-1176, Dec. 1989.
[55] Y. Sheiretov, and M. Zahn, ñDielectrometry measurements of moisture dynamics in oil-impregnated pressboardò, IEEE Transactions on Dielectrics and Electrical Insulation, vol. 2, no.3, pp. 329-351, Jun 1995.
[56] Muhammad A. Ansari , Daniel Martin and Tapan Kumar Saha,ò Investigation of distributed moisture and temperature measurements in transformers using fiber optics sensors, IEEE Transactions on Power Delivery, vol. 34, no. 4, pp. 1776-1784, Aug. 2019.
[57] W. Zhang and D. J. Webb, ñPMMA based optical fiber bragg grating for measuring moisture in transformer oil, IEEE Photonics Technology Letters, vol. 28, no. 21, pp. 2427-2430, Nov. 2016.

[58] Garcia, B., Burgos, J.C., Alonso, A.M., Sanz, J, ñA moisture-in-oil model for power transformer monitoring ï part II: experimental veriýcationò, IEEE Trans. Power Deliv., vol. 20, no. 2, pp. 1423-1429, 2005.

[59] Gajanan C. Jaiswal , Makarand Sudhakar Ballal and M. M. Renge, ñCondition monitoring of breather for transformer health assessmentò, In proc. on IEEE International Conference on Power Electronics, Drives and Energy SystemsAnnual IEEE India Conf., 2018.

[60] P. A. Von Guggenberg and J. R. Melcher ñA three-wavelength flexible sensor for monitoring the moisture content of transformer pressboardò, Proceedings of the 3rd International Conference on Properties and Applications of Dielectric Materials, Tokyo, Japan, Japan, 8-12 July 1991.

[60] Hongran Zhao, Xiuzhu Lin, Rongrong Qi, Jianxun Dai, Sen Liu, Teng Fei and Tong Zhang ñA Composite Structure of In Situ Cross-Linked Poly(Ionic Liquid)s and Paper for humidity-monitoring applicationsò, IEEE Sensors Journal, vol. 19, no. 3, pp. 833-837, Feb. 2019.

[61] Tarikul Islam and Mohammad Zia Ur Rahman, ñInvestigation of the electrical characteristics on measurement frequency of a thin-film ceramic humidity sensorò IEEE Transaction Instrument and Measurement, vol. 65, no. 3, pp. 694-702, Mar. 2016.

[62] M. Matsuguch, T. Kuroiwa, T. Miyagishi, S. Suzuki, T. Ogura and Y. Sakai, ñstability and reliability of polyimide humidity sensors using crosslinked polyimide filmsò, Sensors and Actuators B, vol. 52, pp. 53-57, 1998.

[63] U. Kang and K. D. Wise, ñA high speed capacitive humidity sensor with on-chip thermal resetò, IEEE Transactions on Electron Devices, vol. 47, pp. 702-710, 2000.

[64] Y. Y. Qui, C. Azeredo-Leme, L. R. Alcacer, J. E. Franca, ñA CMOS humidity sensor with on-chip calibration,ò Sensors and Actuators A, Vol. 92, pp. 80-87, 2001.

[65] D. Lu, Y. Zheng, A. Penirschke and R. Jakoby, ñHumidity sensors based on photo lithographically Patterned PVa films deposited on SAW resonatorsò IEEE Sensors Journal, vol. 16, no. 1, pp. 13-14, Jan. 2016.

[66] António Vaz, Nathalie Barroca; Miguel Ribeiro; André Pereira and Orlando Frazão ñOptical fiber humidity sensor based on polyvinylidene fluoride fabryï perotò IEEE Photonics Technology Letters, vol. 31, no. 7, pp. 549-552, Feb. 2019.

[67] T. Islam, L. Kumar, and S. A. Khan, ñA novel sol-gel thin ýlm porous alumina based capacitive sensor for measuring trace moisture in the range of 2.5ï 25 PPMvò, Sens. Actuators B, Chem., vol. 173, pp. 377ï 384, Oct. 2012.

[68] Debdulal Saha, Dilip Kr. Ghara and Mrinal Pal, ñNano porous ɔ-alumina based novel sensor to detect trace moisture in high temperature and high pressure environmentò, Sens. Actuators B Chem., vol. 222, pp. 1043ï 1049, Jan. 2016.

[69] Tarikul Islam, Md. Rahat Mahboob and Shakeb A. Khan, ñA Simple MOX vapour sensor on polymide substrate for measuring humidity in ppm levelò, IEEE Sensor vol. 15, no. 5, pp. 3004-3013, May 2015.

[70] Y. Sakai, ñHumidity sensors using chemically modified polymeric materialsò, Sensors and Actuators B, vol. 13 pp. 82-85, 1993.

[71] Ning Li, Xiangdong Chen, Xinpeng Chen and Xing Ding, ñUltrafast response humidity sensor based on GOQDs/polyelectrolyte composite filmsò, Electronics Letters, vol. 52, no. 19, pp. 1609-1611, Sept. 2016.

[72] Y. Wang and J. T. W. Yeow, ñHumidity sensing of ordered macro porous silicon with HfO2 thin film surface coatingò, IEEE Sens. J., vol. 9, pp. 541ï 547, 2009.

[73] Z. M. Rittersma, A. Splinter, A. Bödecker and W. Benecke, ñA novel surface micro machined capacitive porous silicon humidity sensor,ò Sensors and Actuators B, Vol. 68, pp. 210-217, 2000.

[74] Foucaran, B. Sorli, M. Garcia, F. Pascal-Delannoy, A. Giani and A. Boyer, ñPorous silicon layer coupled with thermoelectric cooler: a humidity sensor,ò Sensors and Actuators A, vol. 79, pp. 189-193, 2000.

[75] Tarikul Islam , Deb DulalSaha , Prince M. Z. Hasan and Sheikh Safiul Islam ñɔï Al2O3 - coated porous silicon for trace moisture detectionò IEEE Sensors Journal, vol. 11, no. 4, pp. 882-887, Apr. 2011.

[76] T. Islam, S.S. Islam and H. Saha, ñPorous silicon based moisture detector in the PPMv range,ò Sensors Letters vol. 6, pp. 746-751, 2008.
[77] Saakshi Dhanekar, S.S. Islam, T. Islam, A.K. Shukla and Harsh, ñOrganic vapour sensing by porous silicon: influence of molecular kinetics in selectivity studies,ò Physical E, vol. 42, no. 5, pp. 1648-1652, Jun. 2010.
[78] J. J. Steele, M. T. Taschuk, M. .J. Brett, ñNanostructured metal oxide thin. films for humidity sensors,ò IEEE Sens. J., vol. 8, pp. 1422ï 1429, 2008.
[79] Baochang Cheng, Baixiang Tian, CuicuiXie, Yanhe Xiao and Shuijin Lei, ñHighly sensitive humidity sensor based on amorphous Al_2O_3 nanotubes,ò J. Mater. Chem., vol. 21, pp. 1907ï 1912, 2011.
[80] Upendra Mittal , Tarikul Islam , Archibald Theodore Nimal and Manoj Umesh Sharma ñA novel Solï Gelɔ-Al_2O_3thin-film-based rapid SAW humidity sensorò, IEEE Transaction Electron Devices, vol. 62, no. 12, pp. 4242-4250, Dec. 2015.
[81] Zubair Hassan Zargar and Tarikul Islam ñA thin film porous alumina based cross-capacitive humidity sensorò, IEEE Transaction on Instrumentaion and Measurement, early access, Jun. 2019.
[82] T. Islam, D. D. Saha, S. S. Islam, P.M.Z. Mufti, ñɔ-Al_2O_3 coated porous silicon for trace moisture detection,ò IEEE Sensors Journal, Vol. 11, No. 4, pp. 882-887, 2011.
[83] Md. Rahat Mahboob, Zubair Hassan Zargar and Tarikul Islam, ñA sensitive and highly linear capacitive thin film sensor for trace moisture measurement in gasses,ò Sensors and Actuators B Chem., vol. 228, pp. 658ï 664, Jun. 2016.
[84] Lokesh Kumar, Tarikul Islam and Subhas Chandra Mukhopadhyay, ñSensitivity enhancement of a ppm level capacitive moisture sensor,ò Electronics, vol. 6, no. 3, pp. 1-14, May 2017.
[85] Jacob Fraden, ñHandbook of Modern Sensorsò Physics, Designs, and Applicationô (AIP Press: Springer, 2003, 3rd edn.)
[86] B. E. Yoldas, ñA transparent porous aluminaò, Amer. Ceram. Soc. Bull., vol. 54, no. 3, pp. 286ï 288, Jun. 1975.
[87] Hossein-Babaeia and S. Rahbarpour ñAlteration of pore size distribution by solï gel impregnation for dynamic range and sensitivity adjustment in Kelvin condensation-based humidity sensors,ò Sensors and Actuators B 191 pp, 572ï 578, 2014.
[88] G. E. Thompson, R. C. Furneaux, G. C. Wood, J. A. Richardson, and J. S. Goode, ñNucleation and growth of porous anodic films on aluminiumò, Nature vol. 272, pp. 433-435, Mar. 1978.
[89] Chleck , P. Goodman and M. G. Kovac, ñAbsolute humidity sensors and methods of manufacturing humidity sensorsò, U.S. patent No. 4,143,177,1979.
[90] Feiyue Li, Lan Zhang, and Robert M. Metzger, ñOn the growth of highly ordered pores in anodized aluminum oxideò, Chem. Mater., vol. 10, May 1998.
[91] Azadeh Nazemi and Seyed Abolfazl Sseyed Sadjadi, ñControlling the anodizing conditions in preparation of an nano porous anodic aluminium oxide templateò, Materials Science-Poland, vol. 32, no. 4, pp. 565-570, Oct. 2014.
[92] Lujun Yao, Maojun Zheng, Haibin Li, LiMa and Wenzhong Shen, ñHigh-performance humidity sensors based on high-ýeld anodized porous alumina ýlmsò, Nanotechnology, vol. 20, Sept. 2009.
[93] Alaa M. Abd-Elnaiem, A. Gaber, ñParametric study on the anodization of pure aluminum thin film used in fabricating nano-pores templateò, Int. J. Electrochem. Sci., vol. 8, no. 1, pp. 9741-9751, Jul. 2013.
[94] Jihun Oh and Carl V. Thompson, ñThe role of electric ýeld in pore formation during aluminum anodizationò, Electrochimica Acta, vol. 56, no. 1, pp. 4044-4051, Mar. 2011.
[95] Kusum Sharma and S. S. Islam, ñptimization of porous anodic alumina nanostructure for ultra high sensitive humidity sensorò, Sensors and Actuators B , vol. 237, pp. 443-451, Jun. 2016.
[96] Jiawei Li, Ying Liu, Min Tang, Jie Li and Xinhua Lin, ñCapacitive humidity sensor with a coplanar electrode structure based on anodised porous alumina filmò, Micro and Nano Letters, vol. 7, no. 11, pp. 1097-1000, Nov. 2012.

[97] Degao Lan and Xiaofeng Zhao, ñFabrication and characteristics of the high-sensitivity humidity sensor of anodic aluminum oxide based on silicon substratesò, International Journal of Modern Physics B, vol. 32, no. 16, pp. 1-8, May. 2018.
[98] László Juhász and János Mizsei, ñA simple humidity sensor with thin film porous alumina and integrated heatingò, Procedia Engineering, vol. 5, pp. 701-704, Sept. 2010.
[99] Mamadou Balde, Arnaud Vena and Brice Sorlie, ñFabrication of porous anodic aluminium oxide layers on paper for humidity sensorsò, Sensors and Actuators B: Chemical, vol. 220, pp. 829-839, Dec. 2015.
[100] L. Juhász and J. Mizsei, ñHumidity sensor structures with thin film porous alumina for on-chip integrationò, Thin Solid Films, vol. 517, no. 22, pp. 6198-6201, Sept. 2009.
[101] S. W. Chen, O. K. Khor, M. W. Liao, and C. K. Chung, ñSensitivity evolution and enhancement mechanism of porous anodic aluminum oxide humidity sensor using magnetic fieldò, Sensors and Actuators B: Chemical, vol. 199, pp. 384-388, Mar. 2014.
[102] Youngdeuk Kim, Bongbu Jung and Hyunchal Park, ñCapacitive humidity sensor designed based on aluminium oxideò, Sensors and Actuators B: Chemical, vol. 141, pp. 441-446, Jul. 2009.
[103] H. O. Ali, ñReview of porous anodic aluminium oxide (AAO) applications for sensors, MEMS and biomedical devicesò, The International Journal of Surface Engineering and Coatings, vol. 95, no. 6, pp. 290-296, Oct. 2017.
[104] Yoshihiko Sadaoka, Yoshiro Sakai and Shoji Matsumoto, ñElectrical properties of anodized aluminium in a humid atmosphereò, Journal of Material Science, vol. 21, pp. 1269-1274, 1986.
[105] V. K. Khanna and R. .K. Nahar, ñSurface conduction mechanisms and the electrical properties of Al_2O_3 humidity sensorò, Applied Surface Science, vol. 28, no. 3, pp. 247-264, Jun. 1987.
[106] RK Nahar and VK Khanna, ñIonic doping and inversion of the characteristic of thin film porous Al2O3 humidity sensorò, Sensors and Actuators B: Chemical, vol. 46, no. 1, pp. 35-41, Jan. 1998.
[107] Murugaiya Sridar Ilango, Amruta Mutalikdesai and Sheela K Ramasesha, ñAnodization of aluminium using a fast two-step processò, J. Chem. Sci., Vol. 128, no. 1, pp. 153-158, Jan. 2016.
[108] E. Hourdakis and A. G. Nassiopoulou, ñHigh-density MIM capacitors with porous anodic alumina dielectricò, IEEE Transaction on Electron Devices, Vol. 57, pp. 2679-2683, Oct. 2010.
[109] Arshi Salamat and Tarikul Islam, ñFabrication of an anodized porous alumina relative humidity sensor with improved sensitivityò, Instrumentation Science and Technology, vol. 47, no. 6, pp. 1-19, Sept. 2019.
[110] M. Almasi, A. Ramzani, H. Abbasian and A. Khayyatian, ñCapacitive humidity sensors based on large diameter porous alumina prepared by high current anodizationò, Sensors and Actuators A Physical, vol. 174, pp. 69-74, Feb. 2012.
[111] Masanobu Matsuguchi, EtsuroHirota, TakaakiKuroiwa, Sachiko Obara, Tsutomu Ogura and Yoshiro Sakai, ñDrift Phenomenon of capacitive-type relative humidity sensors in a hot and humid atmosphereò, Advancing Solid State and Electrochemical Science and Technology, vol. 147, no. 7, pp. 2797-2799, Jan. 2000.
[112] S. A. Bell1, P. A. Carroll1, S. L. Beardmore1, C. England and N. Mander, ñA methodology for study of in-service drift of meteorological humidity sensorsò, Metrologia, vol. 54, no.1, pp. 1681-7575, May 2017.
[113] Masanobu Matsuguchi, Yasunori Takahashi, Takaaki Kuroiwa, Tsutomu Ogura, Sachiko Obara and Yoshiro Sakaia, ñEffect of sensing film thickness on drift phenomenon of capacitive-type humidity sensorsò, Journal of The Electrochemical Society, vol. 150, no. 8, pp. 92-95, July 2003.
[114] F R G Cruz, A H Ballado Jr, A K A Alcala, A K S Legaspi1, E L Lozada and V L P Portugal, ñWireless soil moisture detection with time drift compensationò, AIP Conference Proceedings, vol. 2045, pp. 1-7, Dec. 2018.

[115] Chia-Yen Lee and Gwo- Bin Lee, ñMEMS-based Humidity Sensors with Integrated Temperature Sensors for Signal Drift Compensationò, IEEE Sensor Conference, Toronto, Ont., Canada, 22-24, Oct. 2003.
[116] Almudena Rivadeneyraa, José Fernández-Salmerón, Manuel Agudo,Juan A. López Villanueva, Luis Fermín Capitan-Vallvey and Alberto J. Palmaa, ñDesign and characterization of a low thermal drift capacitive humidity sensor by inkjet-printingò, Sensors and Actuators B: Chemical, vol. 195, no. 1, pp. 123-131, Jan. 2014.
[117] G. J. W. Visscher and J. G. Kornet, ñLong-term tests of capacitive humidity sensors,ò Meas. Sci. Technol., vol. 5, no. 10, pp. 1294ï 1302, Oct. 1994.
[118] T. Islam and H. Saha, ñStudy of long-term drift of a porous silicon humidity sensor and its compensation using ANN technique,ò Sensors Actuators A Phys., vol. 133, no. 2, pp. 472ï 479, Feb. 2008.
[119] L. H. Mai, P. T. M. Hoa, N. T. Binh, N. T. T. Ha, D. K. An, ñSome investigation results of the instability of humidity sensors based on alumina and porous silicon materials,ò Sens. Actuators B vol. 66, pp. 63ï 65, 2000.
[120] Almudena Rivadeneyra, José Fernández-Salmerón, Manuel Agudo and Alberto J. Palma, ñDesign and characterization of a low thermal drift capacitive humidity sensor by inkjet-ò, Sensors and Actuators B Chemical, vol. 195, no. 2, pp. 123-131, Jan. 2014.
[121] J. Salonen, E. Laine, L. Niinisto, ñThermal carbonization of porous silicon surface by acetyleneò, J. Appl. Phys. ; vol. 91, no. 1, pp. 456ï 461, 2002.
[122] J. Kiilunen and L. Frisk, ñHygrothermal aging of an ACA attached PET þex-on-board assemblyò, IEEE Trans. Compon. Packag. Manuf.Technol., vol. 4, no. 2, pp. 181ï 189, Feb. 2014.
[123] V. K. Khannaa, ñA plausible ISFET drift-like aging mechanism for Al_2O_3 humidity sensorò, Sensors Actuators B Chem., vol. 213, pp. 351ï 359, Jul. 2015.
[124] Filho RWND, Rocha GA, Montes CR and Vieira-Coelho AC, ñSynthesis and characterization of boehmites obtained from gibbsite in presence of different environments,ò Materials Research, vol. 19, no. 3, pp. 659ï 668, Oct. 2016.
[125] J. C. Harding Jr., ñOvercoming limitations inherent to aluminum oxide humidity sensorsò, Roc. Int. Symp. on Moisture and Humidity, Washington D. C, pp 367-378, 1985.
[126] Emmer, Z. Hajek and P. Repa, ñSurface adsorption of water vapor on hydrated layers of $A1_20_3$ ò Surf. Sci. , vol. 162, pp. 303-309, 1985.
[127] Z. Chen, M. C. Jin , and C. Zhen, ñHumidity sensors with reactively evaporated Al_20_3 films as porous dielectricsò, Sens and Actuators B vol . 2, pp. 167-171, 1990.
[128] Z. Chen, M. C. Jin, C. Zhen, and G. H. Chen, ñProperties of modified anodic-spark-deposited alumina porous ceramic films as humidity sensorsò, J. Am. Cmm. Soc. , vol. 74, no. 6, pp. 1325- 1330, June 1991.
[129] M. C. Jin, Z. Chen, and G. H. Chen, ñAlumina ceramic thin film humidity sensorsò, Tech. Rept. U. of Elec. Sci. &. Tech. of China, Dec. 1990.
[130] R. S. Alwitt, ñSome physical and dielectric properties of hydrious alumina filmsò, J. Electrochem. Soc., vol. 118, pp. 1730 - 1733, 1971.
[131] Rafiee, K., Feng, Q.and Coit, D.W., ñ Condition-based maintenance for repairable deteriorating systems subject to generalized mixed shock modelò,. IEEE Trans. Reliab. Vol.64, pp.1164ï 1174, 2015.
[132] R. K. Nahar, ñPhysical understanding of moisture induced degradation of nano porous aluminum oxide thin ýlms,ò J. Vac. Sci. Technol.,Vol. B 20, no. 1, pp. 382ï 385, Feb. 2002.
[133] T. K. Mehrhoff, ñComparison of continuous moisture monitors in the range 1 to 15 ppm,ò Rev. Sci. Instrum., vol. 56, no. 10, pp. 1930ï 1933, Oct. 1985.
[134] A. R. K. Ralston, C. F. Klein, P. E. Thomas, and D. D. Denton, ñAmodel for the relative environmental stability of a series of polyimide capacitance humidity sensors,ò in Proc. 8th Int. Conf. Solid-State Sensors Actuators Eurosensors IX, Stockholm, Sweden, Jun. 1995, pp. 821ï 824.
[135] A. Tetelin and C. Pellet ñModeling and optimization of a fast response capacitive humidity sensorò, IEEE Sensors Journal , vol. 6, no. 3, pp. 714-720, Jun. 2006.

[136] Wen-He Zhou, Liang-Cheng Wang, and Liang-Bi Wang ñNumerical study of the structural parameter effects on the dynamic characteristics of a polyimide film micro-capacitive humidity sensorò, IEEE Sensors Journal, vol. 16, no. 15, pp. 5979-5986, Aug. 2016.
[137] A. Tetelin, V. Pouget; J.-L. Lachaud, C. Pellet ñDynamic behavior of a chemical sensor for humidity level measurement in human breathò, IEEE Transactions on Instrumentation and Measurement, vol. 53, no. 4, pp. 1262-1267, Jul. 2004.
[138] Sumy Jose et al. ñReliability tests for modelling of relative humidity sensor driftsò IEEE International Reliability Physics Symposium (IRPS), Monterey, CA, USA, 2-6 April 2017.
[139] Jia Qi, Zhen Zhou , Chenchen Niu, Chunyu Wang and Juan Wu, ñReliability modeling for humidity sensors subject to multiple dependent competing failure processes with self-recoveryò, sensors, vol. 18, pp. 1-17, Aug. 2018.
[140] Keyvan Narimani, Fatemeh D. Nayeri and Praveen Ebrahimi, ñFabrication, modeling and simulation of high sensitivity capacitive humidity sensors based on ZnO nanorodsò, Sensors and Actuators B: Chemical, vol. 224, no. 1, pp. 338-343, Mar. 2016.
[141] Jerzy Weremczuk, Grzegorz Tarapata and Ryszard S Jachowicz, ñThe ink-jet printing humidity sorption sensorð modelling, design, technology and characterizationò, Measurement Science and Technology, vol. 23, no. 1, pp. 1-10, Dec. 2011.
[142] N. Wildmann, F. Kaufmann, and J. Bange, ñAn inverse-modelling approach for frequency response correction of capacitive humidity sensors in ABL research with small remotely piloted aircraft (RPA)ò, Atmos. Meas. Tech., vol. 7, no. 1, pp. 3059ï 3069, Sept. 2014.
[143] Souhil Kouda, Zohir Dibi and FaycalMeddour, ñModeling of a smart humidity sensorò, International Conference on Microelectronics, Sharjah, United Arab Emirates, 14-17 Dec. 2008.
[144] Bartosz Dzikowski and Jerzy Weremczuk, ñFlexible humidity sensors impedance modelling, Proc. SPIE 10808, Photonics application in astronomy, communications, industry and high energy physics experiments, Oct. 2018.
[145] Karim Feroudji, Nabil Benoudjit, and Fayçal Medjili, ñModdeling of smart thin film thermal conductivity humidity sensor using ANNò1er Congrès National de Physique et Chimie Quantique, 2015.
[146] Derek M. Hall, Timothy Duffy, Margaret Ziomek-Moroz, and Serguei N. Lvov ñElectrochemical impedance spectroscopy and finite element analysis modeling of a 4-electrode humidity sensor for natural gas transportation pipelinesò, Review of Scientific Instruments, vol. 90, no. 1, pp. 1-10, Jan. 2019.
[147] Yang Wang, Jun-Ning Chen, Dao-Ming Ke and Jiang Hu ñModeling of a CMOS Capacitive Relative Humidity Sensorò, First International Workshop on Education Technology and Computer Science, Wuhan, Hubei, China, 7-8 March 2009
[148] Ashis Kumar Sen and Jeff Darabi, ñModeling and optimization of a microscale capacitive humidity sensor for HVAC applicationsò, IEEE Sensors Journal, vol. 8, no. 4, pp. 333-340, April 2008.
[149] Navjot K. Sidhu, P. Abedini Sohi, S. Samadi and M. Kahrizi, ñModeling of FBG Moisture Sensor in COMSOLò, 2018 Photonics North (PN), Montreal, QC, Canada, 5-7 June 2018.
[150] P.M. Faia, C.S. Furtado and A.J.Ferreria, ñAC impedance spectroscopy: a new equivalent circuit for titania thick film humidity sensorsò, Sensors and Actuators B: Chemical, vol. 107, no. 1, pp. 353-359, May 2005.
[151] Henrik Lensch, Manuel Bastuck, Tobias Baur, Andreas Schütze, and Tilman Sauerwald, **"**Impedance model for a high-temperature ceramic humidity sensorò, Journal of Sensors and Sensor Systems, vol. 8, no. 1, pp. 161-169, Apr. 2019.
[152] A. E. Falk, B. M. Lacquet and P. L. Swart,ñDetermination of equivalent circuit parameters of porous dielectric humidity sensorò, Electronics letter, vol. 28, no. 2, pp.166-167, Jan. 1992.
[153] J. J. Velasco-Velez, A. Chaiyboun, C. Wilbertz, S. Scheinert, and T. Doll, ñDrift modeling of electrically controlled nano scale metalï oxide gas sensors,ò IEEE Electron Device Letters, vol. 29, no. 7, pp.677-680, Jul. 2008.
[154] Jia Qi, Zhen Zhou 1, Chenchen Niu , Chunyu Wang and Juan Wu, ñReliability Modeling for Humidity Sensors Subject to Multiple Dependent Competing Failure Processes with Self-Recoveryò, Sensors MDPI,ò vol. 18, pp., 1-17, Aug. 2018.

[155] Stoyan Nihtianov, Zhichao Tan and Boby George ñNew trends in smart sensors for industrial applicationsð Part Iò, IEEE Transaction on Industrial Electronics, vol.64, no. 9, pp. 7281-7283, Sept. 2017.
[156] A. Chatterjee, S. Munshi and A. Rakshit, ñANN based linearizing technique for constant temperature anemometer systemò, Journal of the Instrument Society of India, vol. 30, no. 2,- pp. 109-114, 2000.
[157] Tarikul Islam , Shakeb A. Khan and Md. Firoz A. Khan and Subhas Chandra Mukhopadhyay ñA relaxation oscillator-based transformer ratio arm bridge circuit for capacitive humidity sensorò, IEEE Transactions on Instrumentation and Measurement, vol. 64, no. 12, pp. 3414-3422, 64, no.12, Dec. 2015.
[158] Anwar Ulla Khan , Tarikul Islam and Jamil Akhtar ñAn oscillator-based active bridge circuit for interfacing capacitive sensors with microcontroller compatibilityò, IEEE Transactions on Instrumentation and Measurement, vol. 65, no. 11, pp. 2560-2568, July 2016.
[159] P. Vooka and B. George ñCapacitance-to-digital converter for leaky capacitive sensorsò, Electronics Letter, vol. 52, no. 6, pp.456-458, Mar. 2016.
[160] Moupali Chakraborty , Anindita Kalita and Karabi Biswas ñPMMA-coated capacitive type soil moisture sensor: design, fabrication, and testingò, IEEE Transactions on Instrumentation and Measurement, vol. 68, no. 1, pp. 189-196, Jan. 2019.
[161] S. Pennisi, ñHigh-performance and simple CMOS interface circuit for differential capacitive sensors,ò IEEE Trans. Circuits Syst. II Express Briefs, vol. 52, no. 6, pp. 327-300, 2005.
[162] P. Bruschi, D. Navarrini, G. Barillaro, and A. Gola, ñA Precise Capacitance-to-Pulse width converter for Integrated Sensors,ò Analog Integr. Circuits Signal Process., vol. 41 no, 1, pp. 93-97, Oct. 2004.
[163] Tarikul Islam, Anwar Ulla Khan, Jamil Akhtar and Zia Ur Rahman, ñA digital hygrometer for trace moisture measurementò IEEE Trans. Ind. Electron., Vol. 61, no. 10, pp. 5599-5605, Jan. 2014.
[164] J. Park, J. Park, Y. Choi, K. Sim, and D. Baek,ñA Fully-Differential Complementary Hartley VCO in 0.18 m CMOS Technology,ò IEEE Microw. Wirel. Compon. Lett., vol. 20, no. 2, pp. 91-93, 2010.
[165] Sougata Kumar Kar , Procheta Chatterjee , Banibrata Mukherjee , Kenkere Balashantha Murthy, Mruthyunjaya Swamy and Siddhartha Sen ñA Differential Output Interfacing ASIC for Integrated Capacitive Sensorsò, IEEE Transactions on Instrumentation and Measurement, vol. 67, no. 1, pp. 196-203, Oct. 2017.
[166] Anwar Ulla Khan , Tarikul Islam , Boby George and Mahfoozur Rehman ñAn Efficient Interface Circuit for Lossy Capacitive Sensorsò, IEEE Transactions on Instrumentation and Measurement, vol. 68, no. 3, pp. 829-836, Mar. 2019.
[167] Kupershtokh, A.L., Karpov, D.I., Medvedev, D.A., ñStochasticmodels of partial discharge activity in solid and liquid dielectricsò, IET Sci. Meas. Technol., vol. 1, no.6, pp. 303ï 311, 2007.
[168] K. Dutta, A.Hazra and P. Bhattacharyya, ñTi/TiO2 nano tube Array/Ti capacitive device for non-polar aromatic hydrocarbon detection,ò IEEE Transactions on Device and Materials Reliability, vol. 16, no. 2, pp. 235-242, Jun 2016.
[169] Jianlin Huang, Duġan S. Golubovi´, SauKoh, Daoguo Yang, Xiupeng Li, Xuejun Fan, and G. Q. Zhang, ñRapid degradation of mid-power white-light LEDs in saturated moisture conditions,ò IEEE Transactions on Device and Materials Reliability, vol. 15, no. 4, pp. 478-483, Dec. 2015.
[170] Sanae Taouýk, Pascal Dherbécourt, Ahmed El Oualkadi, and Farid Temcamani, ñReliability and failure analysis of UHF RFID passive tags under thermal storageò, IEEE Transactions on Device and Materials Reliability, vol. 17, no. 3, pp. 531-538, Sept. 2017.
[171] Jianlin Huang, Duġan S. Golubovi´c, Sau Koh, Daoguo Yang, Xiupeng Li, Xuejun Fan, and Guoqi Zhang, ñDegradation mechanism decoupling of mid-power white-light LEDs by SPD simulation,ò IEEE Transactions on Electron Devices, vol. 63, no. 7, pp. 2807-2814, Jul. 2016.

[172] Ketul B., Sutaria, Jyothi Bhaskarr, Velamala, Chris H. Kim, Takashi Sato, and Yu Cao, ñAging statistics based on trapping/detrapping: compact modeling and silicon validationò, IEEE Transactions on Device and Materials Reliability, vol. 14, no. 2, pp. 607-615, Jun. 2014.
[173] SHAW Moisture Meters [UK] Ltd., Westgate Bradford, BD13SQ (www. shawmeters.com).
[174] M. M. Dubinin, V. A. Astakhov and L. V. Radushkevich,in D.A. Cadenhead, J.F. Danielli and M.D. Rosenberg (Eds.), ñPhysical adsorption of gases and vapors in microporesò, In Progress and Membrane Scienceô(New York: Academic Press, 1975), pp. 1-70.
[175] S.J. Gregg and K. S. W. Sing, ñAdsorption, Surface Area and Porosityò, (LondonAcademic Press, Chapter 4, 1991).
[176] A. Gil and P. Grange, óApplication of the Dubinin-Radushkevich and Dubinin-Astakhovequations in the characterization of microporous solidsò, Colloids and Surfaces A physicochemical and engineering aspects, vol.113, pp. 39-50, 1996.
[177] F.P. Incropera: õFundamental of Heat and Mass Transferô(New York: Wiley, 1990, 3rd edn.)
[178] Bombay Engineering Company, ñ2D-RH/100 relative humidity indicatorò, Available at https://www.tradeindia.com/Seller-7944739-Bombay-Engineering-Company.
[179] A. Shahin, M. Hinaje, J. P. Martin, S. Pierfederici, S. Rael, and B. Davat, ñHigh voltage ratio DC-DC converter for fuel-cell applicationsò, IEEE Trans. Ind. Electron., vol. 57, no. 12, pp. 3944ï 3955, Dec. 2010.
[180] D. Li, M. Shen, J. Huangfu, J. Long, Y. Tao, J. Wang, C. Li, and L. Ran, ñWireless sensing system-on-chip for near-ýeld monitoring of analog and switch quantitiesò, IEEE Trans. Ind. Electron., vol. 59, no. 2, pp.1288ï 1299, Feb. 2012.
[181] H. M. El-Bolok, ñ A microprocessor- based firing circuit for thyristor working under three-phase variable- frequency supplyò, IEEE Trans. Ind. Electron., Vol. 37, no. 2, pp. 152-155, Apr. 1990.
[182] H. M. EL-Bolek and S. ABD-EL Hamid, ñ A microprocessor based self- adjusting system for integral cycle power control of RL loadò, IEEE Trans. Ind. Electron., Vol. 37, , no. 2, pp. 156-159, Apr. 1990.
[183] Mohammed T. Lazim, ñPower frequency converter based on integral cycle triggering mode of thyristors with mult-icontrol periodsò, Electric Power Components and Systems, Vol. 41, no. 12, pp. 1173-1187, Jul. 2013.
[184] A. De Marcellis, G. Ferri, and P. Mantenuto, ñUncalibrated operational ampliýer-based sensor interface for capacitive/resistive sensor applicationsò,.IET Circuits Devices Syst., vol. 9, no. 4, pp. 249ï 255, 2015.
[185] S. N. Nihtianov, G.P. Shterev, B. Iliev, and G. C. M. Meijer, ñAn interface circuit for Rï C impedance sensors with a relaxation oscillatorò,. IEEE Trans. Instrum. Meas. Vol. 50, no. 6, pp. 1563ï 1567, 2001.
[186] Y. Liu, S. Chen, M. Nakayama, and K. Watanabe, ñLimitations of a relaxation oscillator in capacitance measurementsò, IEEE Trans. Instrum. Meas., vol. 49, no. 5, pp. 980ï 983, 2000.
[187] T. Islam, K. K. Mistry, K. Sengupta, and H. Saha, ñMeasurement of gas moisture in the ppm range by porous silicon and porous alumina sensors. Int. J. Sens. Mater., vol. 16, no. 7, pp. 345ï 356, 2004.
[188] T. Islam, Md. F. Khan, S.A. Khan, and H. Saha, ñA sensitive digital moisture detector for nano structured thin ýlm sensor. Int. J. Smart Sens. Intell. Syst., Vol. 7, no. 3, pp. 1059ï 1076, 2014.
[189] S. Malik, K. Kishore, T. Islam, Z.H. Zargar, S.A. Akbar, ñA time domain bridge-based impedance measurement technique forwide-range lossy capacitive sensorsò, Sens. Actuators A, Vol. 234, pp. 248ï 262, 2015.
[190] S. Malik, D. Sharma, K. Kishore, M. Maharana, S.A. Akbar, T. Islam, ñA CCII-based wide frequency range square/triangular wave generatorò, in 2015 IEEE 2nd International Conference on Recent Trends in Information Systems July 9-11, 2015, Jadavpur University, Kolkata.
[191] Babaei, F.H.; Rahbarpour, S., ñAlteration of pore size distribution by solï gel impregnation for dynamic range and sensitivity adjustment in Kelvin condensation-based humidity sensorsò, Sens. Actuators B Chemical, vol. 191, pp. 572ï 578, Oct. 2014.

List of Publications of Thesis Work

Journal Publications

1. Shailesh Kumar, L. Kumar, Tarikul Islam and K.K.Raina, **"**Condition Monitoring of Transformer Breather Using a Capacitive Moisture Sensorò, **IEEE Transactions on Industrial Electronics,** Vol. 67, no. 11, pp. 9779-9789, Nov. 2020. **(SCI), IF-7.503**
2. Shailesh Kumar, Tarikul Islam and Kuldeep Kumar Raina, ñStudy of long term drift of aluminium oxide thin film capacitive moisture sensorò, **IEEE Transactions on Device and Materials Reliability**, Vol. 18, no. 2, pp.180-188, Mar. 2018. **(SCIE), IF-1.583**
3. Shailesh Kumar, Tarikul Islam and Kuldeep Kumar Raina, ñModelling of breather for transformer health assessmentò, **IET Science Measurement and Technology**, Vol. 11, no. 2, pp. 194-203, Mar. 2017.**(SCI), IF-1.895**
4. Shailesh Kumar, L. Kumar, T. Islam and Kuldeep Kumar Raina, ñElectrical Circuit Model of an Aged Ceramic Humidity Sensorò **Materials Today: Proceeding- Journal – Elsevier,** vol. 18, pp. 822-829, 2019. **(SCOPUS)**
5. Shailesh Kumar, Kuldeep Kumar Raina and Tarikul Islam ñAnodic Aluminium Oxide based Humidity Sensor for Online Moisture Monitoring of Power Transformerò, **Sensors and Actuators B Chemical** (Under revision). .**(SCI), IF-7.1**

Conference publication

1. Shailesh Kumar, Tarikul Islam and K.K.Raina, ñA Moisture-in-Breather Model for Transformer Health Monitoringò, 12th Annual IEEE India Conference (INDICON) Dec. 17-20, 2015, at Jamia Millia Islamia, New Delhi. (Available at IEEE Explore, **DOI: 10.1109/INDICON.2015.7443326**).
2. Shailesh Kumar, L. Kumar, T. Islam and Kuldeep Kumar Raina, ñElectrical Circuit Model of an Aged Ceramic Humidity Sensorò, Proc. of International Conference on Nanotechnology: Ideas, Innovations & Initiatives, Dec. 6-8**,** 2017, IIT Roorkee.
3. Shailesh Kumar, Tarikul Islam and K.K.Raina, ñ Design and Fabrication oh Humidity Sensor for Condition Monitoring of Breather of Transformerò, International Conference on Condition Assessment Techniques in Electrical Systems, 21-23, Nov. 2019 at IIT Chennai. (Available at IEEE Explore, **DOI: 10.1109/CATCON47128.2019.CN0079**).